Report No. FAA-RD-77-118

12

AD A047887

TEST AND EVALUATION OF THE MOVING TARGET DETECTOR (MTD) RADAR

Ronald S. Bassford

William Goodchild

and

Alfred De La Marche

OCTOBER 1977

FINAL REPORT

Prepared for

U. S. DEPARTMENT OF TRANSPORTATION
FEDERAL AVIATION ADMINISTRATION
Systems Research & Development Service
Washington, D.C. 20590

NOTICE

This document is disseminated under the sponsorship of the Department of Transportation in the interest of information exchange. The United States Government assumes no liability for its contents or use thereof.

METRIC CONVERSION FACTORS

Approximate Conversions to Metric Measures

Symbol	When You Know	Multiply by	To Find	Symbol
		LENGTH		
in	inches	*2.5	centimeters	cm
ft	feet	30	centimeters	cm
yd	yards	0.9	meters	m
mi	miles	1.6	kilometers	km
		AREA		
in^2	square inches	6.5	square centimeters	cm^2
ft^2	square feet	0.09	square meters	m^2
yd^2	square yards	0.8	square meters	m^2
mi^2	square miles	2.6	square kilometers	km^2
	acres	0.4	hectares	ha
		MASS (weight)		
oz	ounces	28	grams	g
lb	pounds	0.45	kilograms	kg
	short tons (2000 lb)	0.9	tonnes	t
		VOLUME		
tsp	teaspoons	5	milliliters	ml
Tbsp	tablespoons	15	milliliters	ml
fl oz	fluid ounces	30	milliliters	ml
c	cups	0.24	liters	l
pt	pints	0.47	liters	l
qt	quarts	0.95	liters	l
gal	gallons	3.8	liters	l
ft^3	cubic feet	0.03	cubic meters	m^3
yd^3	cubic yards	0.76	cubic meters	m^3
		TEMPERATURE (exact)		
°F	Fahrenheit temperature	5/9 (after subtracting 32)	Celsius temperature	°C

*1 in = 2.54 (exactly). For other exact conversions and more detailed tables, see NBS Misc. Publ. 286, Units of Weights and Measures, Price $2.25, SD Catalog No. C13.10:286.

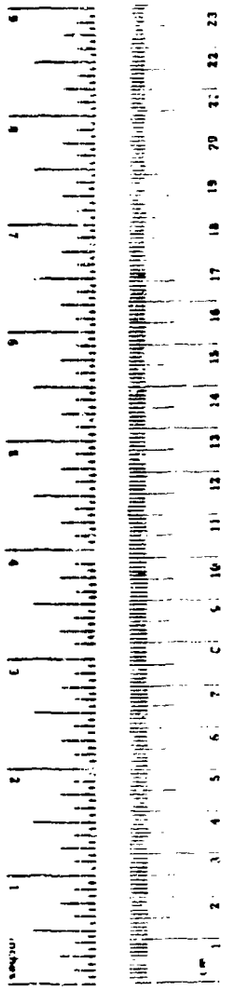

Approximate Conversions from Metric Measures

Symbol	When You Know	Multiply by	To Find	Symbol
		LENGTH		
mm	millimeters	0.04	inches	in
cm	centimeters	0.4	inches	in
m	meters	3.3	feet	ft
m	meters	1.1	yards	yd
km	kilometers	0.6	miles	mi
		AREA		
cm^2	square centimeters	0.16	square inches	in^2
m^2	square meters	1.2	square yards	yd^2
km^2	square kilometers	0.4	square miles	mi^2
ha	hectares (10,000 m^2)	2.5	acres	
		MASS (weight)		
g	grams	0.035	ounces	oz
kg	kilograms	2.2	pounds	lb
t	tonnes (1000 kg)	1.1	short tons	
		VOLUME		
ml	milliliters	0.03	fluid ounces	fl oz
l	liters	2.1	pints	pt
l	liters	1.06	quarts	qt
l	liters	0.26	gallons	gal
m^3	cubic meters	35	cubic feet	ft^3
m^3	cubic meters	1.3	cubic yards	yd^3
		TEMPERATURE (exact)		
°C	Celsius temperature	9/5 (then add 32)	Fahrenheit temperature	°F

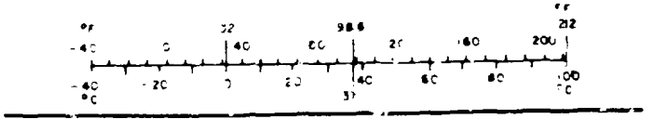

(18) FAA/P-
(19) 77-11

Technical Report Documentation Page

1. Report No.	2. Government Accession No.	3. Recipient's Catalog No.
FAA-RD-77-118		

4. Title and Subtitle (6)
TEST AND EVALUATION OF THE MOVING TARGET DETECTOR (MTD) RADAR

5. Report Date (11)
Oct[redacted]77

6. Performing Organization Code

8. Performing Organization Report No. (12) 226 p.

7. Author(s) (10) Ronald S. Bassford, William Goodchild, Alfred De La Marche

FAA-NA-77-29 (17)

9. Performing Organization Name and Address
Federal Aviation Administration
National Aviation Facilities Experimental Center
Atlantic City, New Jersey

10. Work Unit No. (TRAIS)

11. Contract or Grant No.
022-243-510

13. Type of Report and Period Covered (9)
Final rept.
Oct[redacted]74-Oct[redacted]76

12. Sponsoring Agency Name and Address
U.S. Department of Transportation
Federal Aviation Administration
Systems Research and Developmental Service
Washington, D.C. 20590

14. Sponsoring Agency Code
ARD-243

15. Supplementary Notes

16. Abstract

The moving target detector (MTD) terminal radar processor system was evaluated to determine its capability to provide radar data suitable for utilization by the Automated Radar Terminal System.

The major objective of testing was to compare the target detection in clutter performance of the MTD system with that of the best terminal radar processor system in the FAA inventory. The comparative tests were conducted using test signals and flight test aircraft. The test signals were used to determine false alarm rates, probability of detection, accuracy, velocity response, and subclutter visibility capabilities. Flight testing was performed to determine subclutter visibility, subweather visibility, and target resolution capabilities.

Additional tests were performed to determine the compatibility of the MTD processor with terminal radar systems currently in use in the Federal Aviation Administration (FAA).

The results of the tests demonstrated that the MTD system capability to detect targets in a clutter environment was much better than that of present FAA systems. It effectively eliminated all clutter experienced in the National Aviation Facilities Experimental Center (NAFEC) radar environment. The MTD processor is compatible with present FAA radar systems.

17. Key Words	18. Distribution Statement
Airport Surveillance Radar Moving Target Detector Radar Processors Radar Quantizers	Document is available to the public through the National Technical Information Service, Springfield, Virginia 22151 240 550

19. Security Classif. (of this report)	20. Security Classif. (of this page)	21. No. of Pages	22. Price
Unclassified	Unclassified	123	

Form DOT F 1700.7 (6-72) Reproduction of completed page authorized

PREFACE

Acknowledgement is made to the following personnel for their contribution to this project:

1. Mr. Lincoln Cartledge, Lincoln Laboratory, for his assistance in MTD operation and data collection.

2. Mr. Gerald Decker, NAFEC project pilot, for arranging and participating in the test flight program.

3. Mr. Edward Ezekiel, NAFEC, for his expertise as project air traffic controller.

4. Mr. Mark Schoenthal, NAFEC, for his help in developing and debugging software used with the Automated Radar Terminal System (ARTS) for Moving Target Detector (MTD) operation and data collection.

5. Mr. Ken Tschetter, Sperry Univac, for his assistance in developing and debugging clutter reduction software for the ARTS III Radar Input Processor (RIP) MTD report processing.

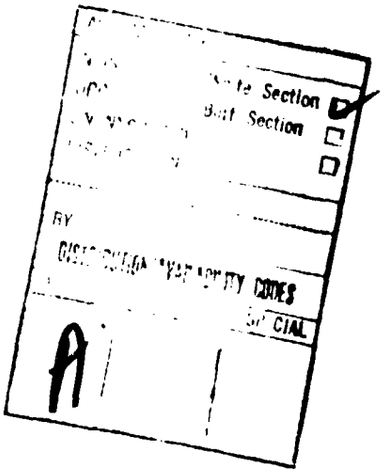

TABLE OF CONTENTS

LIST OF ILLUSTRATIONS

LIST OF ILLUSTRATIONS (Cont'd)

LIST OF ILLUSTRATIONS (Cont'd)

LIST OF TABLES

INTRODUCTION

PURPOSE.

The purpose of this project was to test and evaluate the Moving Target Detector (MTD) radar/processor system to determine its capability to provide Airport Surveillance Radar (ASR) data suitable for Automated Radar Terminal System (ARTS III) processing. The primary area of concern was the ability of the MTD to function acceptably in a terminal radar clutter environment.

BACKGROUND.

The MTD radar/processor was developed for the Federal Aviation Administration (FAA) by the Massachusetts Institute of Technology (MIT) Lincoln Laboratory under tasks B and G of interagency agreement DOT-FA71-WAI-242. It was designed to provide radar data suitable for utilization by the ARTS III system. Primarily, this was to be accomplished by providing improved target detection in ground, weather, and angel clutter. To this end, the MTD was designed to provide stable linear operation with wide dynamic range and sophisticated digital processing. The MTD was integrated into the Terminal Facility for Automated Surveillance Testing (TFAST) ARTS III system at the National Aviation Facilities Experimental Center (NAFEC) and tested by a joint Lincoln Laboratory and NAFEC team. Software for integration of the MTD/processor and the ARTS III system was developed by Sperry Univac and NAFEC.

DESCRIPTION OF EQUIPMENT.

System processing was performed in two stages. First, the MTD system (figure 1) developed by Lincoln Laboratory provided coherent radar signal processing using adaptive thresholding techniques to discriminate against undesirable signals caused by nonsynchronous interference, ground clutter, and weather clutter. Second, further processing was performed in the ARTS III radar input processor (RIP) software developed for MTD operation. This additional adaptive thresholding was performed to remove any false alarms caused by residue from clutter, interference, and angels, thereby preventing initiation of false tracks. The ARTS III tracker provided further velocity discrimination against false alarms. Descriptions of MTD and ARTS III processing are given below.

Figure 2 shows the basic components of the MTD radar digital signal processing system. In the NAFEC tests, intermediate frequency (IF) signals input to the processor were taken from the preamplifier output of the radar system being used. A modified Military Fixed Radar Detector (FPS)-18 klystron-type radar was used for the basic MTD testing. Modifications included a new analog IF receiver subsystem designed to provide stable, wide-dynamic-range signals suitable for MTD processing and a Coherent Oscillator (COHO) and video detectors for providing the in-phase (I) and quadrature (Q) bipolar videos to the input processor. A description of the modified FPS-18 system is contained in appendix A.

The input processor shown in figure 2 consisted of two analog-to-digital (A/D) converters and two 8K memories. A 10-bit A/D converter was used for each (I or Q) video channel. The digitizer video from each A/D was stored in memory until data from 10 interpulse periods had been accumulated. This group of data was termed a coherent processing interval (CPI). There were 480 CPI's per antenna scan. The 10 samples in each range gate were then outputted to the canceller, beginning with the first range gate and continuing in range order. The first two azimuth samples from each range gate were used to "charge up" the three-pulse canceller, and the remaining eight provided the necessary inputs for the eight-point discrete Fourier transform. The MTD operated with a 1/16 nautical mile (nmi) range gate length and a maximum range of 47.5 nmi.

The saturation detector determined if any of the 10 samples saturated the A/D converter resulting in distorted information. If so, the information from that range cell was discarded.

The interference eliminator compared the magnitude of each of the 10 samples with the average magnitude of the 10. If any sample was greater than five times the average, it was considered to be interference from another radar, and the informationin that range cell was discarded.

The three-pulse canceller removed low-velocity information (ground clutter) prior to discrete Fourier transform (DFT) filtering. Since low radial velocity (tangential) targets were removed along with the clutter echoes, a separate zero velocity filter (ZVF) was implemented. It allowed detection of a low-radial-velocity target when its echo strength exceeded the level of the clutter in the same range-azimuth cell. The ZVF was implemented using a disc memory to store the clutter level information in every range azimuth cell from scan to scan. This information was used to establish thresholds for deciding whether a low-velocity return represented clutter or a target. ZVF range azimuth cells were 10-pulse repetition periods by 1 range cell in extent.

A moving target would, in most cases, occupy a different range azimuth cell each antenna scan. Therefore, the threshold which built up over a number of scans, did not inhibit its being outputted in the ARTS III Input Output Processor (IOP).

The DFT circuitry performed an eight-point DFT implementation of the fast Fourier transform (FFT). The eight time samples from each range gate were thereby converted to frequency (Doppler) information. Seven filter outputs from the DFT were utilized. The DFT zero filter output was replaced with the output from the separate ZVF.

In the weights and magnitudes circuits, the sidelobes generated in the DFT were lowered, and the I and Q signals were combined.

Thresholding was performed on each filter output. For the seven nonzero (weather) filters, the threshold was controlled by the average level of the returns in 1-nmi range segments centered on the cell of interest. The threshold for the ZVF was based on the clutter value stored on the disc memory for the

range azimuth cell of interest. Both thresholds adaptively adjusted to the environment.

The IOP interface performed the necessary timing and buffering between the MTD and ARTS III systems. Azimuth, velocity, range, amplitude, and pulse repetition frequency (PRF) information were outputted by the MTD. A complete description of the MTD processor is contained in reference 1. Figure 3 shows the basic ARTS III RIP processing unique to MTD operation (discussed fully in appendix A). The input function shown provided handshaking between the MTD and the RIP processor. The range and Doppler consolidation function combined adjacent MTD range and Doppler filter information into a single target response for each CPI. The target record processor merged these new target responses into existing target record stores. It outputted completed target records to the target report processor. The target report routine processed target records into target reports or noise responses. It outputted finalized target reports containing range, azimuth, strength, number of CPI's involved, and Doppler filter numbers.

The second-level thresholding capability shown in figure 3 was developed at NAFEC to eliminate residual MTD clutter from angels, weather, nonsynchronous interference, and inversion. Each of these areas is discussed fully under FALSE ALARM TESTING. Targets determined to be valid by the above processing were outputted to the ARTS III correlation and tracking functions.

DISCUSSION

The basic philosophy followed in testing was to compare the capabilities of the MTD/processor system to that of the best radar data acquisition system (RDAS) then in the FAA inventory. This was determined to be the combination of an airport surveillance radar (ASR-7) and the radar video digitizer (RVD-4).

First, the parameters of the two systems were investigated to insure valid test results. This also provided the basis for system normalization in later tests so that a valid system-to-system comparison could be made.

Second, each system was tested to determine its capability with respect to standard radar performance factors. These included probability of false alarm (P_{fa}), probability of detection (P_d), subclutter visibility (SCV), Sub-Weather Visibility (SWV), and velocity response. Coherent S-Band radio-frequency (RF) test targets were generated for the P_d, SCV, SWV, and velocity response tests using the NAFEC TFAST Test Target Generator (TTG). The TTG output was variable in frequency, pulse width, phase, range start, range rate, azimuth position, antenna scan modulation, amplitude modulation (scintillation), and radar cross section (strength). A description of the TTG is contained in appendix B.

Third, flight testing was conducted to determine the target detection capabilities of the two systems in the clear, over clutter (both tangentially and radially), and in weather. Target resolution capabilities were tested by directing a pair of aircraft through a series of crossing tracks.

Tests were also conducted to determine the capability of the MTD to function as the processor for present FAA ASR-type radars. This is discussed below under ASR-5 and ASR-7 compatibility testing.

Concurrent with the MTD/RVD-4 comparison testing, a separate investigation of the RVD-4 system was conducted. The resulting NAFEC report containing pertinent parameter and performance data has been published (reference 2). Results from the above investigation were used to establish system operating parameters and will be referred to throughout this report.

SYSTEM TESTS AND RESULTS

TEST CONFIGURATION.

The basic system for data acquisition for the comparison of the ASR-7/RVD-4 and FPS-18 (S-band coherent radar)/MTD systems is shown in figure 4. The two radars located at the NAFEC TFAST facility were operated independently (asynchronously) by means of a waveguide diplexer. The normal, log normal, and moving target indicator (MTI) video outputs of the ASR-7 were available to the RVD-4. Low-level IF information from the FPS-18 was sent to the MTD receiver/processor.

The RVD-4 output was processed with the All Digital Tracking Level (ADTL) program in real time in the ARTS III IOP with the extracted system data being recorded on magnetic tape via the ARTS III Integral Magnetic Tape (IMT) unit. Meanwhile, the MTD output was recorded on magnetic tape via a Bucode digital recorder. Subsequent to this operation, the Bucode tape was played back into the ADTL program in the ARTS III IOP, and the MTD system data were extracted on magnetic tape via the ARTS III IMT.

The two comparative system data extractions were then reduced at the NAFEC Terminal Automated Test Facility (TATF). Scan and run summaries of each system were printed out for comparative analysis (tables 1 and 2). The extracted data tapes from both systems could also be displayed on ARTS III Data Entry and Display System (DEDS) indicators. This allowed data control with the DEDS keyboard and visual analysis of system performance.

Beacon data were sent to the IOP via the Beacon Data Acquisition System (BDAS). It was processed with both the RVD-4 and MTD data for correlation analysis. The ASR-7 analog videos were also recorded on magnetic tape via the TFAST FR-950 video recorder. This analog information was used for backup in case of incorrect video processing and was also used as a repeatable source for optimizing the RVD-4 processor parameters.

TABLE 1. RUN SUMMARY (REDUCED DATA)

1. Run Parameters

   Scan start number
   Scan stop number
   Selected track gate (R1, R2, AZ1, AZ2)
   Selected track beacon code
   Threshold (RVD)

2. All Report Statistics

   Beacon reports/scan
   Radar reports/scan
   Radar-beacon correlating reports/scan
   Beacon false alarms/scan
   Radar false alarms/scan

3. All Track Statistics

   Number beacon tracks
   Number radar only tracks
   Mean beacon track life
   Mean radar only track life
   Beacon blip/scan
   Radar blip/scan

4. Selected Track Statistics

   Beacon blip/scan
   Radar blip/scan
   Beacon report standard deviation (R, AZ)
   Radar-beacon correlated report deviation (R, AZ)
   Track position deviation (R, AZ)
   Track speed deviation
   Track heading deviation

5. Processing Load

   Radar average and peak/sector
   System average and peak/sector

Legend

R = Range

AZ = Azimuth

TABLE 2. SCAN SUMMARY (REDUCED DATA)

1. Scan Parameters

   Scan number
   Reference azimuth crossing time
   Selected track gate (R1, R2, AZ1, AZ2)
   Selected track beacon code

2. Number of Reports

   Beacon
   Radar
   Radar and beacon correlated

3. Number of Tentative Tracks

   Beacon only or beacon and radar
   Radar only
   Initiating beacon
   Initiating radar
   Terminating beacon
   Terminating radar

4. Number of Firm Tracks

   Beacon
   Radar only
   Initiating beacon
   Initiating radar only
   Terminating beacon
   Terminating radar only
   Coasts beacon
   Coasts radar
   Coasts both beacon and radar

5. Selected Track Data

   Beacon report (R, AZ, H, Code)
   Radar report (R, AZ, S, D)
   Radar and beacon correlated report (R, AZ)
   Track data (X, Y, H, Speed Heading)

Legend

R = Range

AZ = Azimuth

H = Altitude

S = Strength

D = Doppler

A NOVA 1220 minicomputer (figure 5) was provided as part of the MTD system. It functioned as a maintenance aid to perform system stability testing and was also used in some data collection. It provided a numeric output (0 through 7) to the maintenance indicator for each MTD Doppler response output. The associated Imlac graphics display was provided to display system stability data and to examine signal spectra.

Standard ARTS III correlation and tracking processing was performed on MTD radar reports from the RIP module. Detailed test procedures and results are presented in the following sections.

SYSTEM CERTIFICATION.

Test parameters of the FPS-18 radar system are listed in table 3. Basic parameters were monitored throughout the test program using standard techniques and equipments. By monitoring these parameters and the various system meters, optimum system performance was maintained. A list of the test equipment used is contained in appendix B.

Throughout the test program, the FPS-18/MTD system was monitored to assure that the transmitter and receiver equipments were providing the stable operation necessary for MTD operation.

Table 4 gives the ASR-7 system parameters. Spurious frequency signal levels were measured at the output of the A/D converters using MTD test programs to insure that their amplitudes were low enough not to be processed by the MTD. Since the dynamic range of the MTD system was 42 dB, spurious signals had to be at least 42 dB below the desired radar signals. This test is described fully later under ASR-5 and ASR-7 MTD compatibility testing.

RADAR/PROCESSOR PERFORMANCE TESTS.

PROBABILITY OF FALSE ALARM (P_{fa}). The MTD system P_{fa} was determined in environments of thermal noise, ground clutter, weather clutter, interference, and angel clutter. These areas are discussed below.

Probability of False Alarm in Thermal Noise. The MTD system P_{fa} and the corresponding false alarms per scan as a function of the receiver noise level and MTD threshold levels were measured to determine optimum operating levels. The resulting curves are shown in figure 6. The curves shown are composites of the eight separate Doppler filters. The thresholds (level above the average thermal noise level) used with the individual filters are also listed. As a result of this test, the system was operated with approximately a 6 millivolt (mV) root mean square (RMS) noise level at the A/D converter inputs. As shown, this provided a $1x10^{-5}$ P_{fa} and an average of 30 false alarms per scan. A detailed description of the thermal false alarm investigation is given in appendix C.

During the comparison testing described in following sections, the ASR-7/RVD-4 was also operated with a $1x10^{-5}$ P_{fa} in thermal noise (reference 2).

TABLE 3. TEST PARAMETERS, FPS-18/MTD SYSTEM

Transmitter (FPS-18)	
Power Output (Variable PRF)	
Average	57 dBm
Frequency	2710 MHz
Pulse Width	1 μs
Oscillator	Klystron Varian 87-B
Receiver	
Dynamic Range (IF)	42 dB
Noise Level	6 mV
I	6 mV
Q	6 mV
Noise Figure (Diplexer Antenna Port)	8 dB
STC	R^{-4} to 12 nmi
System Timing	
Scan Stagger OFF	
Low PRF	1.1131 kHz
High PRF	1.3677 kHz
Average PRF	1.2320 kHz
Scan Stagger ON	
Low PRF	1.2080 kHz
High PRF	1.3794 kHz
Average PRF	1.2415 kHz

TABLE 4. ASR-7 SYSTEM PARAMETERS

Transmitter	
Power Output (Staggered PRF)	
Average	54.6 dBm
Frequency	2795 MHz
Pulse Width	.833 μs
Oscillator	Magnetron (Amperex DX-276)
Receiver	
MTI System	Three-Pulse Canceller
Noise Figure	(Diplexer Antenna Port) 4 dB
Sensitivity Time Control (STC)	R^{-4} to 12 nmi
System Timing	
Nonstaggered	
1.200, 1.173, 1.120, 1.050, .950, or .713	kHz
Staggered	
Pseudorandom combination of above 6 PRF's, Average = 1.034	kHz
Antenna Parameters (ASR-5 Antenna)	
Rotation (ASR-7 Drive Motor)	12.75 rpm
Tilt	± 2.75°
Polarization Used	Linear
Beamwidth (two-way)	1°
Gain	34 dB

Probability of False Alarm with an Operating System. In order to maintain a 10^{-5} P_{fa} into the tracker with an operating radar system, the following improvements were added to the MTD and RIP:

1. MTD interference eliminator,
2. RIP interference eliminator, and
3. RIP second-level thresholding.

The following discussion defines the need for each of these improvements and any resulting loss in system sensitivity.

Interference Elimination - The MTD experienced an increase in false alarm rate when operating in an RF interference (RFI) environment. An ASR-7 radar and an ASR-4 radar, each located approximately 1 nmi from the TFAST site, were the primary causes of this nonsynchronous interference. To prevent these false alarms from being outputted by the MTD, an interference eliminator capability was added. The interference eliminator algorithm compared the magnitude of any received signal in a CPI range cell with that of the average magnitude level of the possible 10 signals in the same CPI range cell. If a signal magnitude, exceeded five times the average magnitude, it was considered to be an interference signal. Information from that CPI range was inhibited at the MTD thresholding circuitry from being outputted by the MTD.

The MTD output for an equal length of time (multiscan) with and without the interference eliminator is shown in figure 7. The numerics shown were generated using the NOVA minicomputer. Each numeric represented an MTD threshold crossing. The value of the numeric indicated which filter had the threshold crossing.

As shown, virtually all the interference was eliminated. The remaining isolated numerics were caused by thermal false alarms as previously discussed. Those thermal false alarms satisfying the interference elimination algorithm were also eliminated. Due to the small number of thermal false alarms, with amplitudes five times the average, this resulted in no appreciable loss of data or sensitivity.

The following is a brief discussion of the effect of the interference eliminator on system performance as shown in figure 7. The total number of CPI/range cells in the MTD coverage was 364,800 (760 range gates x 480 CPI's per scan). A typical interfering FAA S-band radar would result in a maximum of 9,600 CPI/range cells containing interference signals (assuming one reception per PRF and 100-percent range splits). The above rate of interference would therefore result in inhibiting the information from 2.6 percent of the CPI/range cells. Since the above interference signals were nonsynchronous with the MTD, they would not correlate in range and azimuth on a scan-to-scan basis. Also, when an interference signal occurred in the same CPI/range cell as an aircraft echo signal, the combined information would not necessarily be discarded. That is, if the interference rejection algorithm was not satisfied (interference magnitude not more than five times the average magnitude) and the MTD threshold criteria were met, the combined information was outputted by the MTD. The

resulting target signal, however, necessarily contained spurious frequency information due to the interference.

For those cases of superposition of aircraft and interference signals where the interference algorithm was satisfied, two alternatives were possible. First, when the aircraft signal occurred in more than one CPI (this was true in the majority of cases), the loss of information from one CPI had a minimized effect on subsequent target declaration and tracking. Second, when the aircraft signal occurred in only one CPI, the resulting loss of information was mitigated by the ability of the tracker to coast for up to two scans on uncontrolled tracks and up to 10 scans on controlled tracks.

The above factors indicate why the interference eliminator had a minimal effect on system target detection and tracking performance.

In the presence of ground or weather clutter, the MTD interference elimination algorithm's capability was again a function of the relative interference and clutter signal magnitudes. Therefore, all interference was not removed. To correct this problem, the following interference rejection algorithm was added to the RIP. Interference was detected by counting the number of single-CPI responses occurring in each 5° by 48 nmi sector of radar coverage. Upon detection of 15 or more single-CPI responses in a sector, all single-CPI responses in that sector were discarded. If the antenna coupling between the radars was such that the interference rotated (changed location) from scan to scan, the results would be similar to that discussed previously for the MTD interference eliminator. However, if the antenna coupling resulted in a stationary interference pattern, all single-CPI signals would be eliminated in the affected sectors for the duration of the interference. The resulting effect on system sensitivity will be discussed later under P_d testing. It will be shown that detection of a two-CPI target required a 3-decibels (dB) greater signal level than for a single-CPI target.

Second-Level Thresholding. Second-level thresholding in the RIP to prevent clutter residue and angels from initiating false tracks and to maintain the number of false alarms at desired levels was implemented as follows. The radar surveillance area was divided into 4 nmi by 22.5° sectors for a total of 192 sectors. Each sector contained eight thresholds (one for each Doppler filter) for a total of 1,536 independent sector Doppler thresholds in the coverage area. The threshold level in each sector Doppler filter was based upon the frequency of occurrence of single-CPI signals in it. The threshold level in each sector filter was adaptively set by incrementing it by an amount equal to 2.00 strength numbers (defined under angel false alarm tests) each time a single-CPI signal with a strength number (amplitude) greater than the threshold occurred. The threshold was decremented by 0.125 strength number if there were no single-CPI signals in that sector from the filter being examined during an antenna scan period.

Each MTD output signal was tested against these thresholds. If the signals amplitude was less than the applicable threshold, it was discarded. The thresholds derived by this process were applied in the first 16 nmi against all signals (single and multiple CPI) and from 16 nmi to 48 nmi on single-CPI

returns only. This range-dependent thresholding was based upon the fact that most angel returns occurred within 16 nmi in the NAFEC radar environment. Also, in the first 16 nmi, RIP thresholding was applied before range Doppler, or CPI consolidation. By applying the threshold in this manner, a considerable saving in processing was realized. Beyond 16 nmi, however, since thresholding was only performed against single-CPI signals, consolidation had to be performed first to determine which signals were only in a single CPI.

Angel returns detected by the MTD on occasion exceeded 1,300 targets per scan while using an R^{-4} STC curve extending to 12 nmi. These angels occurred predominantly in the low-velocity filters as discussed below. Runlengths up to four CPI's were observed.

The MTD/processor system virtually eliminated the resulting false alarm and false track initiation by a combination of using an R^{-4} STC curve, second-level thresholding in the RIP, desensitizing the tracker by requiring a two-CPI runlength for track initiation, and the requirement of a target velocity of at least 50 knots for track initiation and continuation. Targets appearing in only one CPI were allowed to initiate tracks beyond 16 nmi and to continue tracks from 0 to 16 nmi.

Figures 8 and 9 show this angel elimination capability in light and heavy angel clutter. Forty scans of data are presented for each case. Tracking parameters used in these and all subsequent figures required data from three scans to initiate a track and one more before it was displayed. If the tracker received no return for a track during a scan, no symbol was displayed (no coasting). Notice that both second-level thresholding and the tracker contribute to angel elimination. In each figure, target reports or tracks caused by automobile traffic at 0° and from 0.5 nmi to 3 nmi can be observed. No attempt was made during this project to eliminate these automobile targets.

Since the tracker was designed to handle a maximum of 100 tracks at a time, the data shown in figure 9(c) represented only about 15 percent of the angels present. Allowing more data into the tracker would have resulted in improper processing. An example of the inability of the ARTS III system to process large angel populations is shown in figure 9(a). The program was unable to display the reports contained in the 270° to 360° sector.

Table 5 lists the single- and multiple-CPI returns corresponding to figures 8(a) and 8(b). Table 6 presents the same data corresponding to figures 9(a) and 9(b). The data contained in these and successive tables were obtained by modifying the ARTS III operational program to provide the desired outputs. Individual filter outputs for the thresholded case are not presented, since the number of reports obtained per filter was too small to give accurate data.

To further analyze the second-level thresholding capability, the level of each of the 1,536 sector/Doppler thresholds was obtained for typical operating conditions. Data for the light angel clutter condition are presented in table 7. Corresponding data for the heavy angel situation are contained in table 8. By comparing the data in tables 7 and 8, the system desensitization necessary to eliminate angels for these typical cases can be determined.

TABLE 5. NUMBER OF MTD REPORTS DURING LIGHT ANGEL ACTIVITY

Before Second-Level Thresholding

Filter Number	Single CPI	Multiple CPI's
0	10	7
1	18	12
2	13	8
3	8	9
4	8	5
5	5	7
6	11	11
7	20	21
Total	93	80

After Second-Level Thresholding

Total	16	13

TABLE 6. NUMBER OF MTD REPORTS DURING HEAVY ANGEL ACTIVITY

Before Second-Level Thresholding

Filter Number	Single CPI	Multiple CPI's
0	145	39
1	110	48
2	128	88
3	90	59
4	80	42
5	95	73
6	142	94
7	115	46
Total	905	489

After Second-Level Thresholding

Total	16	13

TABLE 7. PERCENTAGE OF 128 THRESHOLDS IN EACH 4-NMI RANGE INTERVAL WITHIN A GIVEN STRENGTH RANGE DURING LIGHT ANGEL ACTIVITY

Strength (dB)	Range (nmi) 0-4	4-8	8-12	12-16	16-20	20-24	24-28	28-32	32-36	36-40	40-44	44-48
0	81.3	79.7	71	73	88.4	94	94	93	95.3	93	93.8	96.9
0-3	10.9	7.8	7	8	7	4.7	4	4	3.1	4.7	6.2	3.1
3-6	6.3	8.2	12.5	8	2.3	.8	1.6	2.2	0.8	2.3		
6-9	0.0	4.0	4.7	8.4	2.3	.5	.4	.8	0.8			
9-12	1.5	0.3	0.8	1.4								
12-15			4	0								
15-18				1.2								

TABLE 8. PERCENTAGE OF 128 THRESHOLDS IN EACH 4-NMI RANGE INTERVAL WITHIN A GIVEN STRENGTH RANGE DURING HEAVY ANGEL ACTIVITY

Strength (dB)	Range (nmi) 0-4	4-8	8-12	12-16
0	4.5	18	33.6	57.8
0-3	1.6	7.9	10.9	16.4
3-6	5.3	12.5	18.8	10.9
6-9	7	9.4	14.8	9.4
9-12	22	17.2	10.9	4.7
12-15	16.4	15.6	5.5	.8
15-18	14	6.3	4.7	
18-21	12.5	7	.8	
21-24	7	5.5		
24-27	7.8	.8		
27-30	1.9			

Figure 10 shows the relationship between the second-level thresholds discussed above and system signal-to-noise ratio.

The effects of combined STC and second-level thresholding to eliminate angels are shown in figures 11 through 14. Four levels of STC were tested as indicated. Note that the four individual STC curves had maximum range extents as given in table 9.

The sector/Doppler threshold levels resulting from using the four values of STC as a function of range are given in table 9. Threshold levels were influenced by the STC attenuation only to the maximum extent (range) of each STC value as indicated. Table 9 shows that an overall increase in system sensitivity within the STC range was obtained by using less STC and allowing the second-level thresholds to adapt to the environment. For example, lowering the STC from 54 dB to 48 dB allowed 6 dB more sensitivity, while the average second-level threshold attenuation values for the 54-dB and 48-dB cases from 0 to 4 nmi were (from table 9) 3.42 dB and 8.08 dB, respectively. Thus, within the above range interval, the average increase in system sensitivity was 1.34 dB. From 4 nmi to 8 nmi, the average second-level threshold attenuation values for STC values of 54 dB and 48 dB were 1.22 dB and 4.14 dB, respectively. This provided an overall increase in sensitivity of 3.08 dB for the range interval. Similar calculations can be made for the other STC values using the data in table 9.

The distribution of angel returns as a function of STC attenuation before second-level thresholding is presented in table 10. Data for both single- and multiple-CPI reports by Doppler filter number are included. Table 11 contains corresponding data after second-level thresholding. Due to the small number of reports, in this case only the combined filter total is given.

The benefits derived from the above second-level threshold processing can be summarized as follows. Angels are distributed nonuniformly in range, azimuth, and Doppler. The adaptive sector/Doppler thresholds are able to eliminate angels selectively without desensitizing in a blanket fashion like STC does.

Second-level thresholding complemented STC rather than replacing it. STC remained useful in preventing ground clutter from exceeding the system dynamic range and in preventing too large a data load from angels etc. from overloading the system. A discussion dealing with the effect of STC on system aircraft detection capability is presented later in this report.

Data were taken for two cases of second-level thresholding in weather. Figure 15 shows the plan position indicator (PPI) presentation for both cases. Corresponding to figure 15, table 12 shows the effect of weather on the level of the second-level thresholds throughout the radar coverage area. Table 13 gives the distribution of the data among the individual Doppler filters. Linear polarization was used throughout the MTD testing.

Data for the first case were recorded during the passage of a weather front in April of 1975. The front passed through the radar coverage area at approximately 60 knots velocity. As can be determined from table 13, this resulted in

TABLE 9. PERCENTAGE OF 128 THRESHOLDS IN EACH 4-NMI RANGE INTERVAL WITHIN A GIVEN STRENGTH RANGE DURING ANGEL ACTIVITY FOR FOUR VALUES OF STC

Strength (dB)	Range (nmi) 0-4	4-8	8-12	12-16	STC
0	56	75	86	88	
0-3	4	8	13	8	54 dB
3-6	11	7		3	
6-9	13	9	1	1	(Maximum Extent
9-12	12	1			12.25 nmi)
12-15	2				
15-18	1				
18-21	1				
0	29	42	77	82	
0-3	9	19	6	9	
3-6	11	7	5	3	
6-9	9	13	8	3	
9-12	12	8	3	2	
12-15	6	3	1	1	
15-18	13	8			48 dB
18-21	3				
21-24	3				(Maximum Extent
24-27	4				8.56 nmi)
27-30	1				
0	23	31	70	81	
0-3	5	13	16	8	
3-6	7	14	6	6	
6-9	11	8	2	2	42 dB
9-12	9	8	3	2	
12-15	8	9	3	1	(Maximum Extent
15-18	12	8			6.0 nmi)
18-21	10	5			
21-24	6	3			
24-27	7	1			
27-30	2				
0	18	24	64	79	
0-3	8	14	19	7	
3-6	5	14	9	6	
6-9	9	9	4	7	36 dB
9-12	11	11	1	1	
12-15	8	8	1		(Maximum Extent
15-18	11	10	2		4.31 nmi)
18-21	13	4			
21-24	10	4			
24-27	5	2			
27-30	2				

TABLE 10. NUMBER OF MTD REPORTS BEFORE SECOND-LEVEL THRESHOLDING IN THE FIRST 16 NMI FOR FOUR VALUES OF STC-- INDIVIDUAL DOPPLER FILTERS

	STC							
	54 dB		48 dB		42 dB		36 dB	
Filter Number	Single CPI	Multiple CPI's	Single CPI	Multiple CPI's	Single CPI	Multiple CPI's	Single CPI	Multiple CPI's
0	4	2	28	12	37	20	17	20
1	17	18	28	24	24	31	31	46
2	27	8	35	31	49	47	49	35
3	16	11	24	12	30	13	36	25
4	14	3	15	10	23	9	28	9
5	12	7	20	4	19	8	20	5
6	16	9	25	14	45	19	42	20
7	5	9	23	18	20	28	28	30
Total	111	67	198	125	247	175	251	190

TABLE 11. TOTAL NUMBER OF MTD REPORTS AFTER SECOND-LEVEL THRESHOLDING IN THE FIRST 16 NMI FOR FOUR VALUES OF STC

STC								
54 dB		48 dB		42 dB		36 dB		
Single CPI	Multiple CPI's	Single CPI	Multiple CPI's	Single CPI	Multiple CPI's	Single CPI	Multiple CPI's	
12	11	14	7	18	11	25	15	

TABLE 12. PERCENTAGE OF 128 THRESHOLDS IN EACH 4-NMI RANGE INTERVAL WITHIN A GIVEN STRENGTH RANGE DURING WEATHER ACTIVITY

Strength (dB)	Range (nmi) 0-4	4-8	8-12	12-16	16-20	20-24	24-28	28-32	32-36	36-40	40-40	44-48	
0	74.0	40	19.5	16.4	22.7	31.3	52.3	60.2	60.9	71.9	82	87.5	C
0-3	7.0	11	7.0	0.8	2.3	8.6	2.3	7.8	6.3	11.0	4.0	6.3	A
3-6	4.0	7.0	8.6	2.3	10.2	5.5	6.3	4.0	7.8	6.3	6.3	3.1	S
6-9	2.3	7.8	11.7	7.0	10.2	9.4	7.0	7.8	9.4	3.1	3.1		E
9-12	2.3	10.2	16.4	22.7	11.0	9.4	11.7	2.3	4.7	4.0	1.6		
12-15	3.1	6.3	10.2	14.1	13.3	5.5	5.5	7.8	4.0		0.8		1
15-18	2.3	7.8	7.8	10.9	7.0	11.7	2.3	3.1	2.3	0.8	0.8	0.8	
18-21	3.1	7.0	8.6	10.2	10.2	8.6	3.1	2.3	2.3	1.6			
21-24	1.0	2.3	5.5	5.5	4.7	5.5	5.5	2.3	0.8	1.3		2.3	
24-27	0.9	0.6	1.6	4.7	4.0	4.2	2.3	1.6	1.5		1.4		
27-30			3.1	4.4	4.4	0.5	1.7	0.8					
0	66.4	35.2	48.4	55.5	61.7	58.6	71.0	68.8	74.0	73.4	77.3	83.6	C
0-3	7.0	12.5	7.0	8.6	7.8	8.6	7.0	14.1	8.6	9.4	7.0	4.7	A
3-6	7.0	13.3	10.2	9.4	4.7	4.0	2.3	4.0	4.7	2.3	5.5	4.7	S
6-9	4.7	6.3	11.0	12.5	7.8	6.3	9.4	5.5	2.3	5.5	4.0	4.0	E
9-12	4.0	9.4	7.8	1.6	5.5	6.3	4.7	4.0	5.5	6.3	2.3	0.8	
12-15	4.7	5.5	6.3	4.0	4.0	4.7	2.3	1.6	2.3	1.6	1.6		2
15-18	3.0	7.0	2.3	3.0	4.0	6.3	2.3	1.6	1.0	0.8	0.8	1.6	
18-21	1.6	7.8	4.0	4.0	3.0	4.7		0.4	1.6			0.6	
21-24	1.0	3.0	3.0	1.4	1.5	0.5	1.0			0.7	0.5		
24-27	0.8												
27-30													

TABLE 13. AVERAGE NUMBER OF SINGLE- AND MULTIPLE-CPI RETURNS FROM EACH MTD DOPPLER FILTER FOR ONE ANTENNA SCAN DURING WEATHER ACTIVITY

Case 1

Filter Number	Single CPI	Multiple CPI's
0	97.0	17.4
1	10.6	2.8
2	27.4	1.8
3	26.2	3.0
4	32.4	5.8
5	27.4	5.8
6	33.4	6.4
7	20.6	4.2
Total	275	47.2

Case 2

Filter Number	Single CPI	Multiple CPI's
0	32.2	3.6
1	13.2	5.6
2	44.0	5.8
3	56.2	4.6
4	52.0	9.4
5	50.8	6.6
6	38.8	6.4
7	12.6	3.4
Total	299.8	45.4

a large number of false alarms from the zero Doppler filter. The large group of false tracks shown in figure 15(a) centered at approximately 20 nmi and 120° correspond to the front leading edge. Due to the high velocity of the front, the clutter map was unable to adapt in time, resulting in the false alarms shown. The corresponding case 1 data in table 12 show a high average threshold level (compared to data in table 7), while table 13 shows that the data were fairly evenly distributed among the seven nonzero Doppler filters. The results of this thresholding can be seen in figures 15(a) and 15(b) which show a loss of aircraft tracks with thresholding. A study of the tracks lost when the thresholds were applied showed that they were primarily from single-CPI (weak) targets.

The second weather case is shown in figures 15(c) and 15(d). The weather in this case was accompanied by high winds and extended over the entire display area. The MTD hardware thresholding eliminated the weather except for the two small areas of false tracks shown. The second-level thresholding further reduced the number of false tracks as shown. In this case, table 13 shows that data were concentrated more toward the central Doppler filters.

Taken together, the data show that each weather system had unique characteristics. The combined MTD and second-level thresholding were successful in eliminating false alarms and tracks. System desensitization was experienced in areas in which weather was present.

Due to the inability of the clutter map to adapt to fast moving weather which resulted in excessive false alarms from the zero velocity filter, no track initiation was allowed on zero velocity filter single-CPI reports.

The effect of second-level thresholding on target detection in the clear is shown in figure 16. Note that there was only a small amount of additional target loss. Thus, the level of the thresholds in a clutter environment and the resulting loss of aircraft detection shown previously were caused by the clutter. That is, the thresholds did not rise appreciably as the result of aircraft signals. This compares favorably with the data given in table 7.

SYSTEM STC. Figure 17 shows the STC curves used with the ASR-7 and the FPS 18/MTD systems. Range to the minus fourth power curves (R^{-4}) were used to best match ground-clutter-received signal characteristics. For the NAFEC tests, the FPS-18/MTD curve shown provided a compromise between elimination of angel clutter and detection of small aircraft near the antenna cone of silence. The ASR-7 curve was tailored to match the FPS-18/MTD curve as closely as possible for normalization of system detection capabilities.

The ASR-7 STC PIN diode had a maximum attenuation of 40 dB as shown in figure 17. A typical FAA CSS (cross sectional sensitivity)-1 curve is also shown for reference.

Figure 18 shows the manner in which the MTD STC was implemented. The desired range zero STC attenuation was preset with switches in the MTD timing section. From this maximum attenuation value shown on figure 18, the attenuation was decreased as an R^{-4} function in 1.5-dB steps reaching zero decibels at the range shown.

Investigation determined that the MTD receiver/processor was linear throughout its dynamic range. The STC values shown in figure 17 were used throughout the comparative system testing.

Flight testing was performed to determine the effect of STC attenuation on aircraft detection. For this test, the flight test aircraft was flown on a radial course at 4,000 and 8,000 feet. These tests were conducted near the cone of silence as this antenna radiation region is most affected by STC. The resulting target strength as a function of STC and range is shown in figure 19. The data shown are smooth curve fits to the data collected. The 54-dB tests were made using a Piper Commanche aircraft. All other runs were made using a Piper Arrow. For comparison purposes, the test target strength level required for a 50-percent P_d (from the P_d tests discussed subsequently) is included in figure 19. From this, it can be seen in figure 19 that at an 8,000-feet altitude, an STC value of 60 dB exceeds the maximum value that could be expected to provide a 50-percent P_d. By extrapolating the data shown, it can be determined that at higher altitudes, the desired P_d could be maintained only by lowering the STC attenuation.

Some difficulty was experienced in getting the flight test aircraft to fly exactly over the radar site, both on the inbound and outbound radials. Since the data shown were extracted in a wedge centered on the desired radial (to avoid overloading the ARTS III computer), any significant deviation from an exactly radial course resulted in loss of close-in data. Therefore, the minimum ranges shown are not reliable indicators of sensitivity. Rather, the relative levels of the target strength are intended to show performance.

PROBABILITY OF DETECTION (P_d). The P_d for the ASR-7/RVD-4 and FPS-18/MTD systems in thermal noise was determined using the TEAST test target generator (TTG). Each system was operated with a 10^{-5} P_{fa}. One hundred and twenty eight RF antenna scan-modulated test targets (32 in each of 4 concentric rings) were moved in range (TTG velocity) and azimuth (1 ACP) each antenna revolution. These targets were varied in amplitude using a precision HP-S382C RF attenuator from below noise level to the point where 100-percent P_d was obtained in 1-dB steps. Fifteen scans of data were taken for each step. Pulse widths for both systems were set to 1.0 microsecond (μs). The TTG runlength set to 1.0 microsecond (μs). The TTG runlength (antenna beam shaped) was set to equal the two-way 3-dB antenna (ASR-5) runlength at the pulse repetition rate of the radar system used. Both systems were operated on dummy load. The TTG variable velocity control was set to provide near-optimum speed targets.

The following calibration method was used to determine the signal-equal-to-noise point for both systems. First, the receiver IF noise level was measured using an rms voltmeter. Then, a TTG RF continuous wave (CW) signal was introduced which provided a signal-plus-noise power level 3 dB above that of the noise alone. This TTG signal output level corresponded to a signal-to-noise ratio of approximately unity.

The number of IOP radar target reports (prior to tracking) for each system was used to determine its P_d. The resulting data are presented in figure 20. For the ASR-7/RVD-4, data for the normal receiver are presented. For the MTD

system, the curve for detection in two CPI's is included to show the added signal strength required for multiple CPI detection. Since the test targets were moving in a spiral fashion, possible range and azimuth gate-splitting losses are included in the data shown in figure 20. Separate tests were made to isolate these factors so that the data shown could be compared to theoretically predicted values. For the MTD-equipped system, a test target was moved in range only and then azimuth only, and the resulting variation in P_d was measured. It was thus determined that an average P_d loss of 1 dB was experienced due to range gate-splitting losses, and an average 1.5-dB loss was experienced due to azimuth splitting. These azimuth-splitting losses were ascribed to the following factor. The MTD processing algorithms did not utilize all the possible data. That is, only 3,840 pulse repetition periods (PRP's) (480 CPI's x 8 DFT pulses per CPI) out of a possible 5,828 (1,240 average PRF x 4.70 seconds per antenna scan) were directly processed. The nonused PRP information between CPI pairs required for antenna/processor synchronization (to compensate for antenna wind loading) and the two pulses each CPI required to "charge" the three-pulse canceller resulted in the above reduction in data processed.

Separate tests of the ASR-7/RVD-4 system (reference 2) determined that it experienced a 2.0-dB loss due to range gate-splitting losses.

The IF passbands of both systems were considerably wider than an optimum filter. From the literature, an optimum filter bandwidth for a 1- s pulse would be approximately 1.2 megahertz (MHz). The FPS-18/MTD and ASR-7 bandwidths were measured to be 3.65 and 2.75 MHz, respectively. Each IF was followed by a narrow video bandwidth which increased the signal energy to noise power ratio to approximate a matched filter. A collapsing loss (reference 3) may have resulted from the instrumentation of this type of filtering, since the 50-percent P_d points for both systems were approximately 1.0 dB higher than expected from theoretical P_d data (reference 4) when the above range and azimuth losses were considered.

VELOCITY RESPONSE. The velocity response of the MTD filters individually and combined are shown in figures 21 through 25. These responses were determined by measuring the TTG signal strength (variable velocity ring-around target) necessary to obtain a 50-percent probability of detection. The probability of detection was measured at the maintenance DEDS indicator using numerics generated by the NOVA minicomputer.

Figure 21 shows the velocity response of the nonzero filters. Since filters 1, 2, and 3 are mirror images of filters 7, 6, and 5, they are not included, but can be deduced from the data shown. The effect of the three-pulse canceller on the shape of the individual filters and their sidelobes can be seen. Also note that the low-velocity filter sidelobes were highest in amplitude. This was caused by the effect of the three-pulse canceller preceding the DFT. These sidelobes which extended throughout the Doppler range limited the amount of subweather visibility obtainable. For instance, an aircraft signal with a radial velocity of 110 knots would have its maximum response in the number 7 filter. It would, however, have to compete against any weather entering the filter via its low-velocity sidelobes shown. The number 7 filter sidelobe at

40 knots is seen to have only 14-dB less sensitivity than the main lobe. This collapsing loss is seen to be less for the center filters.

The qualitative subweather visibility as a function of velocity response of the MTD system is shown in figure 22. The weather system shown (normal video) was moving toward the upper right (Northeast) of the photographs. The numerics shown were generated by the NOVA minicomputer and represent MTD filter outputs 0 through 7. The ring-around TTG signal was given a low positive (incoming--filters 2 and 3) Doppler in figure 22(a) and a low negative (outgoing--filters 5 and 6) Doppler in figure 22(b). Figure 22(a) shows loss of subweather velocity with incoming weather, and figure 22(b) a similar loss with outgoing weather. This corresponds to the approximate 12 dB of subweather visibility obtainable in these filters. However, from these figures, it can be deduced that a small propeller-driven aircraft which characteristically has a wide signal spectrum would have a high probability of detection, regardless of its location and heading. This indeed was the case as is discussed later under weather flight testing.

In figure 22(a), the several targets of opportunity (groups of numerics) also show this effect. Figure 23 further shows the effect of the radial velocity component of a weather system on system operation. The photographs shown were taken using the NOVA minicomputer system to perform a 64-point DFT analysis of the weather signals. The center point of the horizontal axis represents zero velocity. Data points to the right of center represent positive Dopplers with the rightmost data point being equivalent to an optimum speed target. Likewise, data to the left represent negative Doppler signals with the leftmost point also corresponding to an optimum speed target. The three photographs were taken with the antenna stopped at azimuths of 90°, 150° and 330°. Two pertinent points can be observed from the photographs. The weather return occupied only a portion of the velocity spectrum which is a function of azimuth and weather spectral spread and large portions of the velocity spectra have no weather signal present. Target detection in these no-weather areas was equivalent to that in thermal noise except for the Doppler filter sidelobes weather problem discussed previously.

The combined velocity response (multiple PRF) of the seven nonzero Doppler filters is shown in figure 24. The data extend to the first multiple PRF blind speed. Figure 25 shows the velocity response of the zero velocity filter. Since the clutter map built up for low-velocity signals resulting in raising the corresponding ZVF threshold and since the information shown repeated at intervals corresponding to 360° shifts between pulses in the test signal, the data shown were measured between velocities corresponding to the first and second multiples of the system nonstaggered pulse repetition rate and translated to zero velocity as shown.

The MTI velocity response of the ASR-7/RVD-4 system was dictated by the ASR-7 three-pulse canceller. This information can be derived from the ASR-7 technical manuals.

SUBCLUTTER VISIBILITY (SCV). The comparative subclutter visibilities of the two systems are shown in figure 26. SCV was determined by exactly superimposing a modulated (antenna beam shaped) TTG test target of the correct system runlength over isolated fixed-clutter echoes of known amplitude. Then, the test signal was adjusted in amplitude until the desired probability of detection was obtained. The resulting difference in amplitude between the clutter echoes and the test signal was defined as the system SCV. The MTD SCV was measured at the maintenance DEDS indicator using the NOVA minicomputer. The RVD-4 SCV was measured using the ARTS III equipment. For this test, a clutter echo with a strength of 42 dB with respect to receiver noise was used.

When the clutter-received echo strength exceeded the dynamic range at the A/D converters (approximately 42 dB), splattering resulted. When this occurred, the MTD outputted spurious Doppler information (nonzero velocity) resulting in false targets. To overcome this problem, the COHO input to the I and Q phase detectors was attenuated. The resulting conversion loss was utilized to maintain clutter echoes within the dynamic range capabilities of the MTD system. This mode of operation resulted in loss of SCV in conjunction with some clutter echoes. This phenomenon is discussed later in this report under ASR-5 and ASR-7 testing. As shown, several test target velocities were used to better define the relative SCV capabilities. The MTD zero-velocity filter provided interclutter and superclutter visibility but not subclutter visibility. This resulted in the loss of SCV at low velocities.

TARGET DETECTION ACCURACY. To determine the relative capabilities of the ASR-7/RVD-4 and FPS-18/MTD systems to provide accurate target location data in both range and azimuth, the following tests and analyses were performed.

Target report data (ARTS III before tracking) were collected for both systems using the same targets of opportunity and identical scan numbers. Thirty scans of data were analyzed for each 30 aircraft tracks. Nearly straight tracks were chosen. The data were recorded on magnetic tape for analysis. A variety of track locations and headings were used.

A least squares fit of the data to a fifth-order polynomial was chosen as the criterion for accuracy. That is, the deviation of the data from the polynomial curve determinated its smoothness and hence accuracy.

The equation of the polynomial used was:

$$Y = \alpha + B_1 X + B_2 X^2 + \text{----------} + B_k X^k$$

Where:

α, B = the coefficients of the polynomial
X = the scan number
Y = range or azimuth

The deviation was calculated as follows:

$$S = \sqrt{\frac{\sum_{K=1}^{N} (Y_k - \bar{Y})^2}{N - 1}}$$

Where:

S = standard deviation
N = number of data points
K = degree of polynomial
Y_k = observed data
$\bar{Y}$ = mean value of observed data

The deviations determined by computer analysis using the above equations are plotted in figures 27 and 28.

Subsequent to the comparison accuracy tests described above, an additional effort was undertaken to determine if additional MTD range accuracy could be obtained by employing a range-centroiding technique similar to that used for azimuth centroiding. The centroiding was performed according to the equation:

$$R(\text{centroid}) = \sum_{j=1}^{N} \frac{R_j S_j}{S_j}$$

where R and S are the ranges and strengths of the signals in each CPI making up the target report.

Seventeen aircraft tracks were analyzed using the techniques described above. The results of this test are shown in figure 27.

SYSTEM FLIGHT TESTS.

Results from five areas of comparative performance flight testing are presented below. These areas are system sensitivity, tangential target detection in clutter, subclutter visibility, subweather visibility, and target resolution. Blip/scan information for both systems was collected at two points in the ARTS III ADTL Program. The data collected at the first point were radar reports from the output of the previously mentioned RIP portion of the program. The second data collection point was at the output of the ADTL program (tracking output).

Both radars were operated with similar R^{-4} STC curves extending out to 12.25 nmi. The transmitter/receiver loop gains of the two systems were normalized based on their respective receiver noise figures and average transmitter powers.

Two factors should be considered in the normalization of the FPS-18/MTD and the ASR-7/RVD-4. Firstly, the MTD system, due to its longer runlength (21.53 hits/3-dB one-way antenna beamwidth versus 17.29 hits for the ASR-7/RVD-4) would have an advantage in detection capability. Secondly, the ASR-7/RVD-4 system would have, at the same time, an offsetting advantage due to its higher energy in each pulse processed. This is, with its lower pulse repetition frequency, each transmitted pulse of the ASR-7 had to contain proportionately more energy to provide the necessary average power for equalizing the transmit/receive loop gains of the two systems. Equalizing the loop gains likewise compensated for the difference in transmitter pulse widths between the two systems. The FPS-18 and ASR-7 radars operate with 1.0-μs and 0.833-μs transmitted pulse widths, respectively.

The average power and noise figure measurements were made at the diplexer antenna port to eliminate differences in waveguide losses.

SENSITIVITY. Sensitivity flight testing was conducted to determine the comparative performance of the two radar/processor systems in detection of a low-flying small aircraft. This was done at the outer limit of radar coverage in a clutter-free environment. To accomplish this, a Piper Arrow test aircraft was orbited between 20 and 22 nmi in range, first at an altitude of 1,000 feet, and then at 1,500 feet. The ASR-7/RVD-4 system used log normal video during this test. Data from 365 antenna scans were analyzed yielding the following blip scan ratios:

ASR-7/RVD-4	Radar Reports	75 percent
FPS-18/MTD	Radar Reports	73 percent

These data show that approximately the same blip/scan ratios were obtained from the two sensors. Their approximately equal performance in this test was expected both from the probability of detection tests discussed previously and from theoretical considerations of detection probability as a function of target runlength and probability of false alarm. Particularly important, it follows that the normalization of the two systems to achieve equal transmitter/receiver loop gain was effective.

Therefore in the subsequent flight tests described below, any disparity between these systems was attributed to the relative performance of the systems in a clutter environment. Figures 29 and 30 illustrate the tracker output of the two systems during the sensitivity tests. It is important to note that these photographs and subsequent photographs represent radar-only tracking. These pictures and subsequent photos were obtained from data extraction tapes. These comparative photographs were made from the same flight test segments and display every scan of information for 50 scans. The symbol "Δ" on the photographs represents a radar track output. Other aircraft tracks shown are from targets of opportunity.

TANGENTIAL TARGET DETECTION OVER CLUTTER. Tangential target detection capability over clutter was determined by making tangential test flights over the Atlantic City area. The flight test aircraft (Piper Arrow) was flown at an altitude of 1,000 feet. The clutter is shown centered at 7.5 nmi and 145°

in figure 31. Maximum clutter peaks in this area are approximately 45 dB above noise level. For the purpose of this test, a tangential target was defined as one with a radial velocity of less than 30 knots. Thirty knots represents approximately the knee of SCV curve in figure 26 for the MTD system. A total of 10 runs over the clutter were analyzed, resulting in the following blip/scan ratios.

ASR-7/RVD-4	Radar Reports	50 percent
FPS-18/MTD	Radar Reports	96 percent
ASR-7/RVD-4	Tracking Outputs	33 percent
FPS-18/MTD	Tracking Outputs	96 percent

Tracking specifications for both systems for uncontrolled tracks are the same; i.e., three scans for automatic track initiation and one more for display with automatic track drop after loss of detection for three consecutive scans. Figures 32 and 33 illustrate 50 scans of tracker outputs during one the tangential detection runs. Radial velocities exceeding 30 knots are also shown in figures. The test aircraft was broadside to the radar during these runs with an average quantized MTD signal strength of 37 dB above noise level. Therefore, this test was not used for SCV determination.

SUBCLUTTER VISIBILITY. Subclutter visibility was determined by having a flight test aircraft (Piper Arrow) perform a holding pattern at the Northeast end of Atlantic City (figure 34). In order to show any SCV improvement of the FPS-18/MTD system relative to the ASR-7/RVD-4 system in ground clutter, it can be determined from figure 26 that a minimum of 20 to 25 dB of ground clutter is required. Figure 34 shows the level of ground clutter in the NAFEC/Atlantic City area after 25 dB attenuation was added to the receiver front end. Figure 34 depicts radar reports (a "+" symbol is used) from the test aircraft for 40 scans. The flight test aircraft made 16 separate runs over a piece of ground clutter approximately 1/3 nmi by 3/4 nmi, resulting in the following blip/scan ratios:

ASR-7/RVD-4	Radar Reports	38 percent
FPS-18/MTD	Radar Reports	95 percent

The maximum SCV capabilities of the respective systems can be ascertained from figure 26.

SUBWEATHER VISIBILITY. Subweather visibility of the two systems was compared by vectoring a flight test aircraft (Piper Arrow) through areas of precipitation and comparing the resulting blip/scan ratios. The weather used in this test consisted of scattered high-amplitude cells (up to 40 dB above receiver noise level).

The aircraft was slow moving and therefore did not provide optimum testing of the MTD's Doppler filtering capability. Figure 35 shows the PPI display of the weather. The flight test aircraft was vectored eastbound and then westbound through the weather. Three hundred and ten scans of information were analyzed with the following blip/scan ratios resulting:

ASR-7/RVD-4	Radar Reports	41 percent
FPS-18/MTD	Radar Reports	96 percent
ASR-7/RVD-4	Tracking Outputs	35 percent
FPS-18/MTD	Tracking Outputs	96 percent

Figures 36 and 37 illustrate part of the flight test. Note the false tracks from the RVD-4 system in the weather.

Blip/scan ratios for hundreds of scans of data necessarily contained data when the aircraft was in light weather or entirely out of the weather. This occurs at the weather system fringe and at areas of light weather within the system. Blip/scan ratios from any actual weather system might therefore be expected to be higher than would be obtained from a theoretical uniform intensity, large-area system. To show this effect, a small portion (51 scans) of data representing one run through a high-amplitude weather cell was analyzed. The plot of this run is shown in figure 38. Blip/scan ratios for the data shown are:

FPS-18/MTD	Radar Reports	94 percent
ASR-7/RVD-4	Radar Reports	22 percent

The average MTD target signal (ARTS III target report) strength for the 51 scans shown was 22 dB above noise level.

The above data show that, as the test was made more stringent, no additional loss in MTD P_d was experienced. The ASR-7/RVD-4, however, experienced a significant additional loss. Note, that this loss was complete at the center (high-level) portion of the weather cell.

AIRCRAFT RESOLUTION. The ability of the two systems to resolve signals was a function of the radar parameters, processor capabilities, and software management of the data in the ARTS III equipment.

The transmitted pulse widths of 1.0 μs and 0.833 μs (for the FPS-18 and ASR-7 radars) limit the minimum range separation capabilities to 0.081 nmi and 0.067 nmi, respectively. The ASR-5 antenna used by both systems had a one-way 3-dB beamwidth of 1.33°.

Each CPI used in the MTD processor subtended 0.618° in azimuth. This contributed to increasing coarseness of azimuth data. The 1/16-nmi range increments used in both processors corresponded to 0.0625-nmi minimum resolution.

The processing algorithms used in the MTD ARTS III RIP consolidated data in adjacent range bins into a single target report, making the minimum possible range resolution 0.125 nmi. Likewise data in adjacent CPI's were consolidated into a target report.

The resolution capabilities of the two systems were tested by flying two flight test aircraft (a Piper Arrow and an Aero Commander) in a series of crossing maneuvers while proceeding radially, tangentially, and obliquely with respect to the radar site.

The resulting data were analyzed in two ways. First, data from 15 aircraft crossings were analyzed from computer printouts to determine the minimum range resolution when the azimuth separation was zero, and conversely, the minimum azimuth resolution when the range separation was zero. The minimum range and azimuth separations obtained for the MTD were 0.125 nmi and 2.2°, respectively.

This agrees closely with predictions based on analysis of the parameters given above; the ASR-7/RVD-4 system provided minimum range and azimuth separations of 0.125 nmi and 2.5°, respectively.

The second analysis was performed by making computer plots (in X-Y coordinates) of the flight tests and measuring the minimum resolution obtained before and after each aircraft crossing. For the MTD, the average minimum resolution for 77 cases was 0.25 nmi. For the ASR-7/RVD-4 system the average minimum resolution for 30 cases was 0.44 nmi. Fewer cases were obtained for the ASR-7/RVD-4 system, since its poorer resolution capability prevented its distinguishing all aircraft separations and mergings.

Figure 39 shows the resulting data on the capabilities of the two systems to provide resolution as a function of combined range and azimuth separation (X-Y coordinates).

The qualitative resolution capabilities of the two systems are shown in figure 40. The photographs show simultaneous outputs of both systems. The data shown are radar reports from the ARTS III system before tracking.

Additional loss of resolution was experienced in the ARTS III tracker due to the size of the primary tracker window. Figure 40 (sheets 7 and 8) show the tracker (radar only) output corresponding to the radar reports shown in figure 40 (sheets 5 and 6). This indicates that further improvements in the tracker algorithms and possibly more use of available MTD information (e.g., Doppler/strength) are required to make full use of the radar data inputted to the tracker.

ASR-5 AND ASR-7 MTD COMPATIBILITY TESTS.

STABILITY TESTS. The MTD processor was also operated with the ASR-5 and ASR-7 radars located in the TFAST. These tests were made to determine if the radars provided operation stable enough for an MTD system. In these tests, the ASR-5 was operated with magnetron tuning from a solid state fixed-frequency STALO being tested for field use. Likewise, the ASR-7 had a tuned magnetron utilizing its own STALO operating at a fixed frequency. The timing of both radars were slaved to the MTD. Otherwise, both systems were unmodified. No attempt was made to optimize the two radars operation for this test. Preamplifier outputs from the radars were used as inputs to the MTD and to the frequency stability test circuitry described below.

Comparative stability photographs of the FPS-18, ASR-5, and ASR-7 radars are shown in figure 41. These photographs were taken using the Single Gate Processor (SGP) Fast Fourier Transform (FFT) analysis routine furnished with the MTD software for the NOVA maintenance/test minicomputer. The resulting information

was then presented on an Imlac graphics display for analysis and photographing. To make these photographs, a fixed target was spotlighted with the antenna beam, and an SGP analysis was performed on its received signal. The center of the horizontal scale in each photograph represents zero frequency. Negative Dopplers are to the left of zero, and positive Dopplers are to the right. The 64 segments of the horizontal axis mark the 64 outputs of the FFT (64-point). These 64 points cover the unambiguous Doppler range of the three radars. Thus, zero Doppler is at the center, and optimum Doppler at both edges of the display. The frequencies of responses seen can be determined by interpolation. The figure of merit in this test is the difference in amplitude between the desired fixed-target zero-Doppler response and any spurious frequencies generated in the radar systems. For the engineering model MTD at NAFEC, these spurious frequency components must be at least 42 dB (the MTD processor dynamic range) below the zero-Doppler signal to avoid being outputted as targets. The low-amplitude responses in each photograph represent system noise. Each of the three radars provided operation stable enough for MTD processing. A description of the ASR-5 and ASR-7 modifications necessary for MTD operation are given in appendix D.

SUBCLUTTER VISIBILITY. The SCV capabilities of the ASR-5 and ASR-7 radars with the MTD were also tested. In preparation for these tests, the effect of limiting the received radar information prior to digitizing was investigated. Two types of limiting were involved. The first was implemented by attenuating the COHO signal to the phase detectors. The resulting conversion loss was utilized to maintain (limit) strong signals within the dynamic range of the MTD system. This was done to avoid limiting in the A/D's, which resulted in generation of spurious frequencies causing false Doppler information to be outputted by the MTD.

Figure 42 shows typical conversion losses caused by attenuation of the COHO signal. Note how strong signals are attenuated (limited) due to lack of sufficient COHO signal. Typical corresponding SCV losses for several clutter levels are shown in figure 43. The SCV was measured using the TTG as described previously under comparative SCV testing. These curves show that some optimization of the phase detector input signal levels can be performed. Thus, in the MTD system tested, COHO attenuation was used to keep clutter echoes within the system dynamic range with nominal sacrifice of SCV. Without COHO attenuation, false alarms were generated by large-amplitude clutter echoes. Note that SCV in excess of the systems dynamic range was obtained from large clutter signals. In conjunction with this phenomenon, the dynamic range of the IF amplifier was investigated. First, the linear dynamic range at the ASR-7 preamplifier output was measured to be at least 75 dB. Therefore, any nonlinearities were attributed to the IF amplifier.

The dynamic range of the IF amplifier was determined by viewing its output on an oscilloscope when large-amplitude signals were inputted to it. Signal saturation occurred at 45 dB above noise level. Strong signals were limited, therefore, in the IF amplifier.

This was the second type of limiting. Thus, the individual effects on SCV of COHO attenuation and IF limiting on large-amplitude clutter (greater than the system dynamic range) were not defined. The combination of COHO attenuation and IF limiting did not generate false Doppler information and did maintain signals within the system's dynamic range capabilities. For example, two cases of large-amplitude clutter were investigated. With the 50-dB clutter depicted in figure 43, an SCV of 45 dB was obtainable (with low COHO attenuation). In the second case, a 62-dB clutter echo yielded an SCV of 47 dB.

The SCV capabilities of the two radars for pertinent velocities are shown in figure 44. The curves shown compare closely with those in figure 26 of the FPS-18/MTD combination. Thus, the MTD provides approximately a 20-dB improvement in SCV compared with conventional MTI systems for each of the radars tested.

SUMMARY OF RESULTS

1. The MTD system was operated with a 10^{-5} false alarm rate. This corresponded to a 6-mV receiver noise level and a 42-dB receiver dynamic range. This false alarm rate produced approximately 30 thermal false alarms per scan.

2. The MTD interference eliminator removed RFI in a clutter-free environment. When clutter was present, the MTD interference elimination algorithm did not function acceptably. In this instance, an ARTS III RIP interference elimination algorithm was used to remove the remaining interference.

3. With an R^{-4} STC curve extending to 12 nmi, the number of MTD reports due to angels on occasion exceeded 1,300 per scan. Second-level thresholding in the ARTS III RIP was developed which prevented these angel reports from causing false tracks.

4. Without second-level thresholding, the ARTS III system was unable to process heavy angel clutter data outputted by the MTD.

5. Angel clutter extended throughout the MTD Doppler range, appearing as both single-and multiple-CPI reports.

6. Second-level thresholding in an angel environment resulted in a loss of sensitivity proportional to the amount of angel clutter present. Since the second-level thresholding adapted to the environment, it was more selective than STC and hence allowed greater overall sensitivity than STC.

8. Weather systems tested with the MTD on occasion extended throughout the unambiguous Doppler range during an antenna scan. The MTD thresholds eliminated almost all of the resulting clutter information. However, sharp leading and trailing edge discontinuities resulted in false targets being outputted by the MTD. This was particularly so for the zero-velocity filter, due to its unique implementation using the clutter map. Most of the false target information was from single CPI's and was fairly evenly distributed in Doppler. Second-level thresholding in the ARTS III was developed which eliminated virtually all remaining false tracks due to weather phenomena.

9. A loss of system sensitivity was experienced due to the MTD hardware and the second-level thresholding in weather. This loss was a function of weather amplitude velocity, and spectral spread.

10. Second-level thresholding resulted in no appreciable loss of system sensitivity when operating in a clutter-free environment.

11. Flight tests showed that at 8,000 feet at a range of between 3 nmi and 6 nmi, 54 dB was the maximum STC value which would allow a 50-percent P_d. This fact precluded use of large-attenuation STC curves to remove all angel clutter.

12. With a 1.0- s test signal moving in range and azimuth, the FPS-18/MTD and ASR-7/RVD-4 systems provided 50-percent P_d at 5.2 dB and 5.7 dB above receiver noise level, respectively.

13. The MTD DFT velocity filtering scheme accurately separated information into eight Doppler filters with target strength numbers for each filter. This Doppler and strength information enabled subsequent selective processing and thresholding of targets and clutter on the basis of strength and radial velocity.

14. The first multiple PRF blind speed occurred at 594 knots.

15. Weather signals typically occupied only a portion of the unambiguous Doppler range. The portion occupied was a function of the radial velocity of the weather as determined by its location and direction with respect to the radar and by the radar pulse repetition frequency.

16. The MTD provided a minimum of 12 dB of subweather visibility. This lower limit was imposed by sidelobes from the combined three-pulse canceller and DFT filtering. The wide spectra of propeller aircraft returns enabled small aircraft detection in several DFT filters (some with possible lower level weather signals) which mitigated the above limitation.

17. The MTD provided a 20-dB improvement in SCV over the ASR-7/RVD-4 system.

18. The MTD zero velocity filter provided superclutter visibility and interclutter visibility for low-velocity targets.

19. The MTD system, as delivered to NAFEC, provided better range and azimuth accuracy than the ASR-7/RVD-4 system.

20. Range centroiding (developed at NAFEC) in the ARTS III RIP provided a further improvement in accuracy.

21. The MTD and ASR-7/RVD-4 systems provided equal target detection capabilities in the clear during controlled aircraft flight tests.

22. The MTD system provided superclutter visibility for tangential targets during controlled aircraft flight tests. In tangential segments (within 30 knots radial velocity of the tangential point), the MTD and ASR-7/RVD-4 systems provided P_d's of 96 and 33 percent, respectively.

23. Controlled aircraft subclutter visibility flight tests of the MTD and ASR-7/RVD-4 systems produced P_d's of 95 and 38 percent, respectively.

24. Controlled aircraft subweather visibility flight tests produced the following P_d's:

ASR-7/RVD-4	Radar Reports	41 percent
MTD	Radar Reports	96 percent
ASR-7/RVD-4	Tracking Outputs	35 percent
MTD	Tracking Outputs	96 percent

25. The average minimum target resolution distances for two flight test aircraft for the ASR-7/RVD-4 and MTD systems were 0.44 and 0.25 nmi, respectively.

26. The ARTS III tracker was not capable of resolving all the target information provided by the MTD. The tracker window size was too large for fine resolution.

27. The FPS-18, ASR-7, and ASR-5 (with solid state STALO) radars provided sufficient stability (greater than 42 dB) for MTD operation.

28. MTD SCV when operated with ASR-5 and ASR-7 radars was equal to that obtainable when operated with the FPS-18 radar.

CONCLUSIONS

From the results, it was concluded that:

1. The MTD/processor system is superior to the ASR-7/RVD-4 system.

2. The MTD/processor provides data suitable (low false alarm rate and high probability of detection) for automated system processing.

3. The combination of MTD and ARTS III processing effectively eliminates clutter (weather, ground, and angel) and nonsynchronous interference experienced in the NAFEC environment.

4. Terminal radars in the FAA inventory are capable with minimal modification of providing outputs suitable for MTD processing.

RECOMMENDATIONS

It is recommended that:

1. The MTD/processor concept be used in all future FAA surveillance radar systems.

2. A cost benefit analysis be performed to determine desirability of retrofitting existing FAA surveillance radar systems for MTD operation.

3. Second-generation MTD's be procured for operational tests at selected field sites, both terminal and en route.

4. Further work be accomplished to refine ARTS III MTD processing algorithms to provide optimum false alarm management and use of Doppler information for improved tracking.

5. Further work be accomplished to determine the best radar system configuration for MTD operation. Radar equipments and concepts such as circular polarization, frequency diversity, and the passive horn should be investigated.

REFERENCES

1. Drury, William H., Improved MTI Radar Signal Processor, Report No. FAA-RD-74-185 (Lincoln Laboratory Report ATC-39, 1975).

2. Holtz, Martin H. and Waplehorst, Leo J., Test and Evaluation of the Radar Processing Subsystem of the All Digital Tracking Level System, Report No. FAA-RD-76-197.

3. Barton, D. K., Radar System Analysis, Prentice-Hall, 1964.

4. Skolnik, M. I., Radar Handbook, McGraw-Hill, 1970.

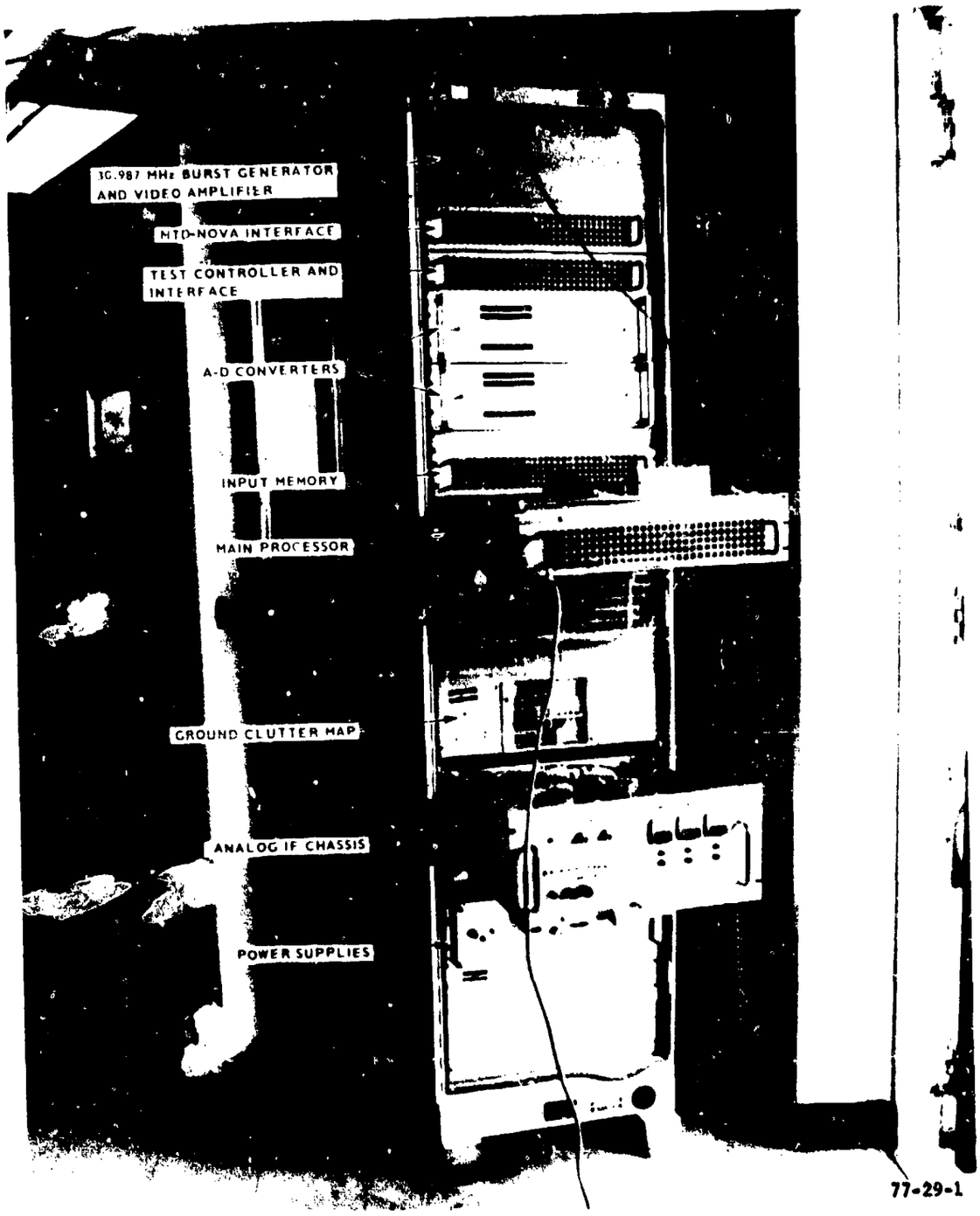

FIGURE 1. MTD EQUIPMENT

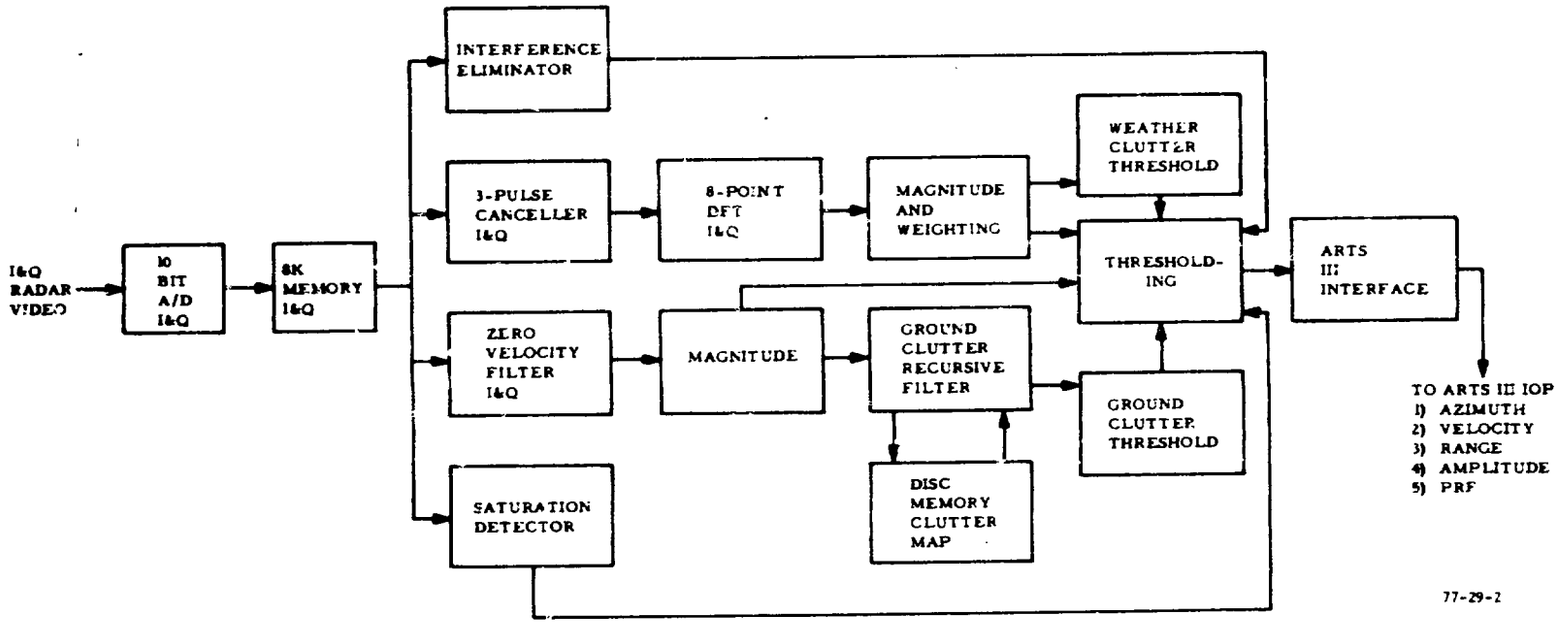

FIGURE 2. SIMPLIFIED MTD PROCESSOR BLOCK DIAGRAM

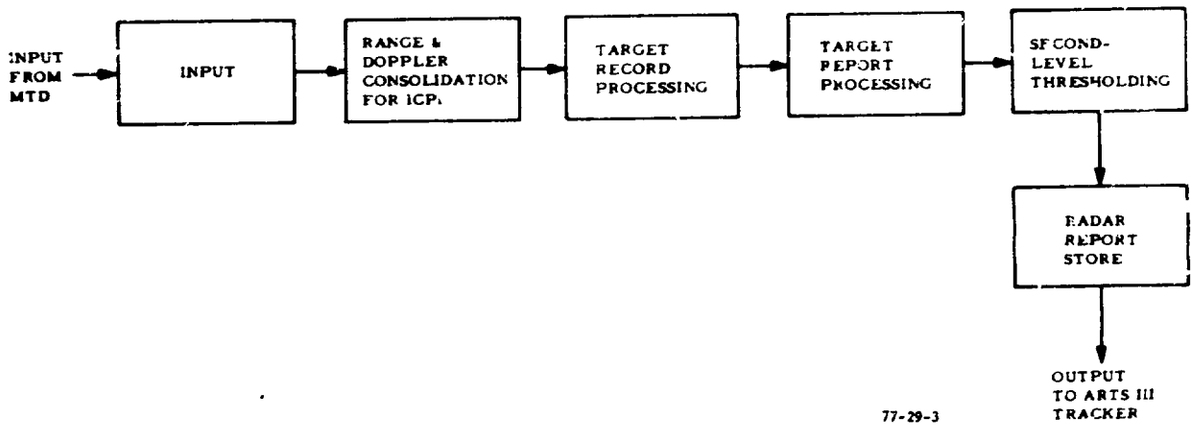

FIGURE 3. ARTS III MTD RIP SIMPLIFIED BLOCK DIAGRAM

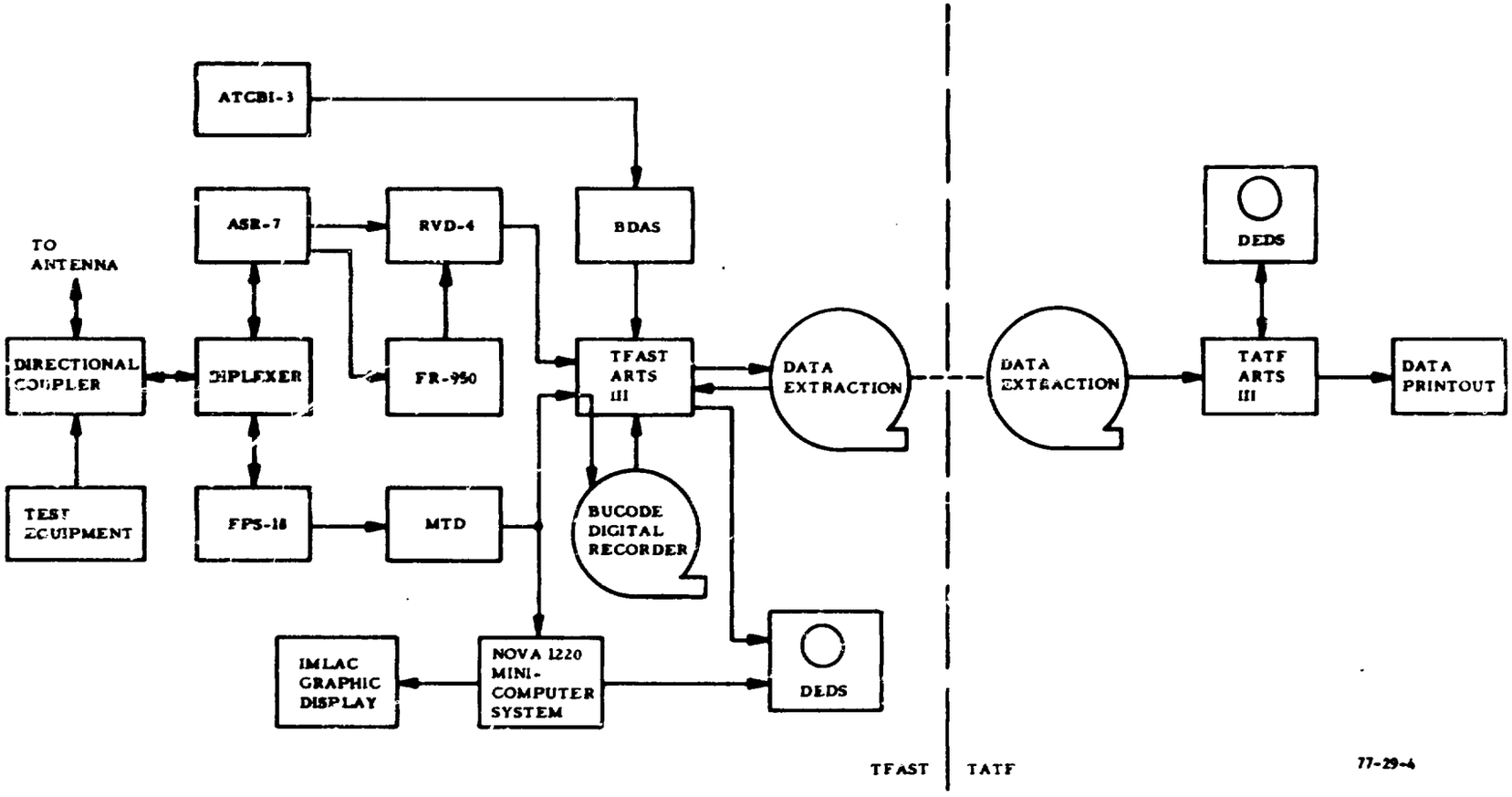

FIGURE 4. COMPARATIVE DATA ACQUISITION AND REDUCTION SYSTEM

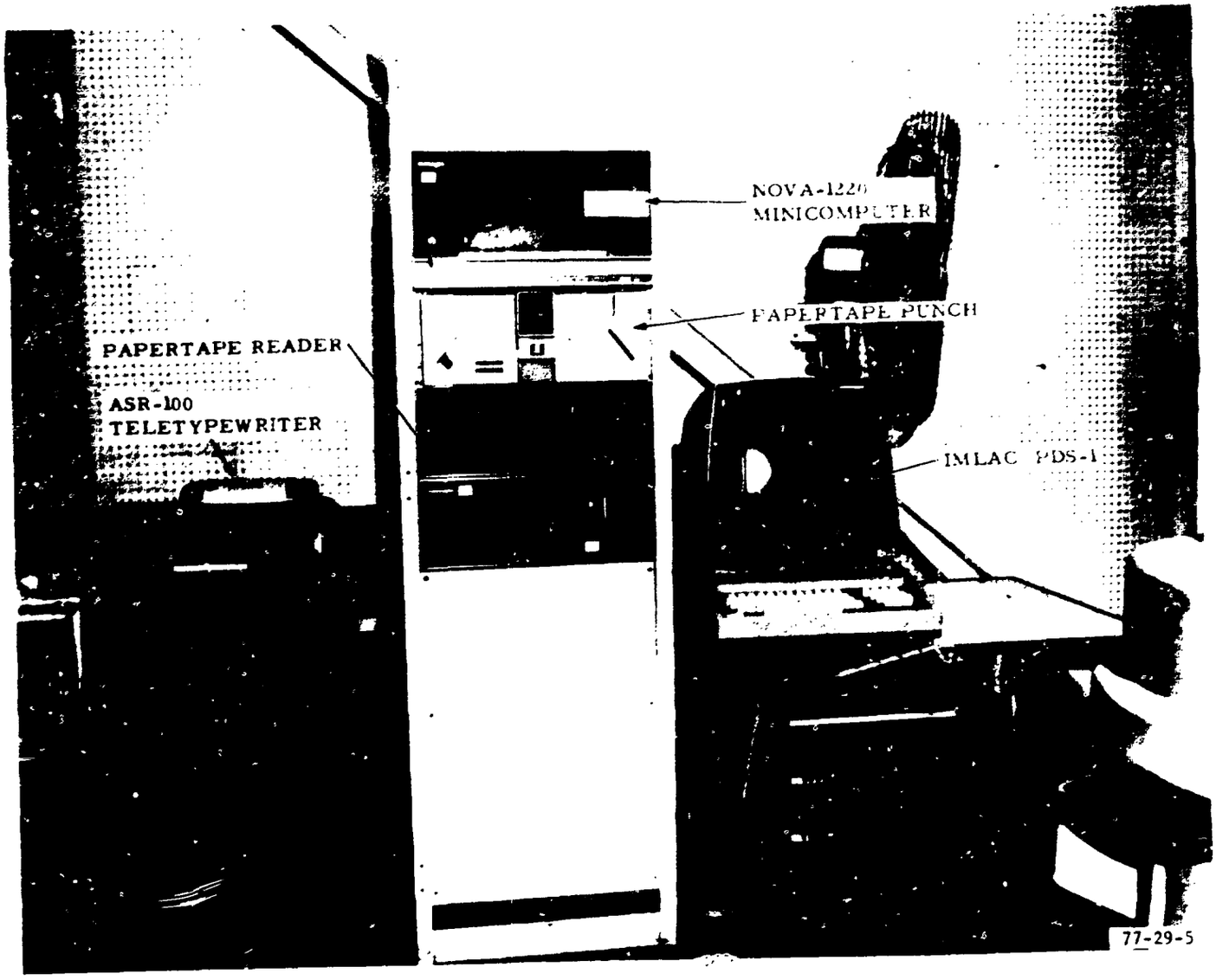

FIGURE 5. NOVA-1220 SUBSYSTEM

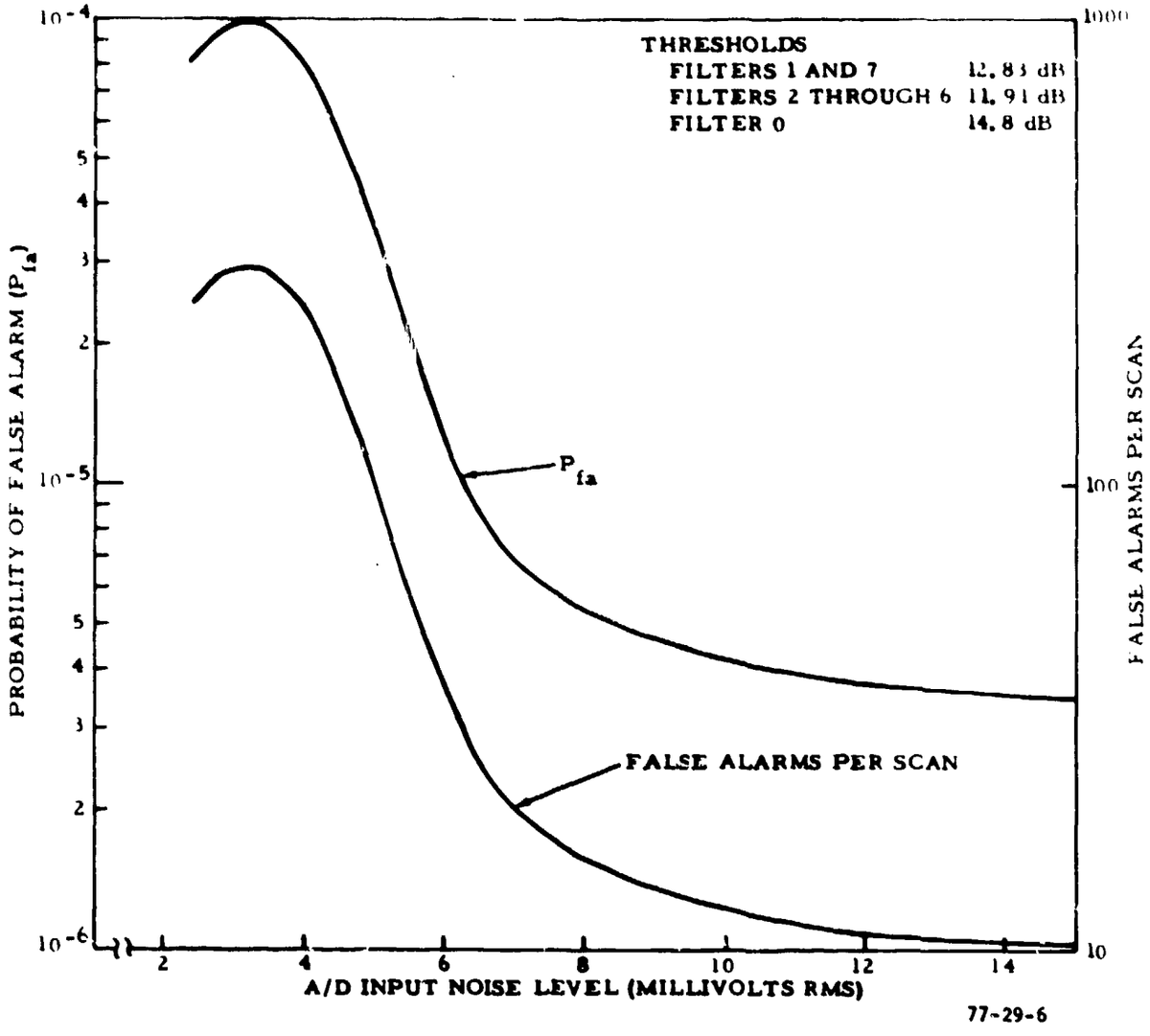

FIGURE 6. MTD THERMAL FALSE ALARM CURVES

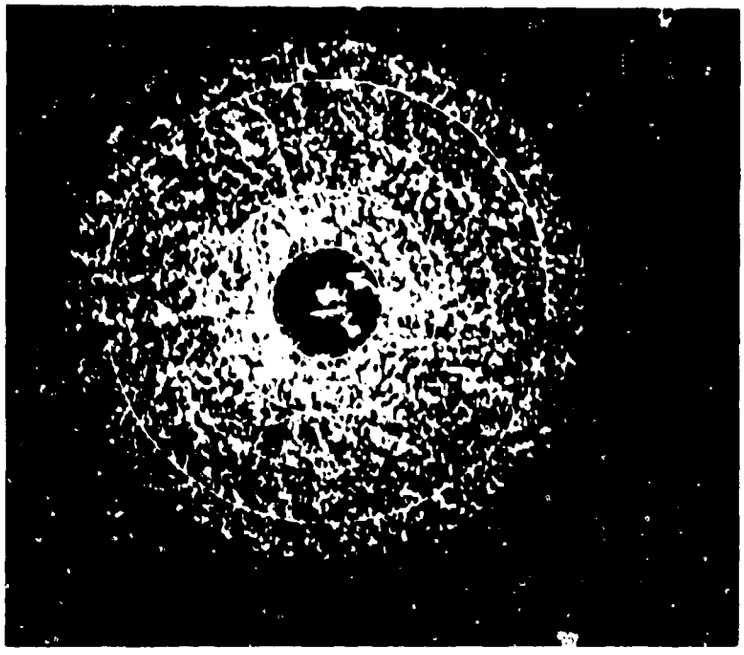

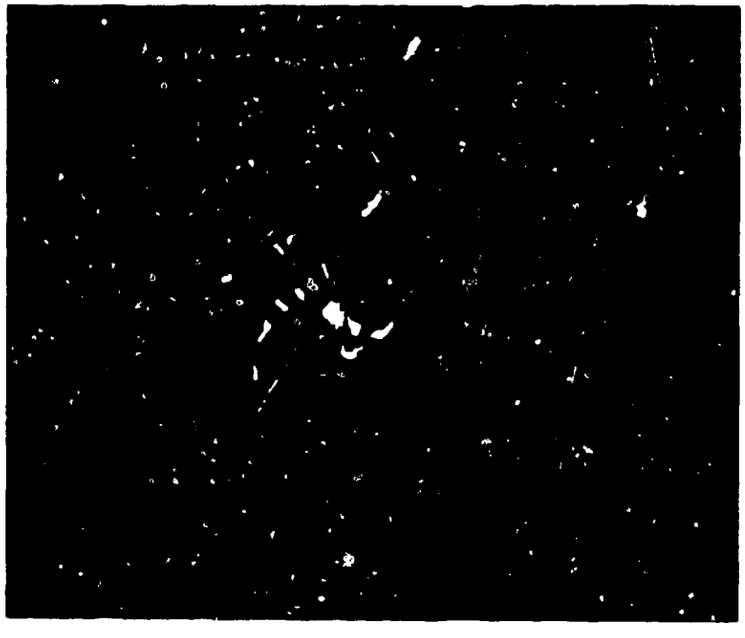

77-29-7

FIGURE 7. MTD INTERFERENCE ELIMINATION

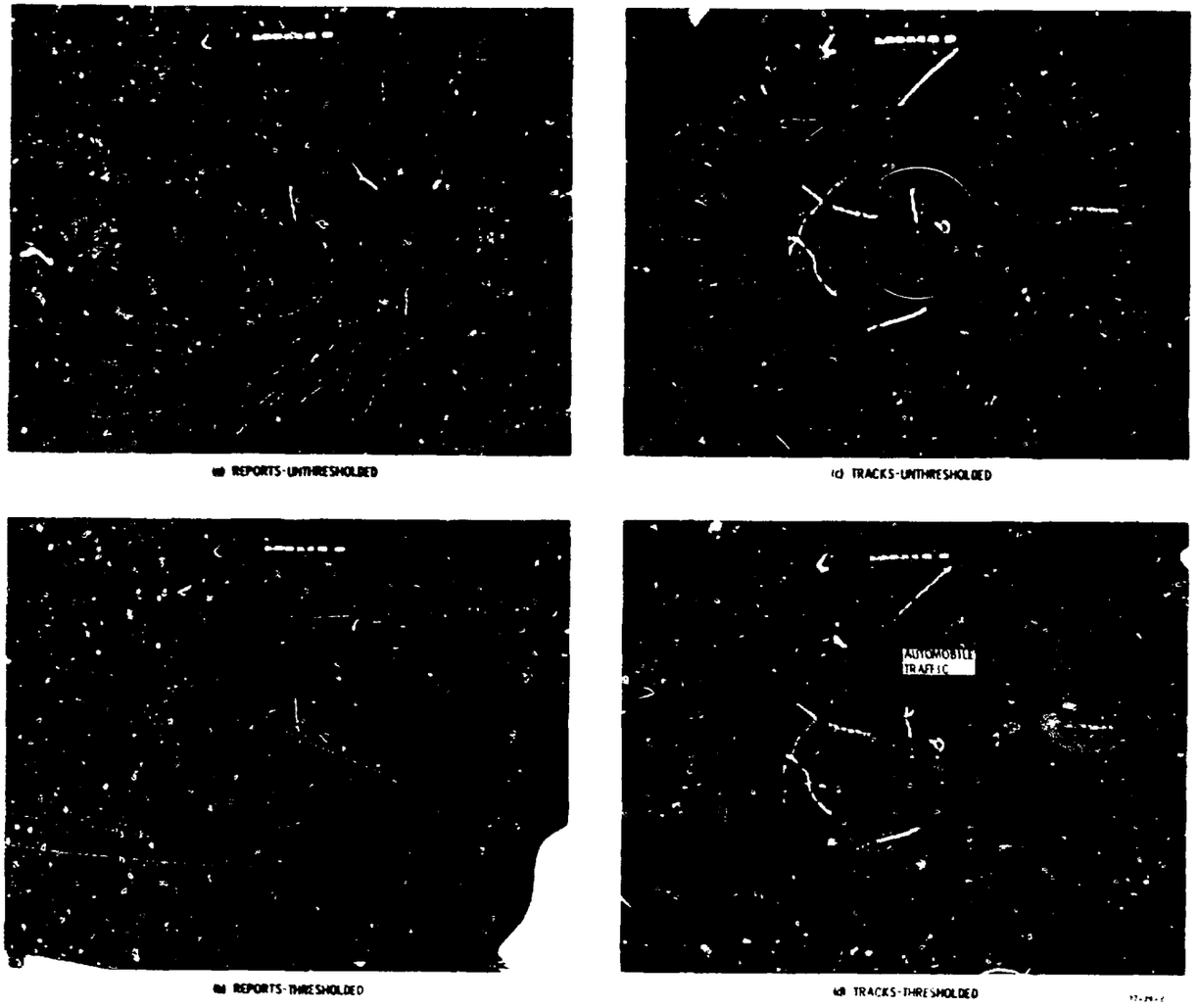

FIGURE 8. TARGET DISPLAYS WITH AND WITHOUT SECOND-LEVEL THRESHOLDING IN A LIGHT ANGEL ENVIRONMENT (5-nmi Range Rings)

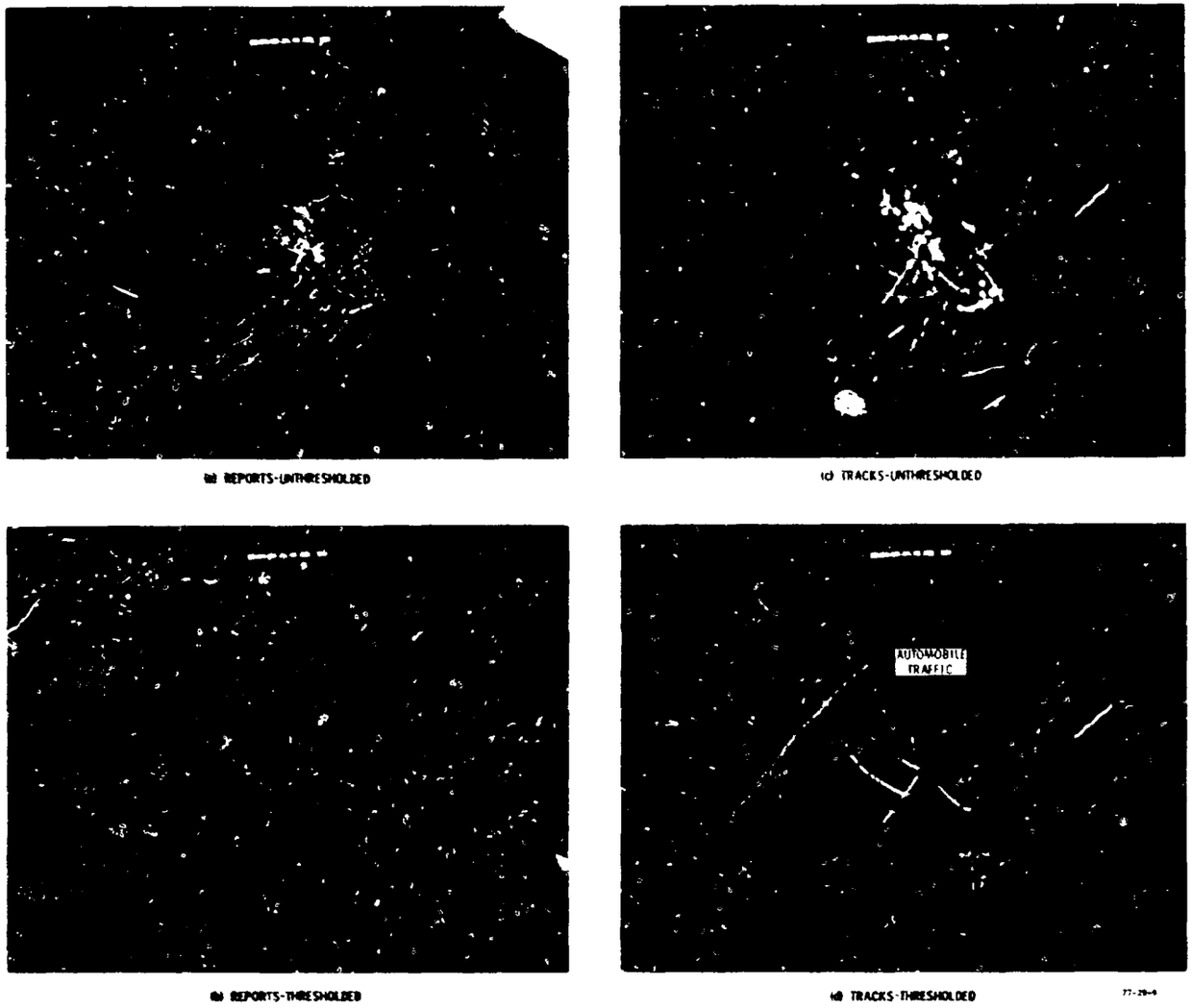

FIGURE 9. TARGET DISPLAYS WITH AND WITHOUT SECOND-LEVEL THRESHOLDING IN A HEAVY ANGEL ENVIRONMENT (5-nmi Range Rings)

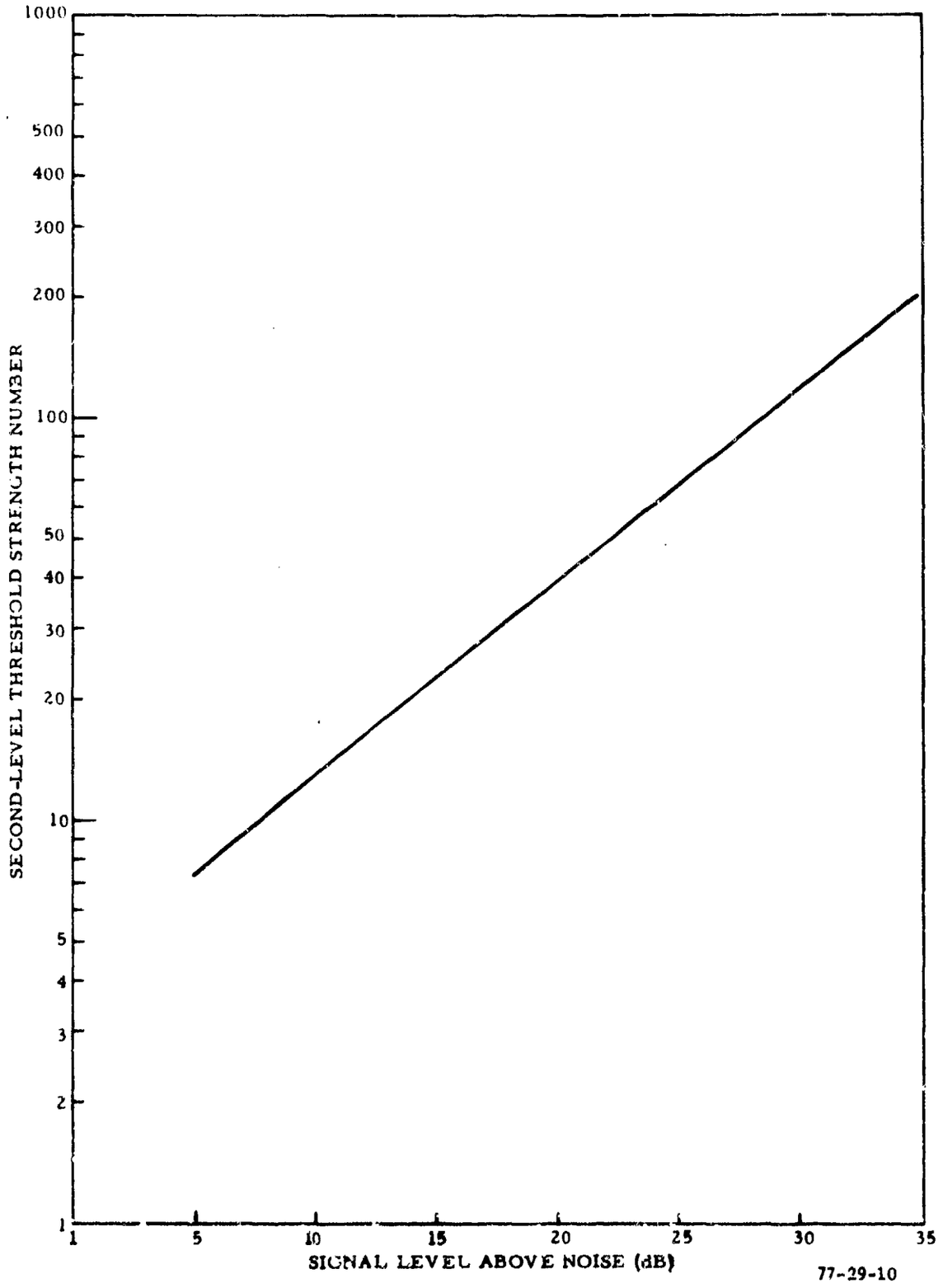

FIGURE 10. SECOND-LEVEL THRESHOLD STRENGTH NUMBER AS A FUNCTION OF SIGNAL STRENGTH

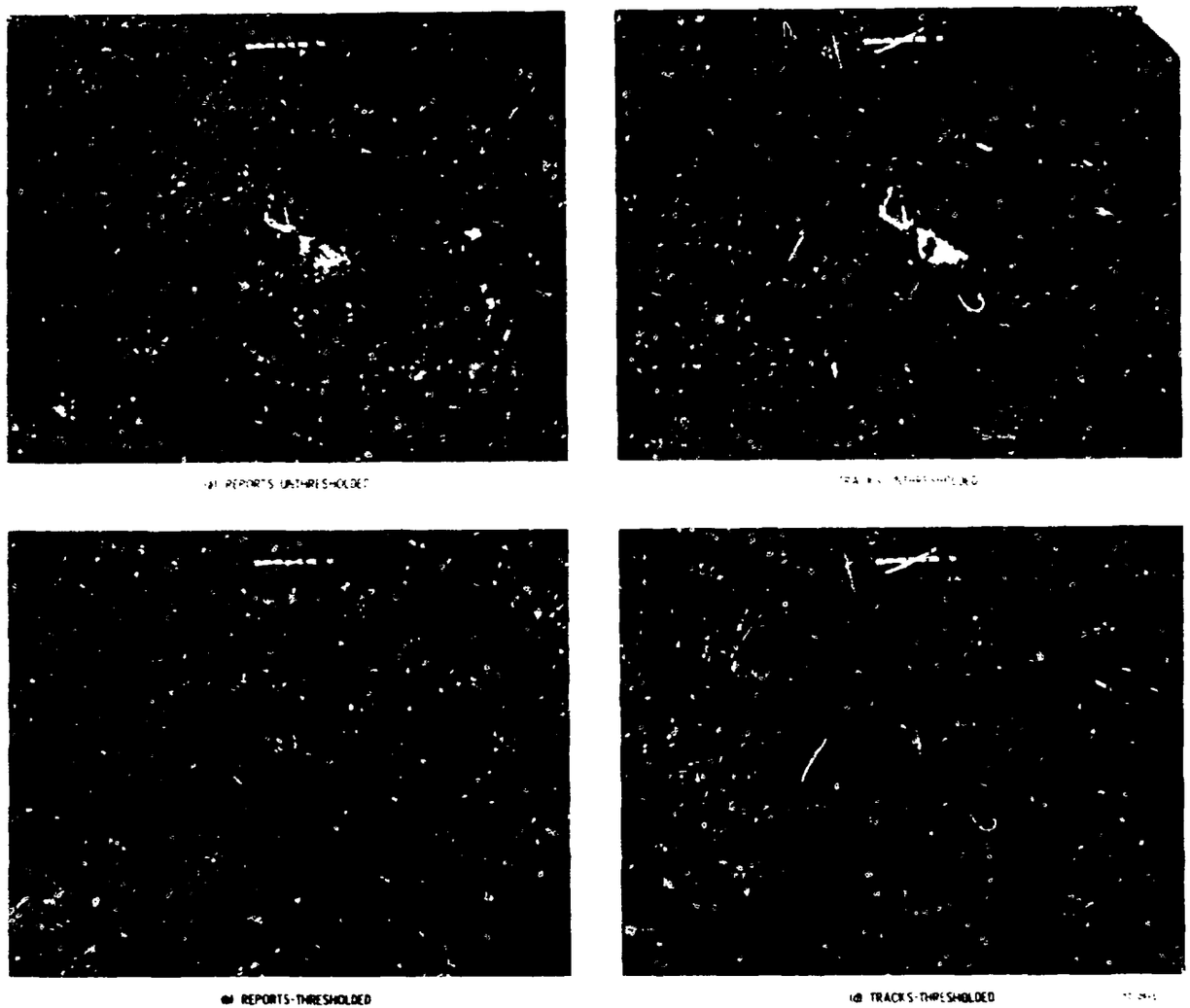

FIGURE 11. TARGET DISPLAY WITH AND WITHOUT SECOND-LEVEL THRESHOLDING IN AN ANGEL ENVIRONMENT, 54-dB STC (5-nmi Range Rings)

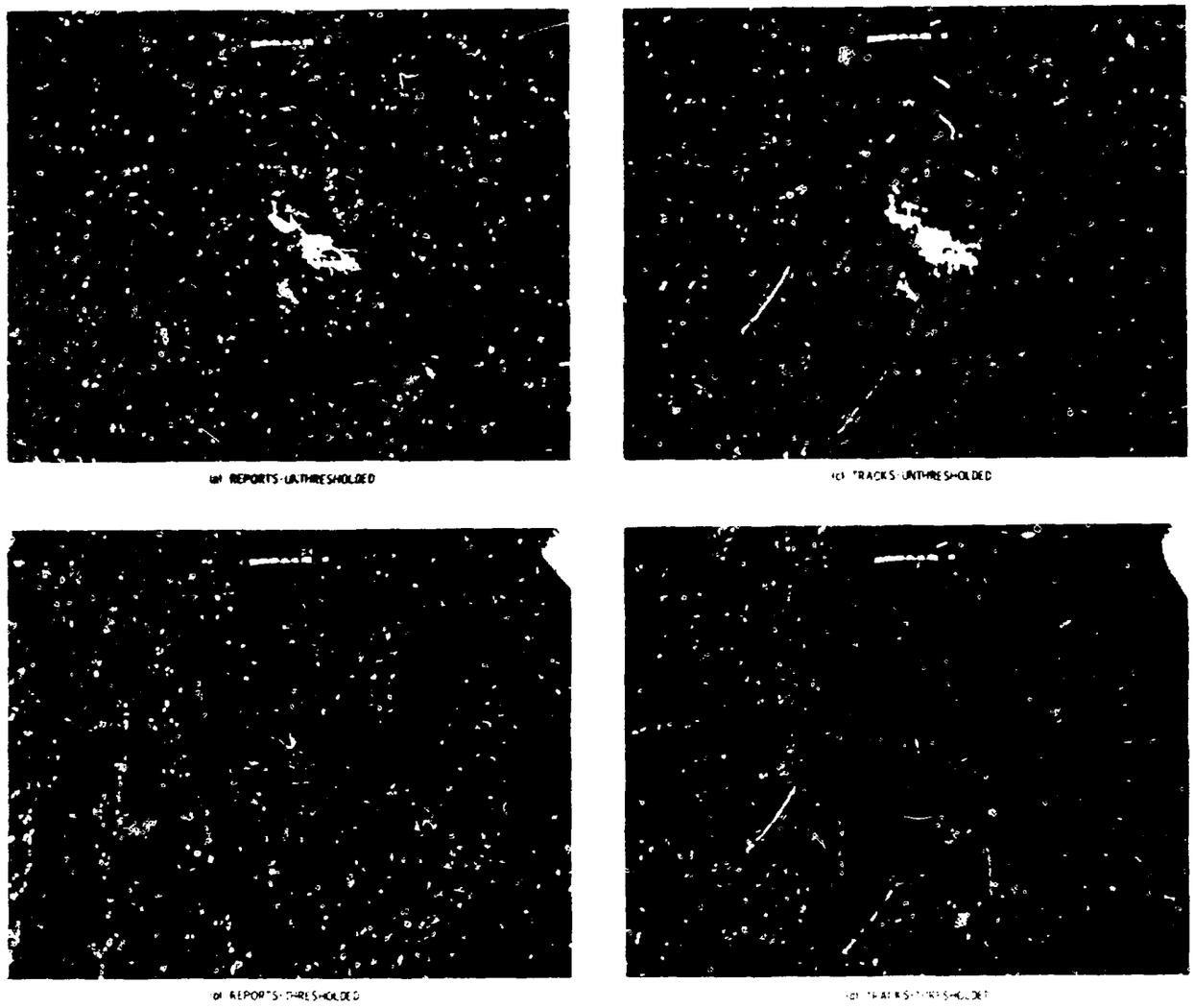

FIGURE 12. TARGET DISPLAY WITH AND WITHOUT SECOND-LEVEL THRESHOLDING IN AN ANGEL ENVIRONMENT, 48-dB STC (5-nmi Range Rings)

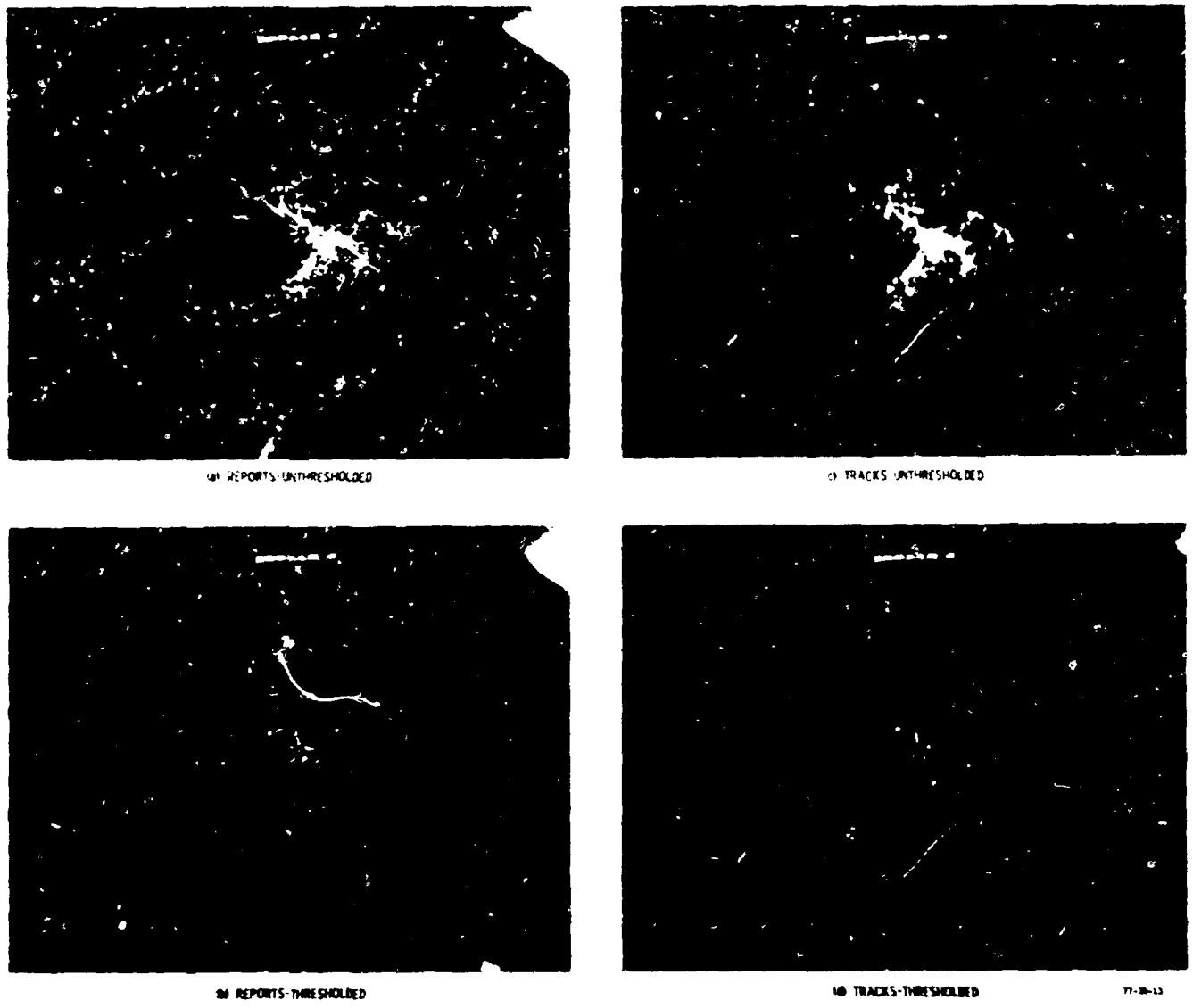

FIGURE 13. TARGET DISPLAY WITH AND WITHOUT SECOND-LEVEL THRESHOLDING IN AN ANGEL ENVIRONMENT, 42-dB STC (5-nmi Range Rings)

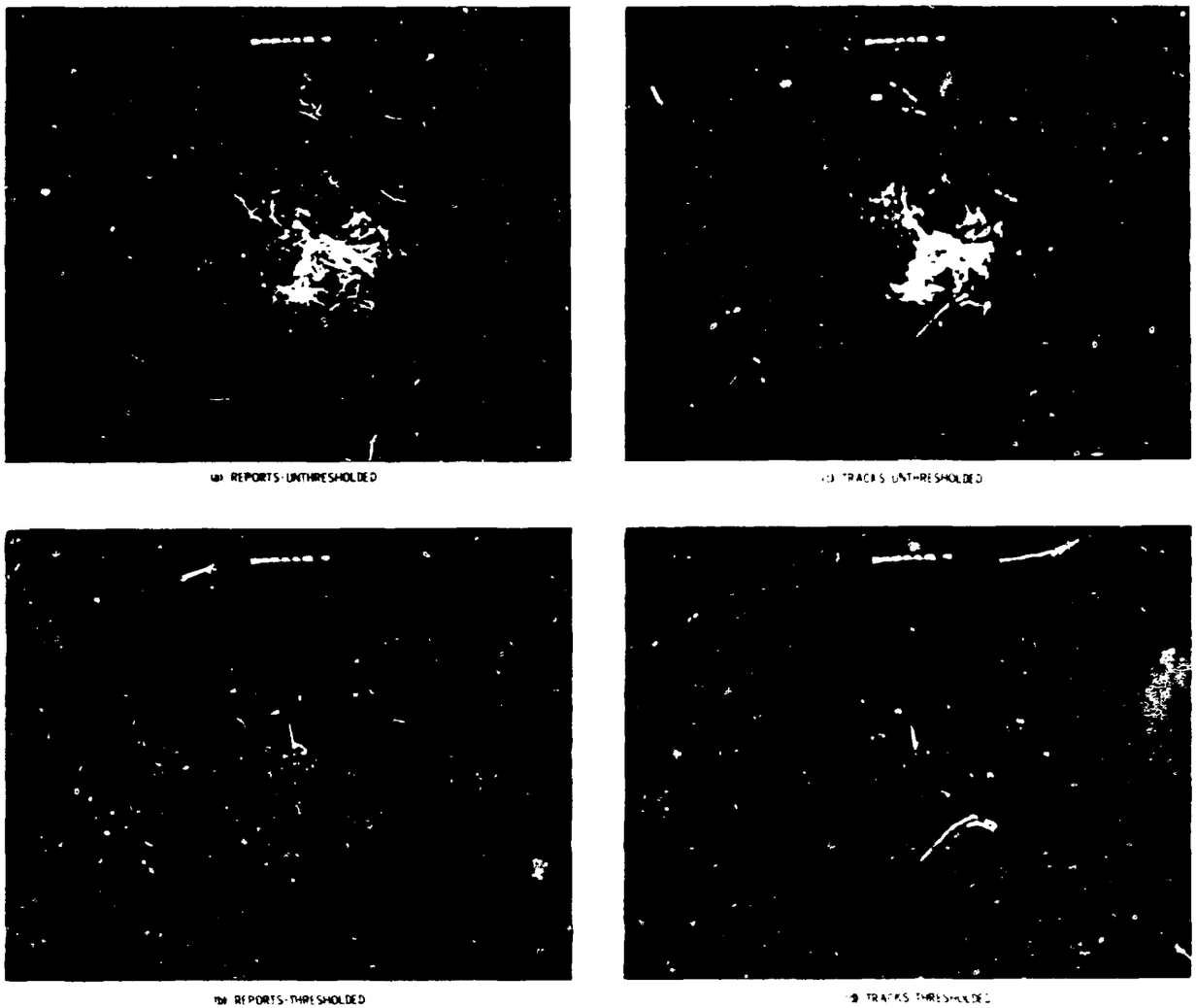

FIGURE 14. TARGET DISPLAY WITH AND WITHOUT SECOND-LEVEL THRESHOLD IN AN ANGEL ENVIRONMENT, 36-dB STC (5-nmi Range Rings)

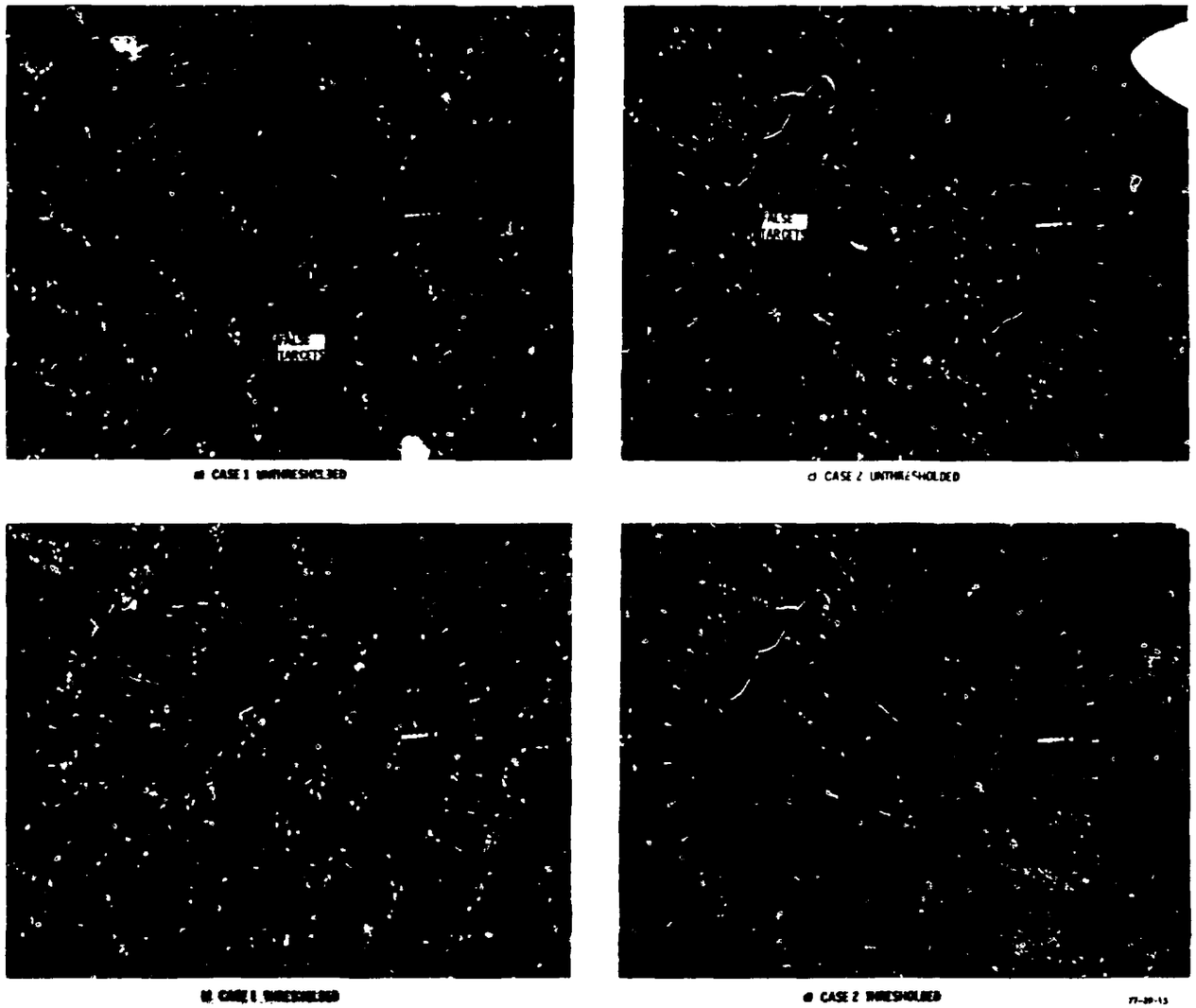

FIGURE 15. ARTS III TRACKER OUTPUT FOR MTD OPERATION IN WEATHER WITH AND WITHOUT SOFTWARE THRESHOLDING (10-nmi Range Rings)

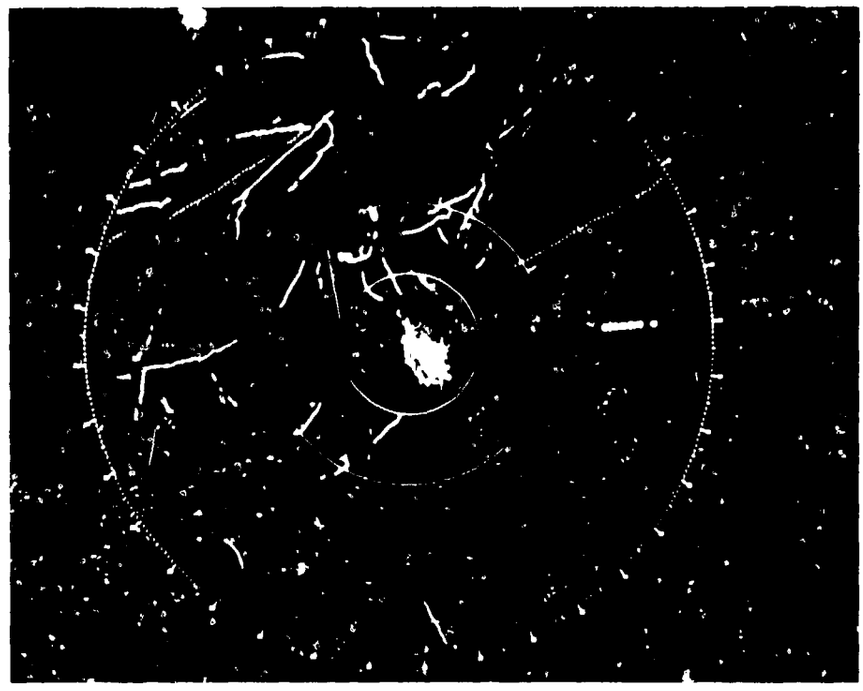

(a) UNTHRESHOLDED

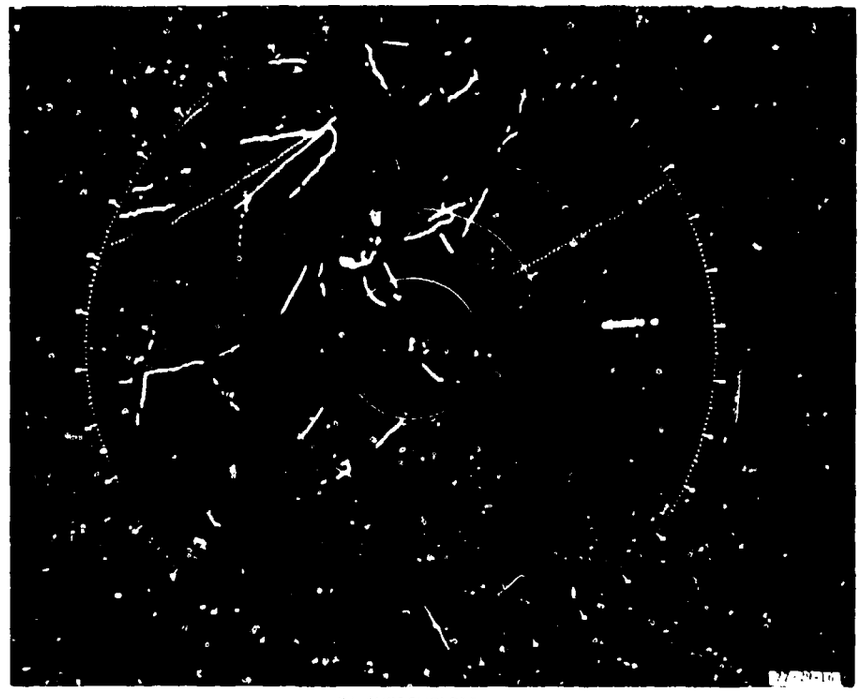

(b) THRESHOLDED

FIGURE 16. ARTS III TRACKER OUTPUT FOR MTD OPERATION ON A CLEAR DAY WITH AND WITHOUT SECOND-LEVEL THRESHOLDING, NO TRACK COASTING (10-nmi Range Rings)

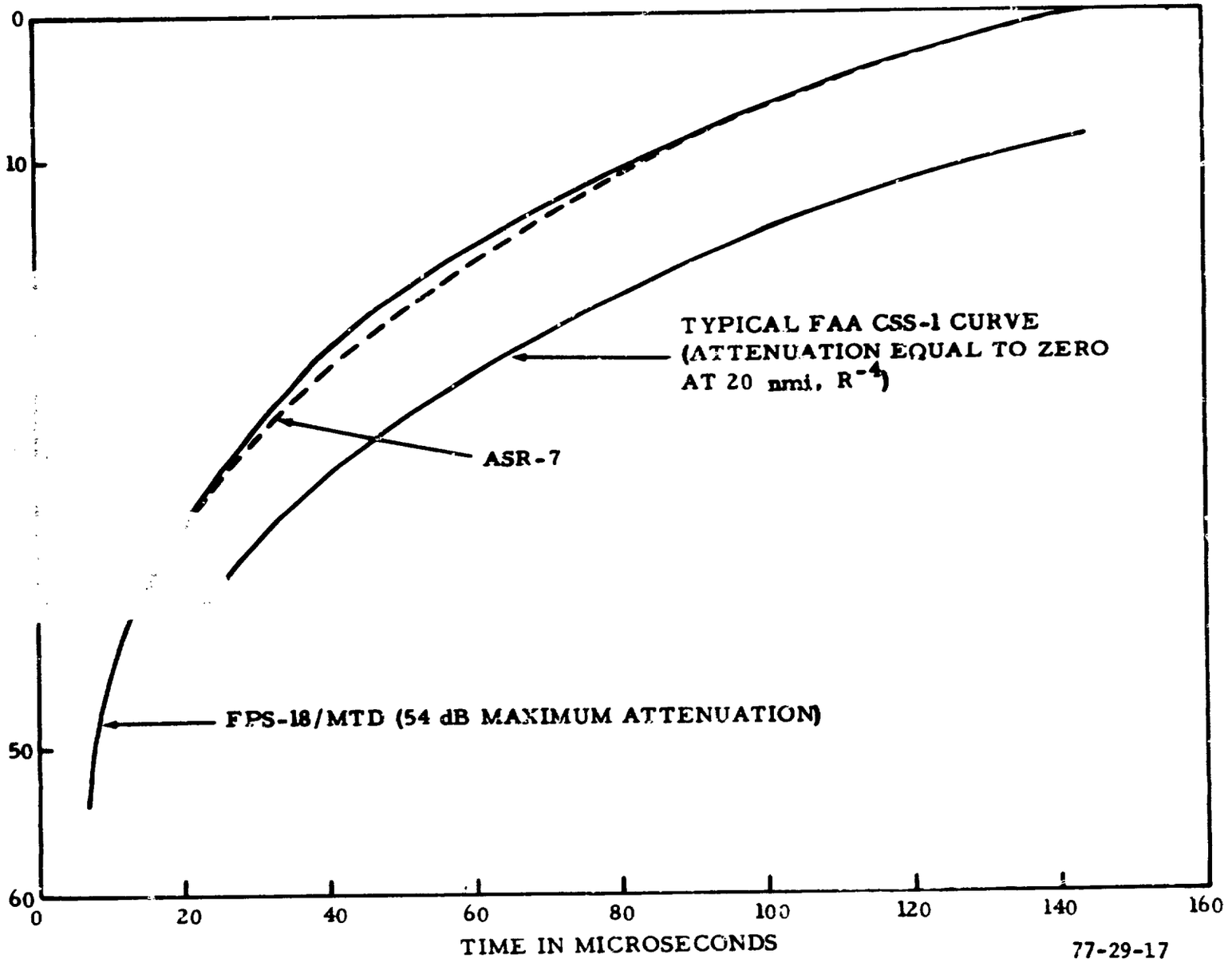

FIGURE 17. SYSTEM STC CURVES

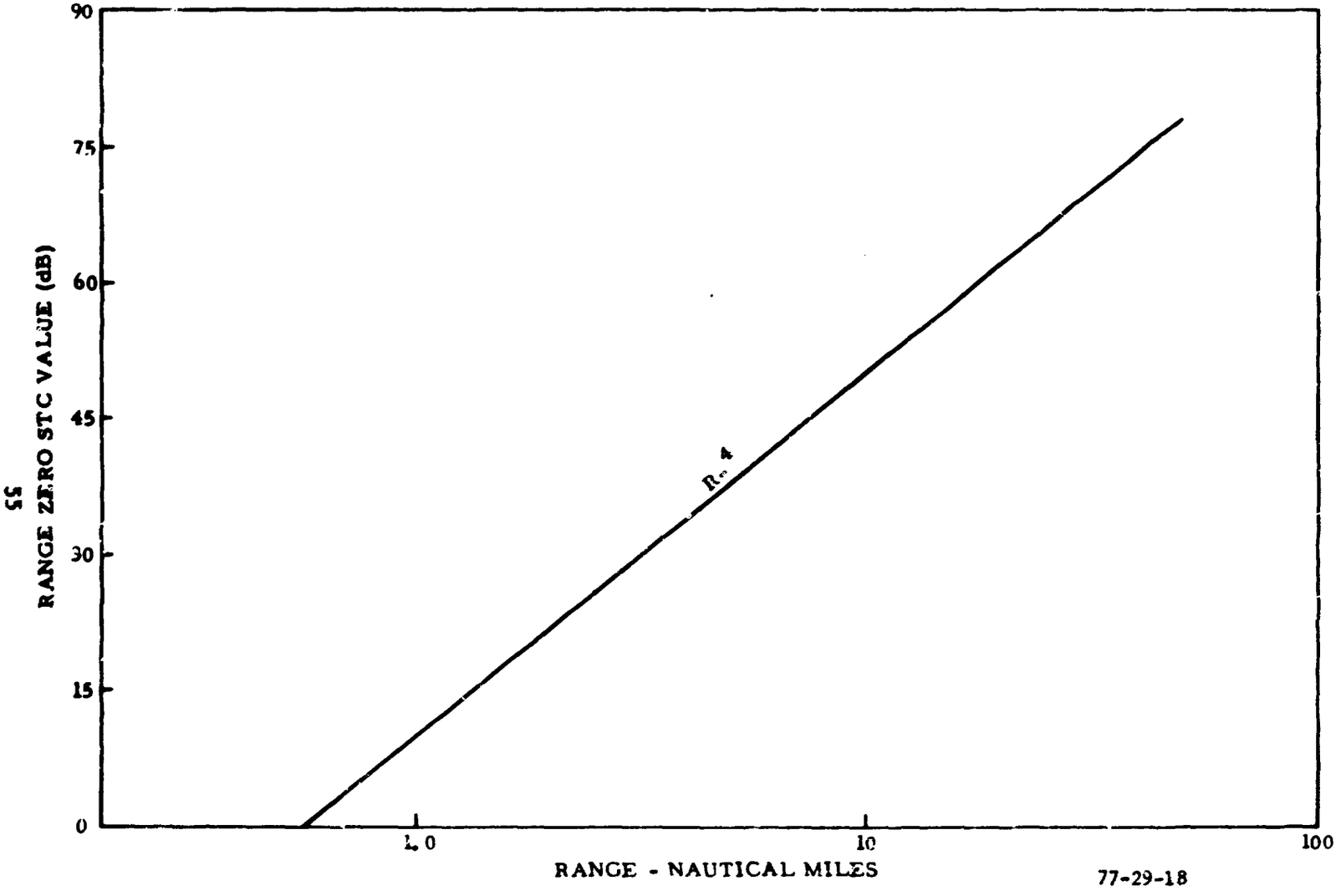

FIGURE 18. MID STC VALUE CURVE

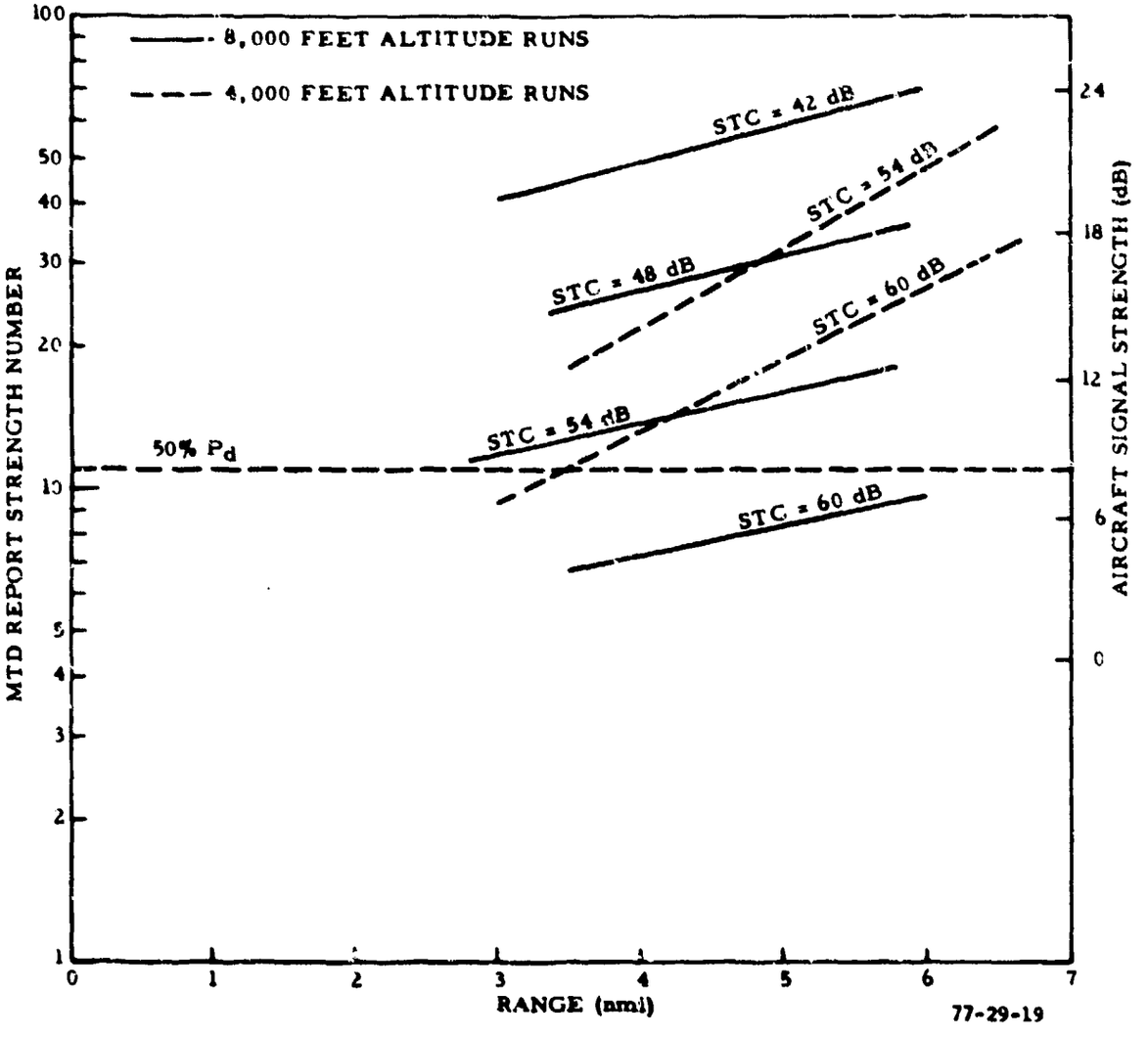

FIGURE 19. AIRCRAFT ECHO STRENGTH VERSUS STC

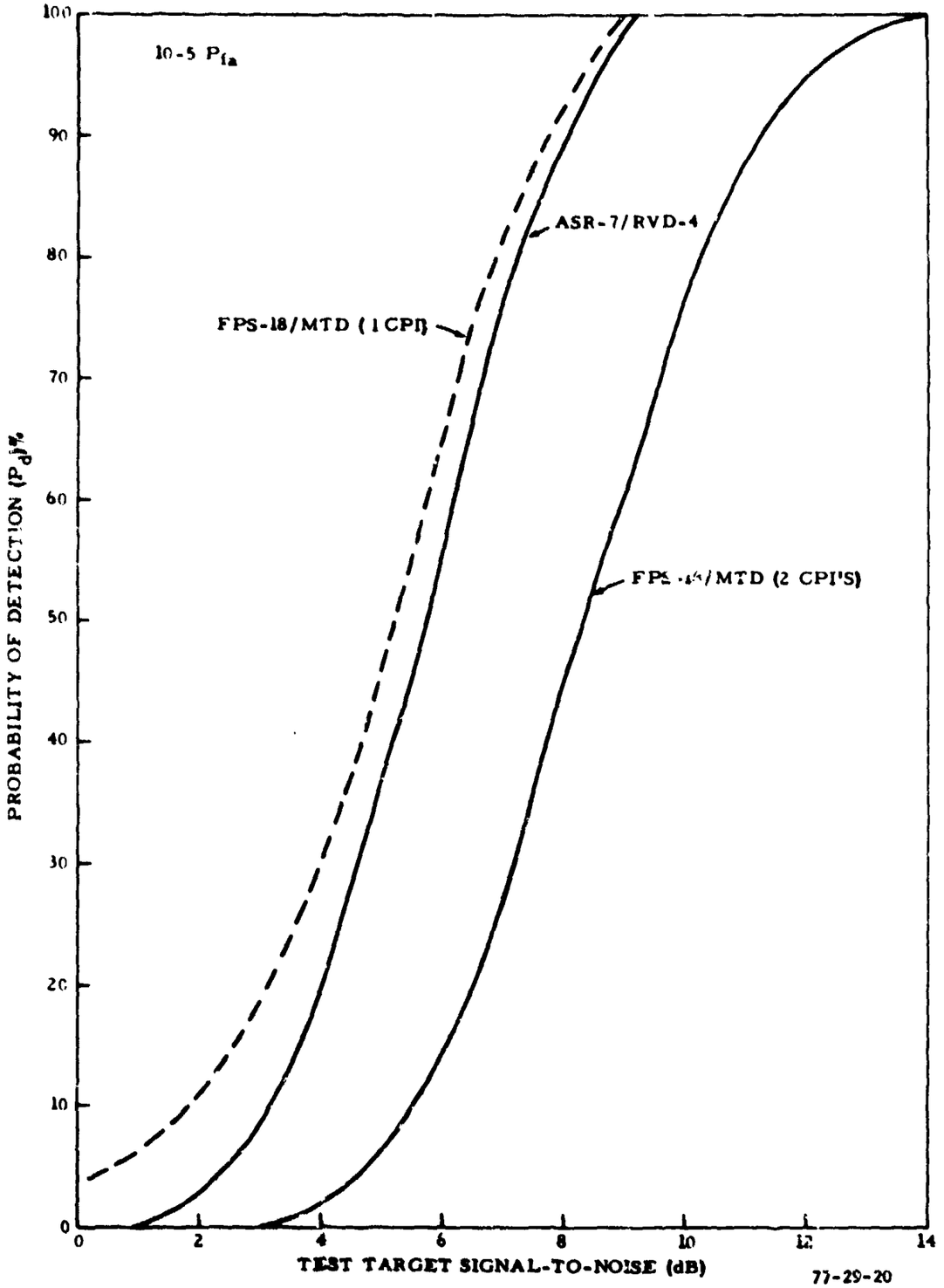

FIGURE 20. MTD/RVD-4 COMPARATIVE PROBABILITY OF DETECTION

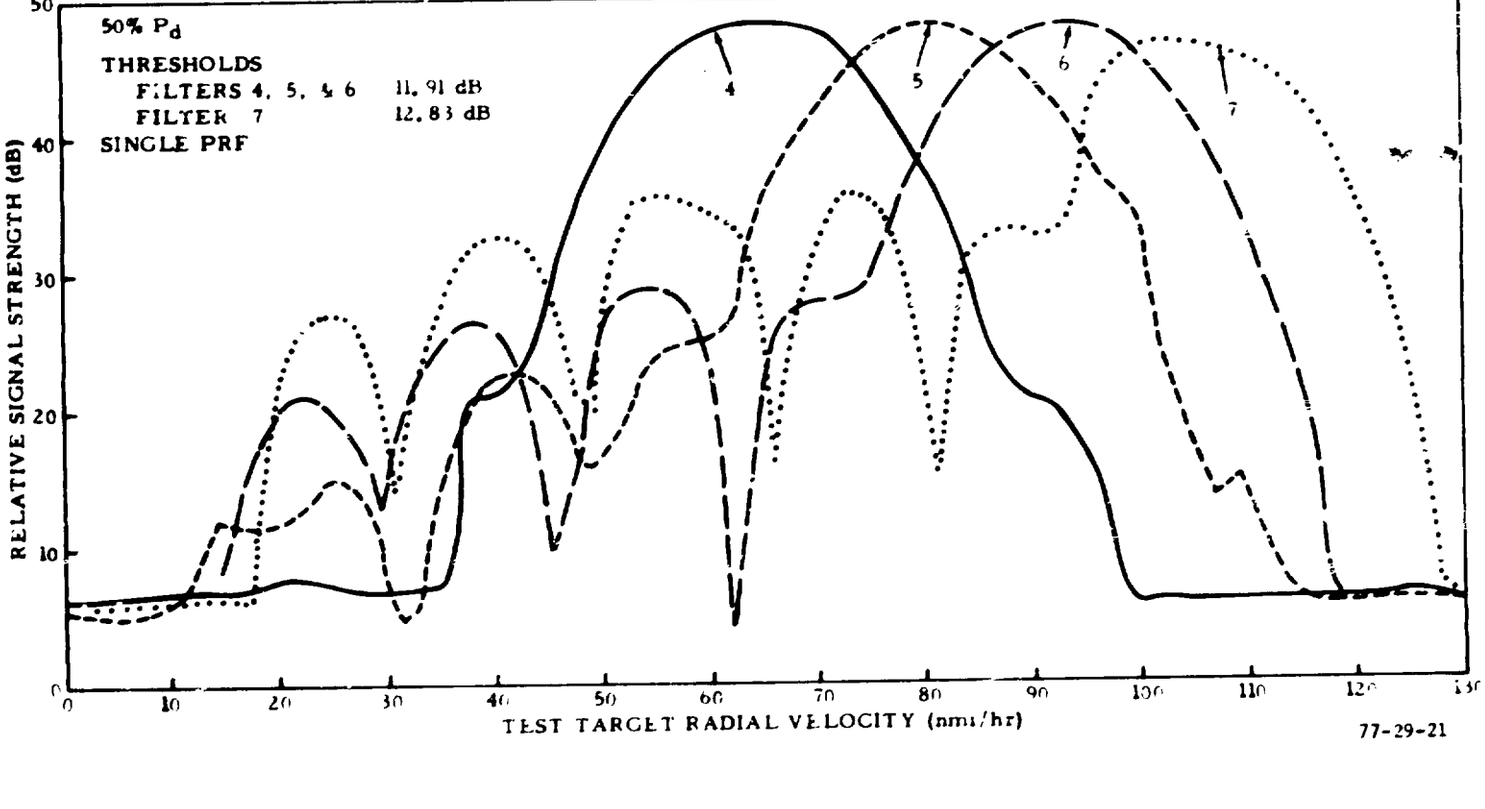

FIGURE 21. VELOCITY RESPONSE OF MTD NONZERO FILTERS

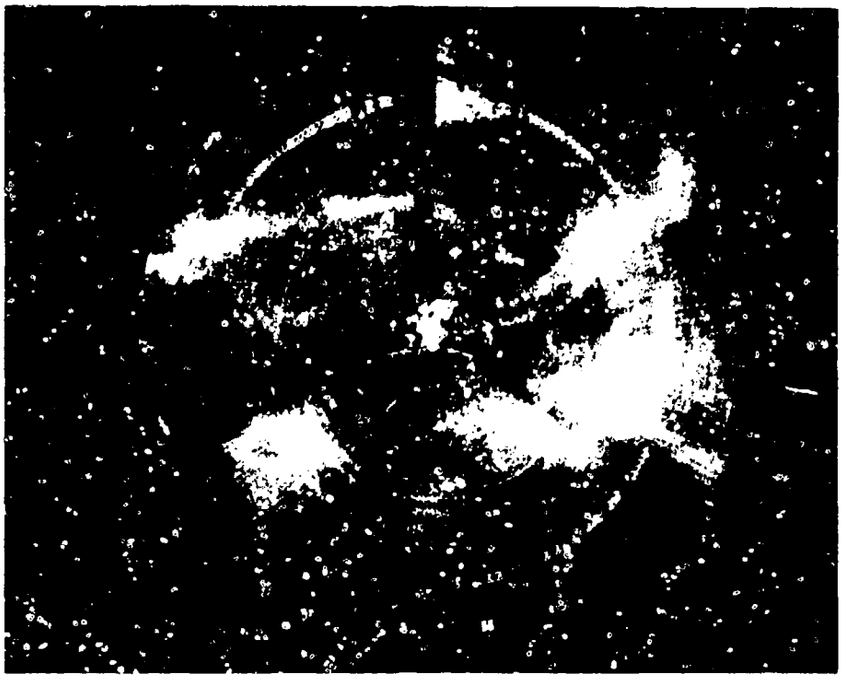

(a)

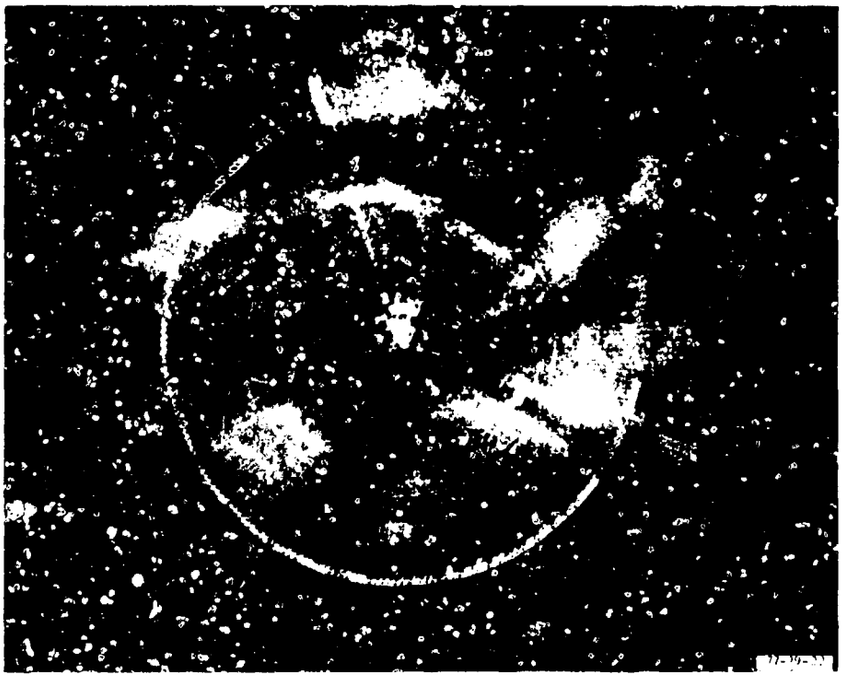

(b)

FIGURE 22. MTD VELOCITY RESPONSE IN WEATHER

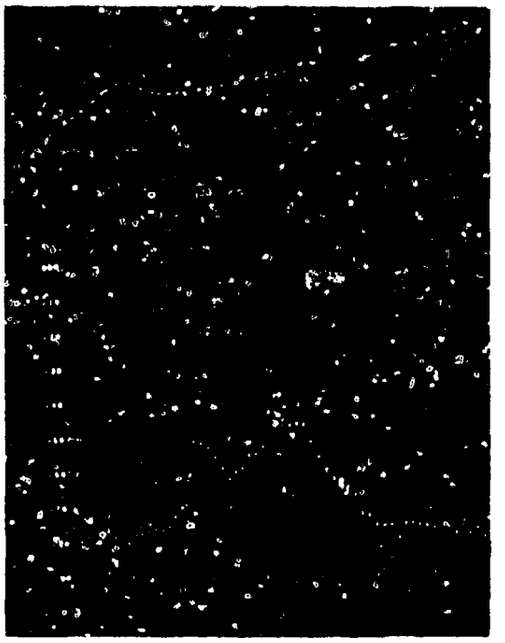

(a) ANTENNA AT [illegible]°

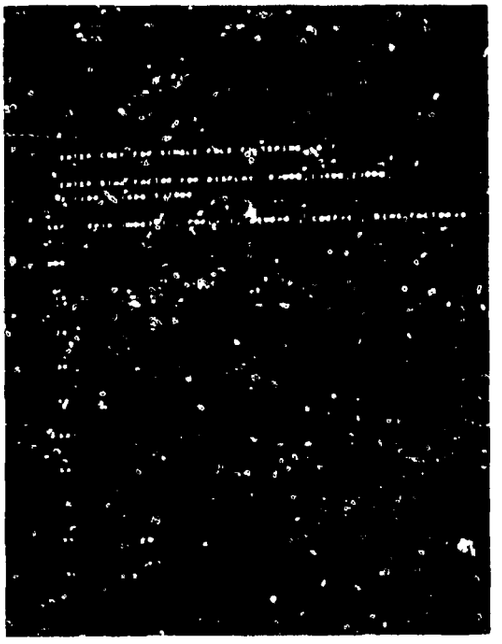

(b) ANTENNA AT 150°

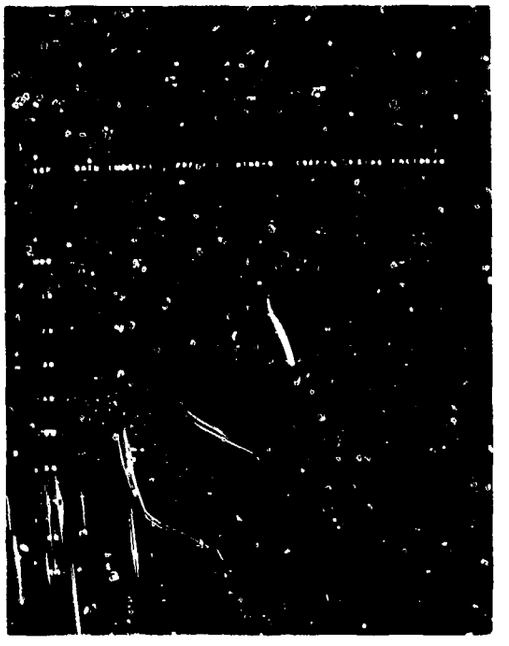

(c) ANTENNA AT 330°

77-29-22

FIGURE 23. PRECIPITATION SPECTRA

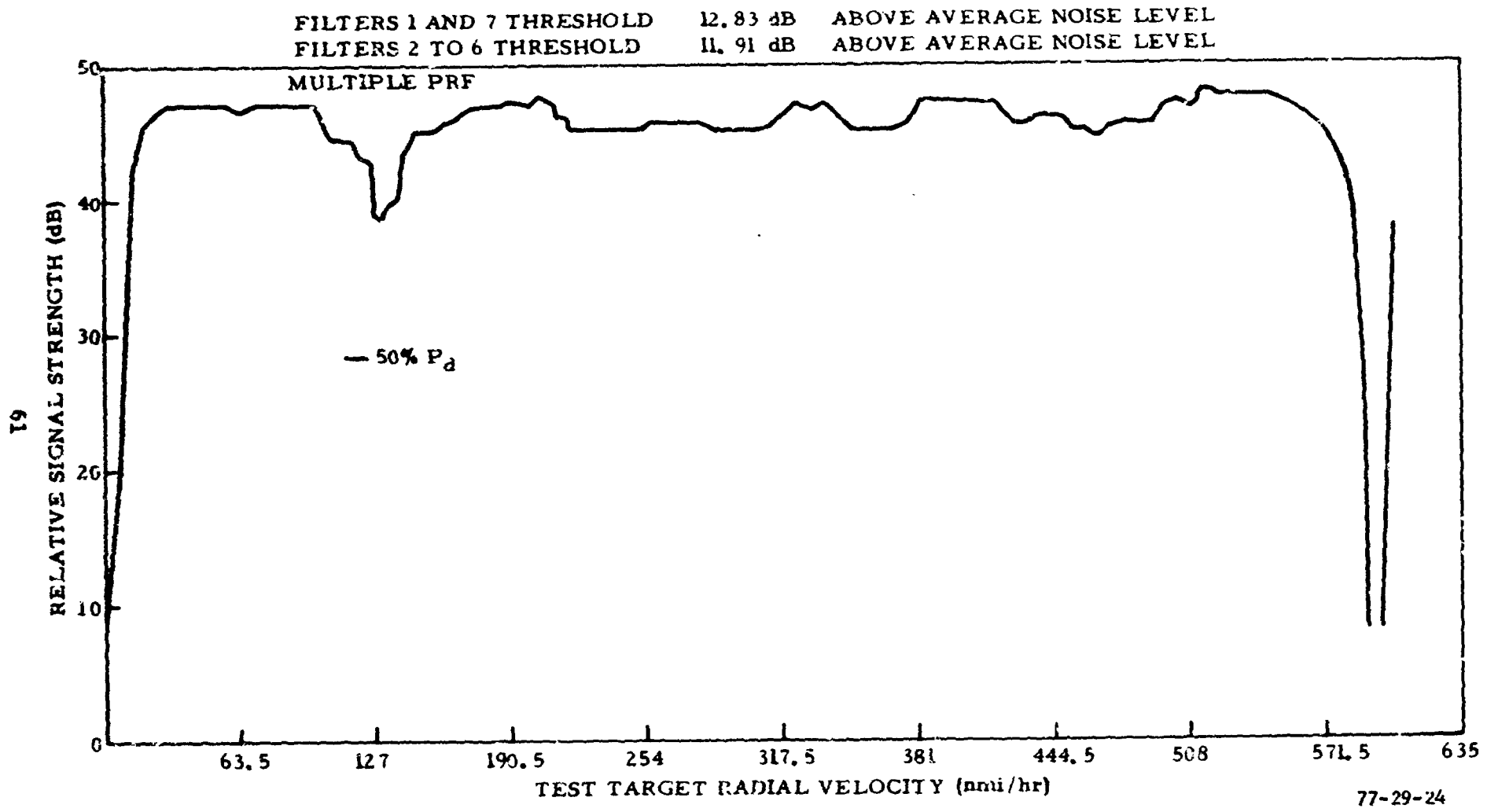

FIGURE 24. MTD VELOCITY RESPONSE FILTERS 1 THROUGH 7 COMBINED

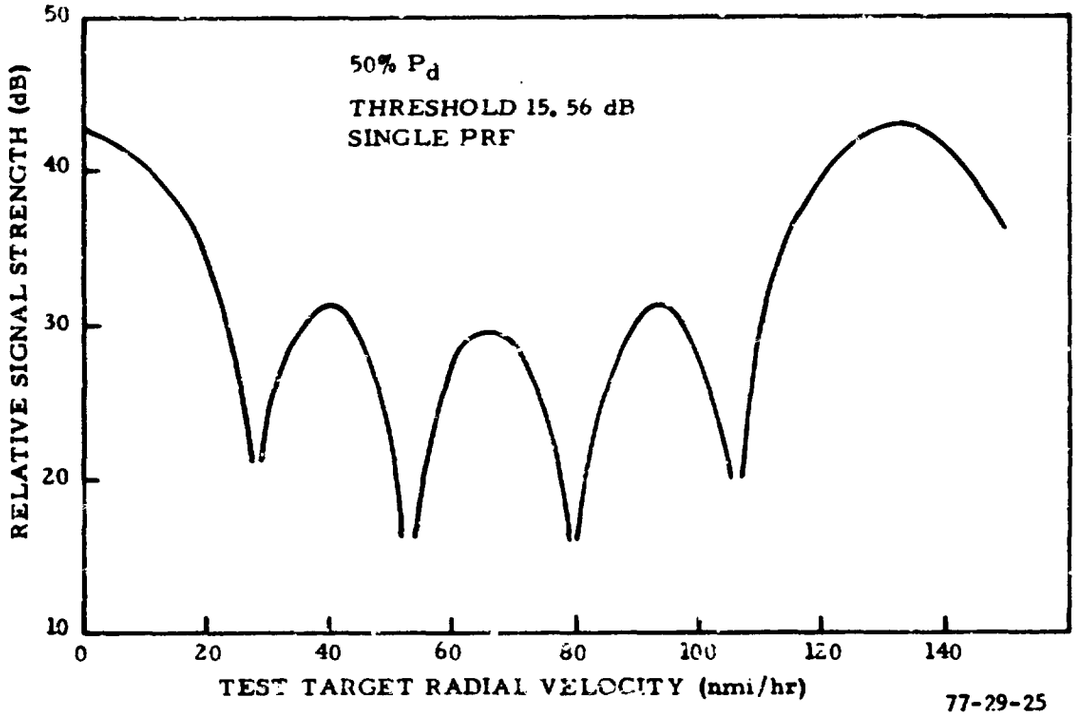

FIGURE 25. VELOCITY RESPONSE OF MTD ZERO FILTER

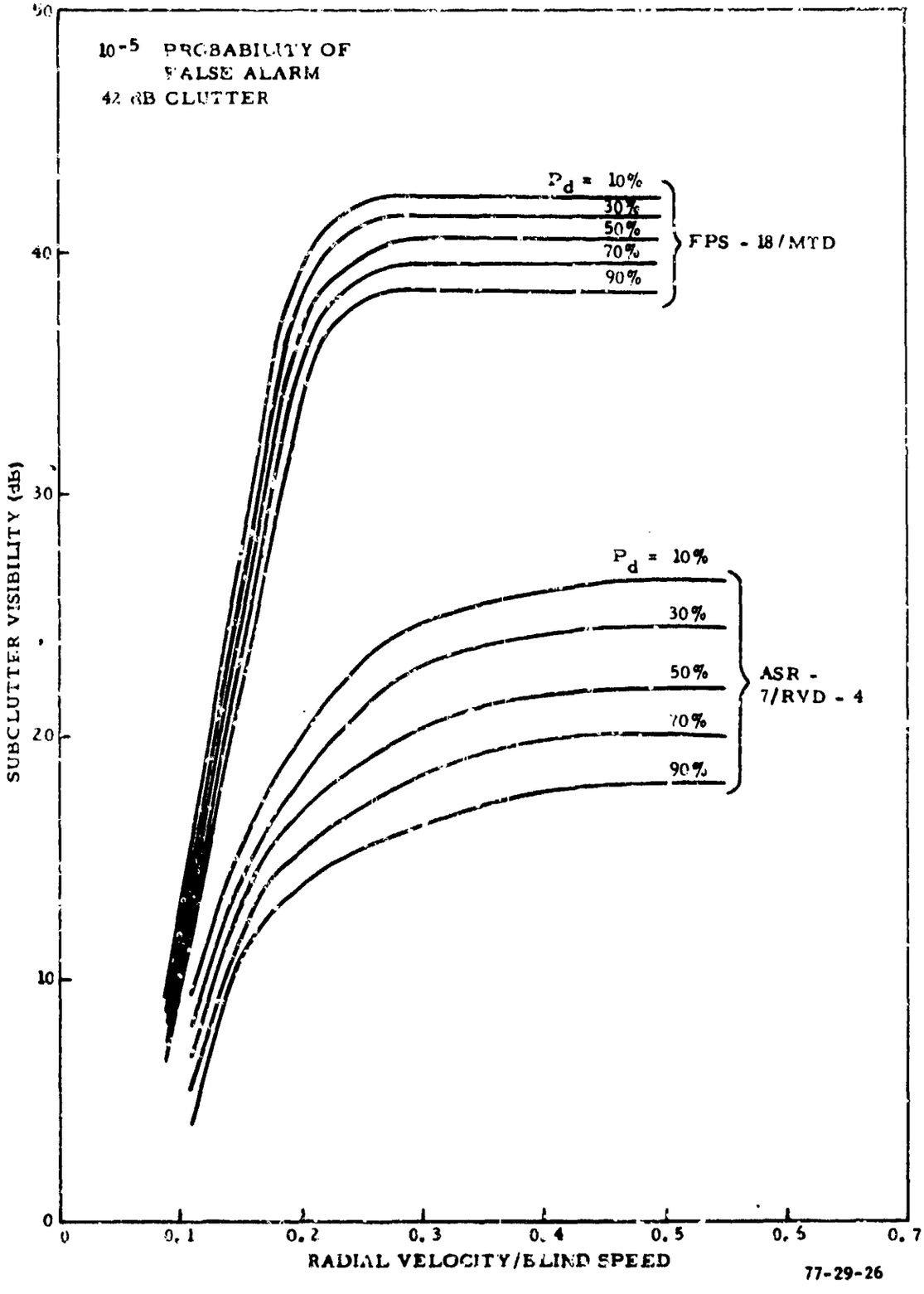

FIGURE 26. COMPARATIVE SUBCLUTTER VISIBILITY

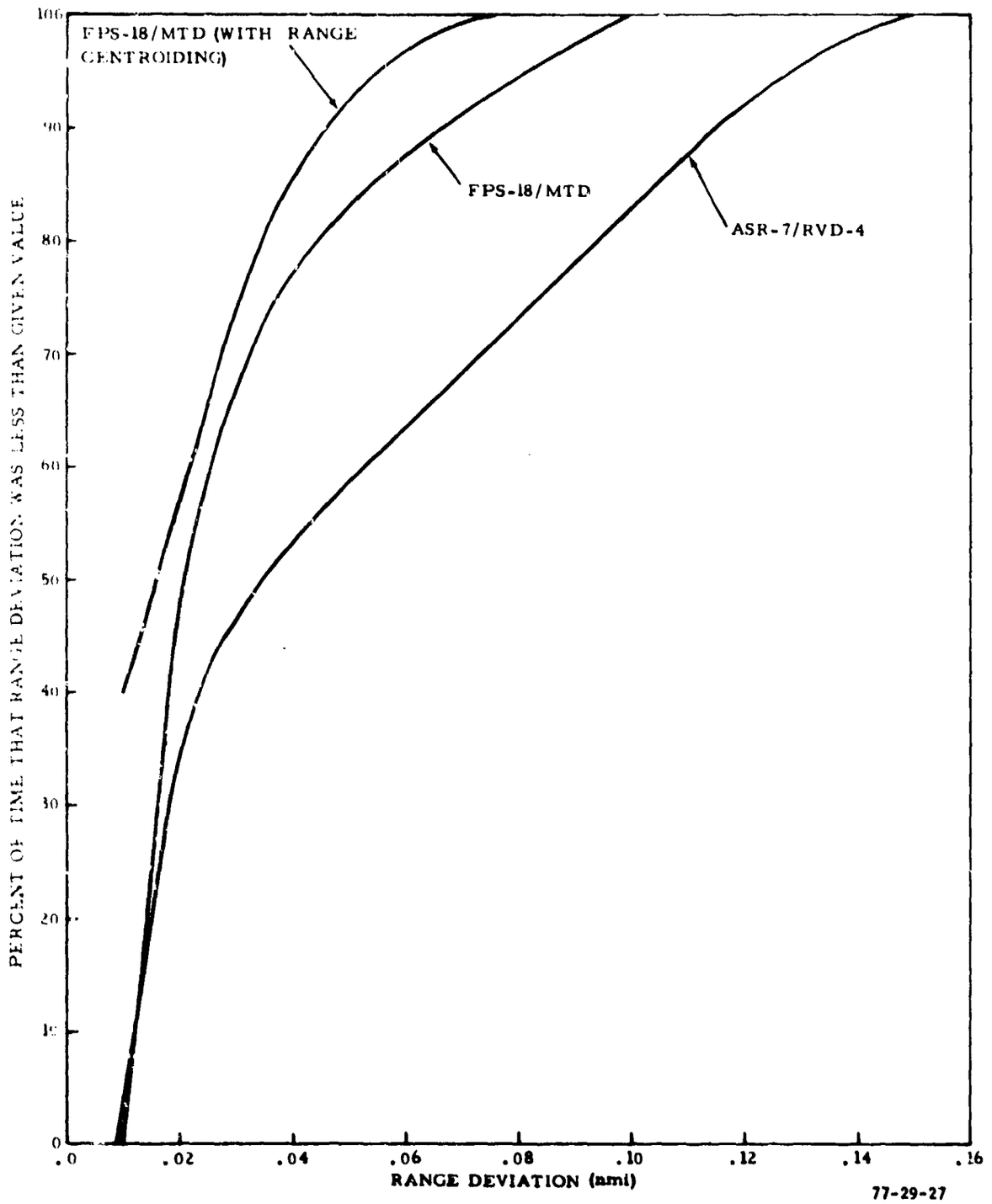

FIGURE 27. COMPARATIVE FREQUENCY DISTRIBUTIONS OF RANGE ACCURACY

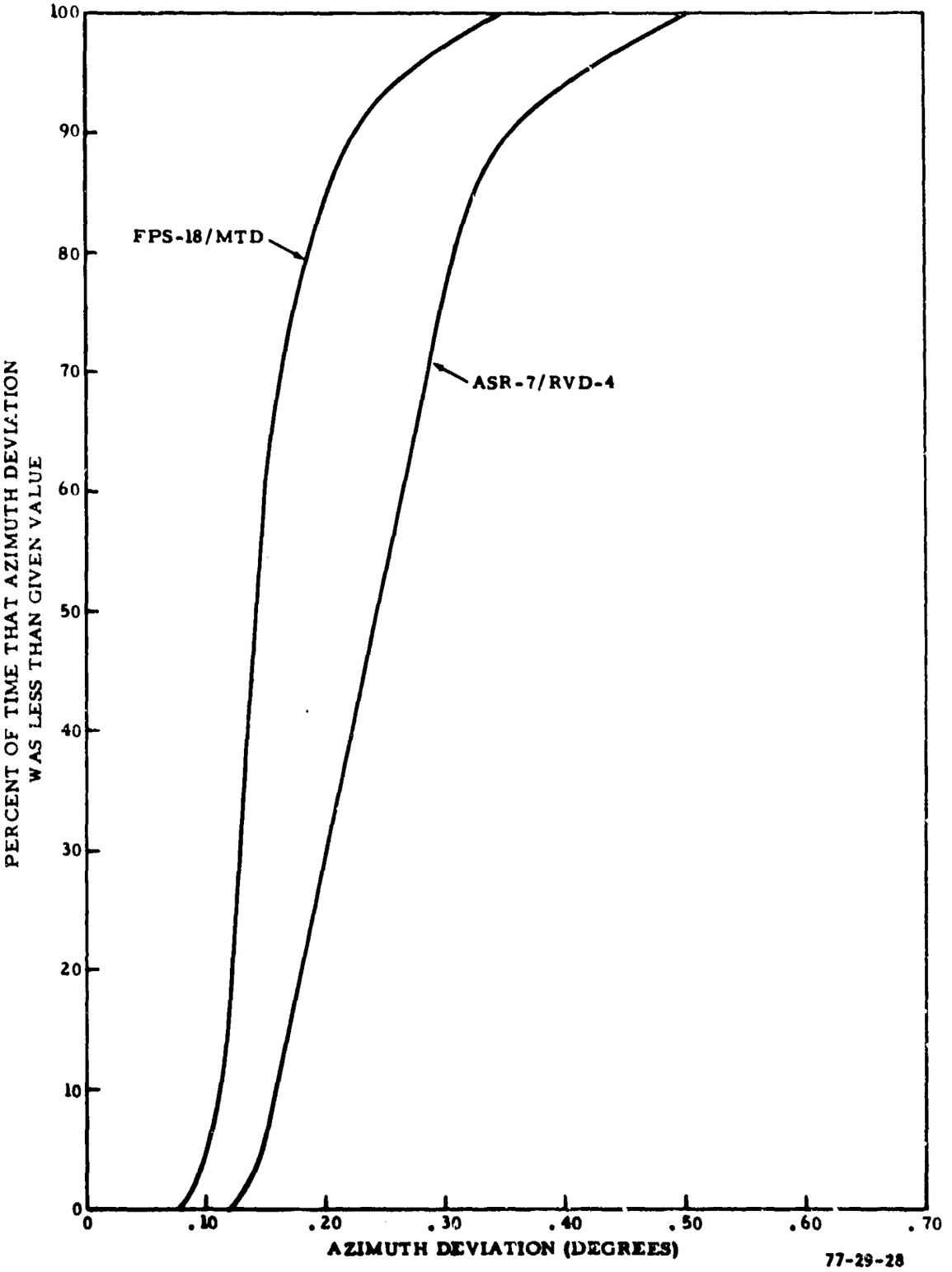

FIGURE 28. COMPARATIVE FREQUENCY DISTRIBUTIONS OF AZIMUTH ACCURACY

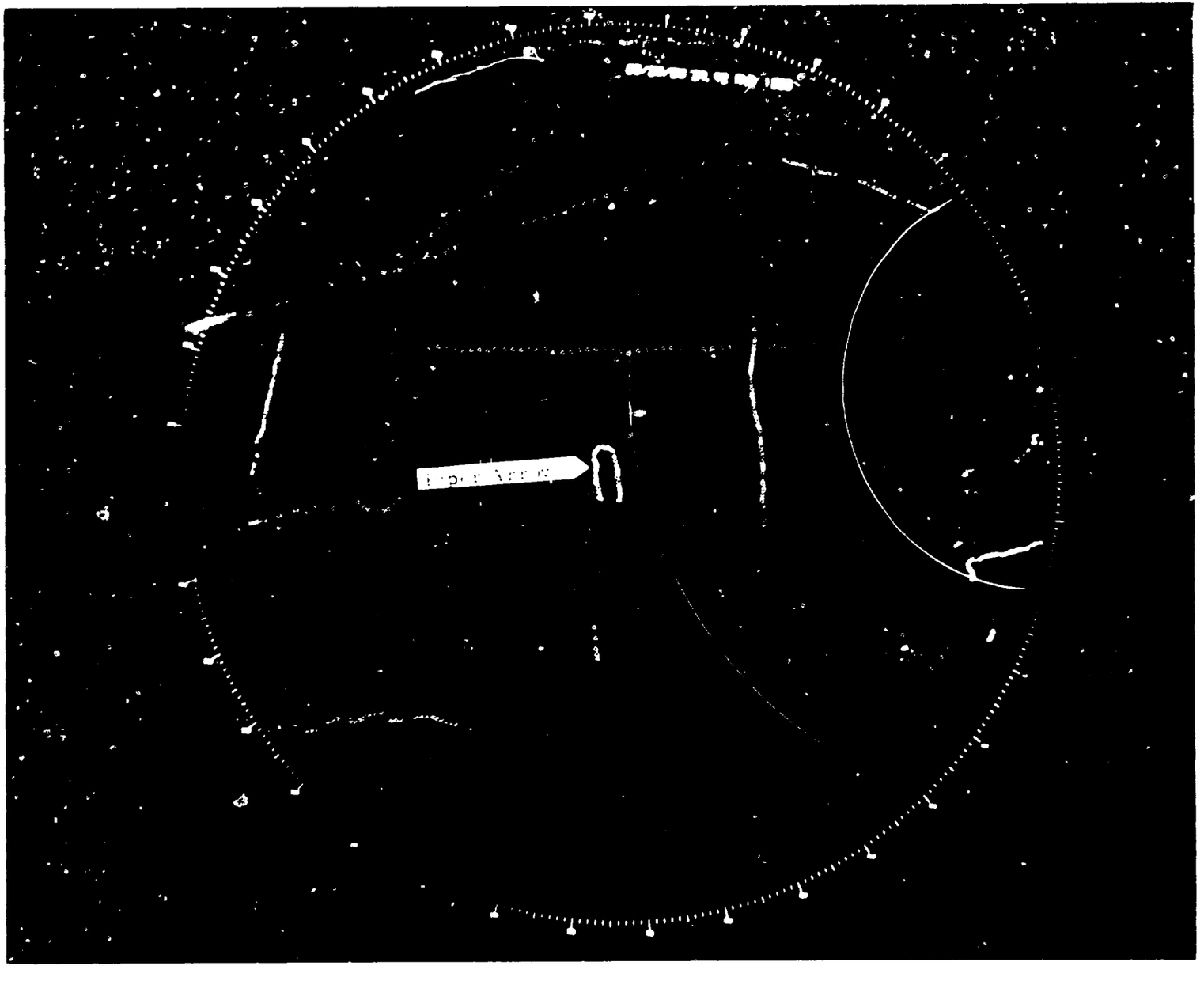

FIGURE 29. ASR-7/RVD-4 SYSTEM SENSITIVITY FLIGHT TEST (10-nmi Range Rings)

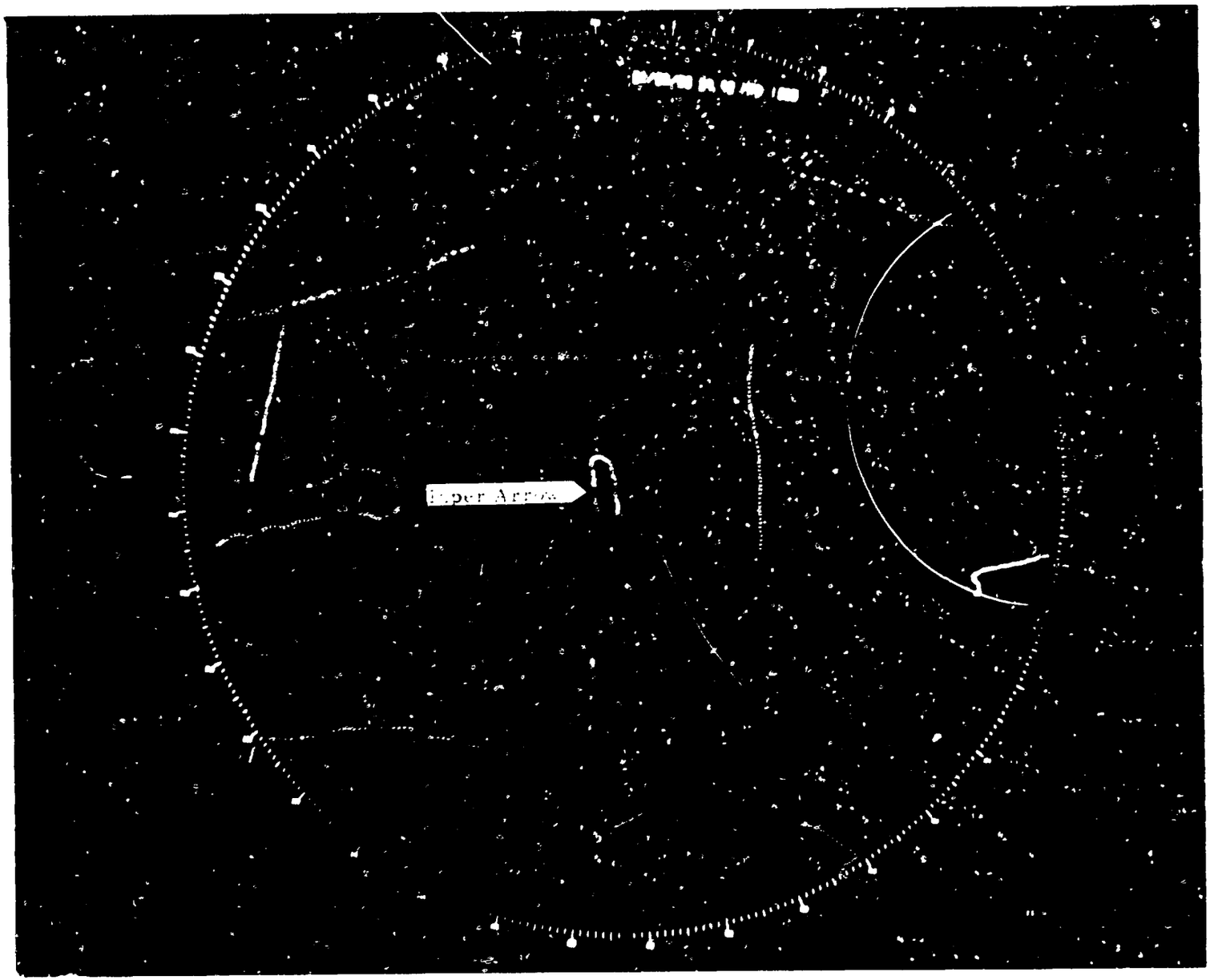

FIGURE 30. FPS-18/MTD SYSTEM SENSITIVITY FLIGHT TEST (10-nmi Range Rings)

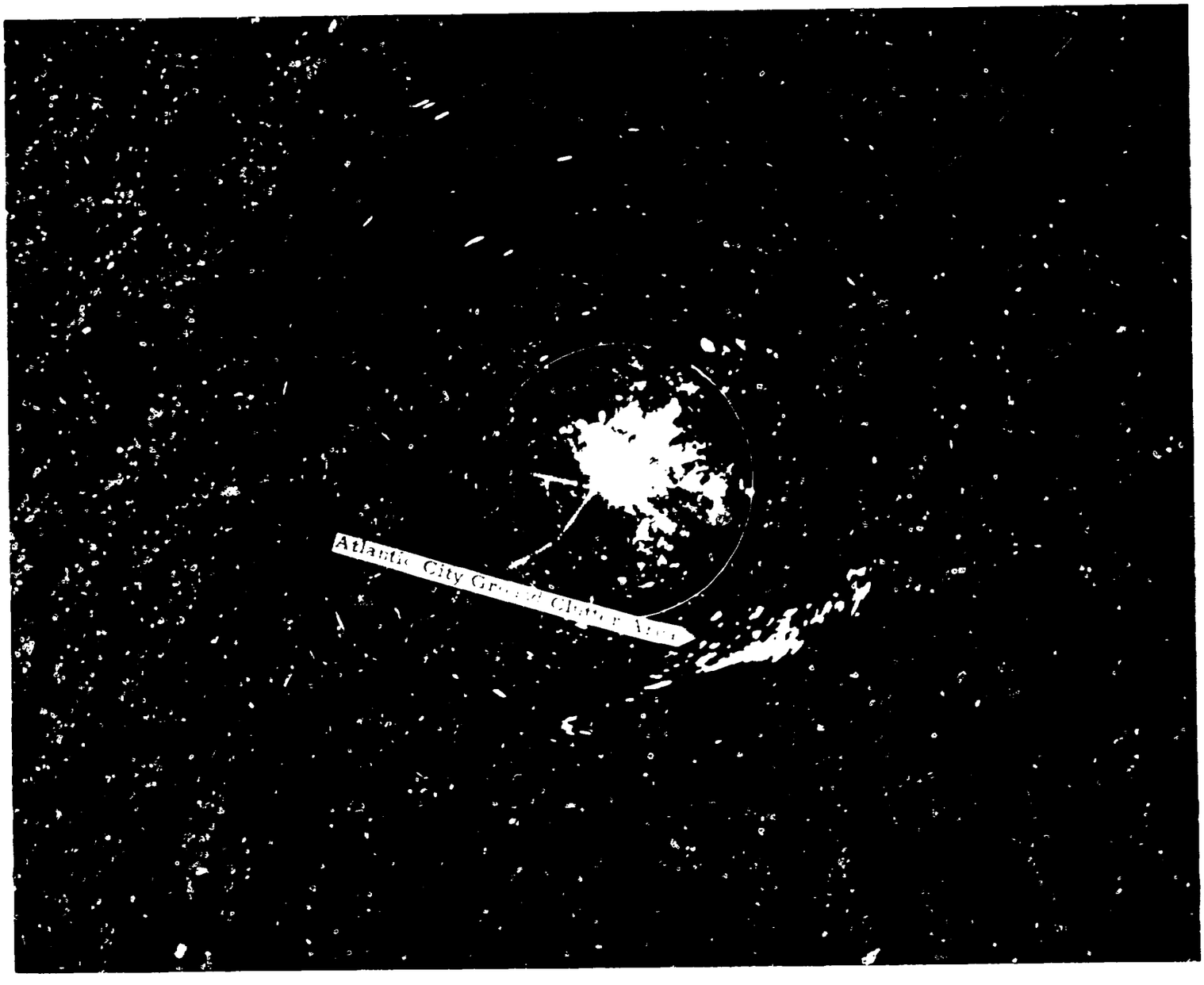

FIGURE 31. GROUND CLUTTER IN THE NAFEC/ATLANTIC CITY AREA (5-nmi Range Rings, 54-dB STC)

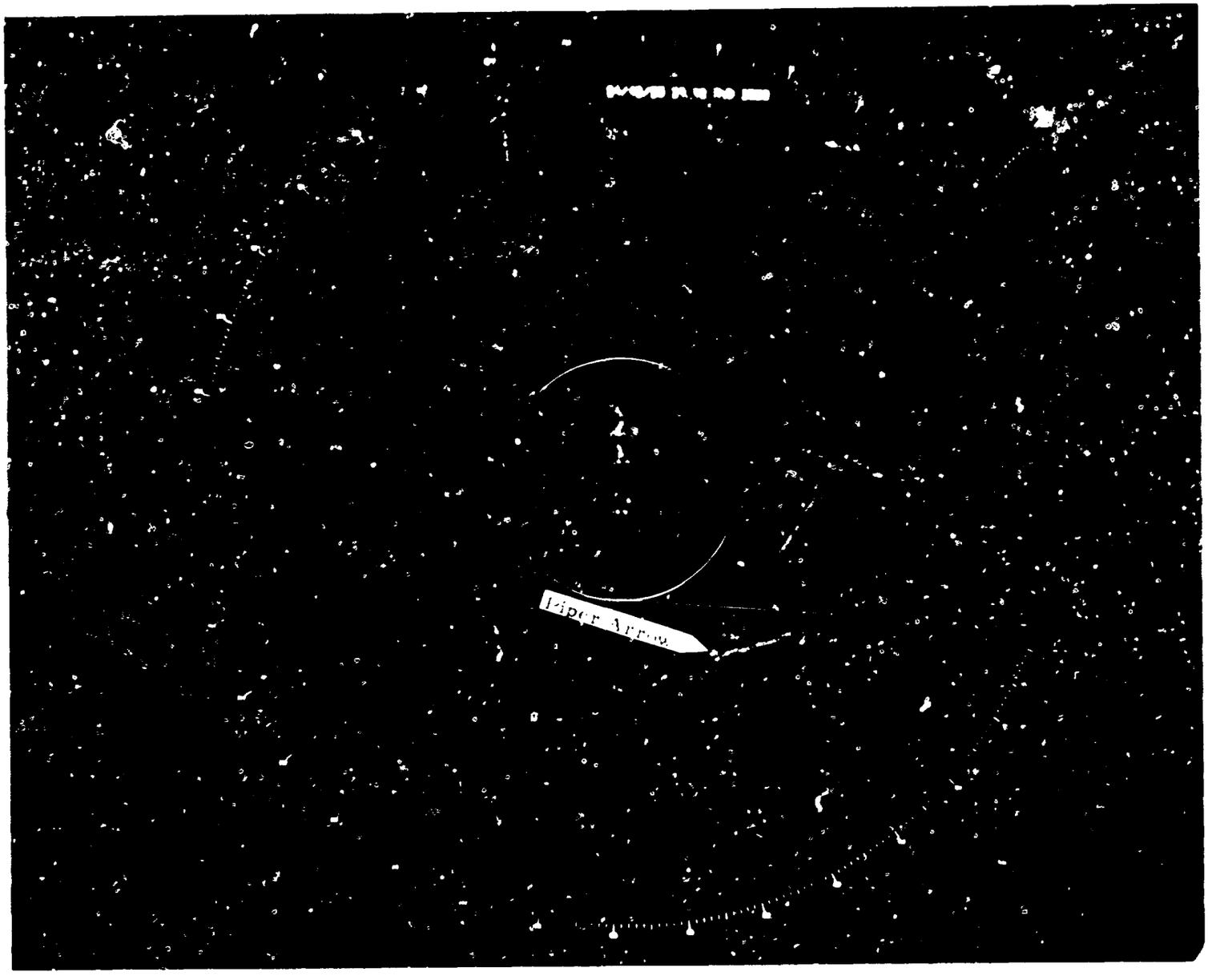

FIGURE 32. ASR-7/RVD-4 TANGENTIAL DETECTION IN CLUTTER (5-nmi Range Rings)

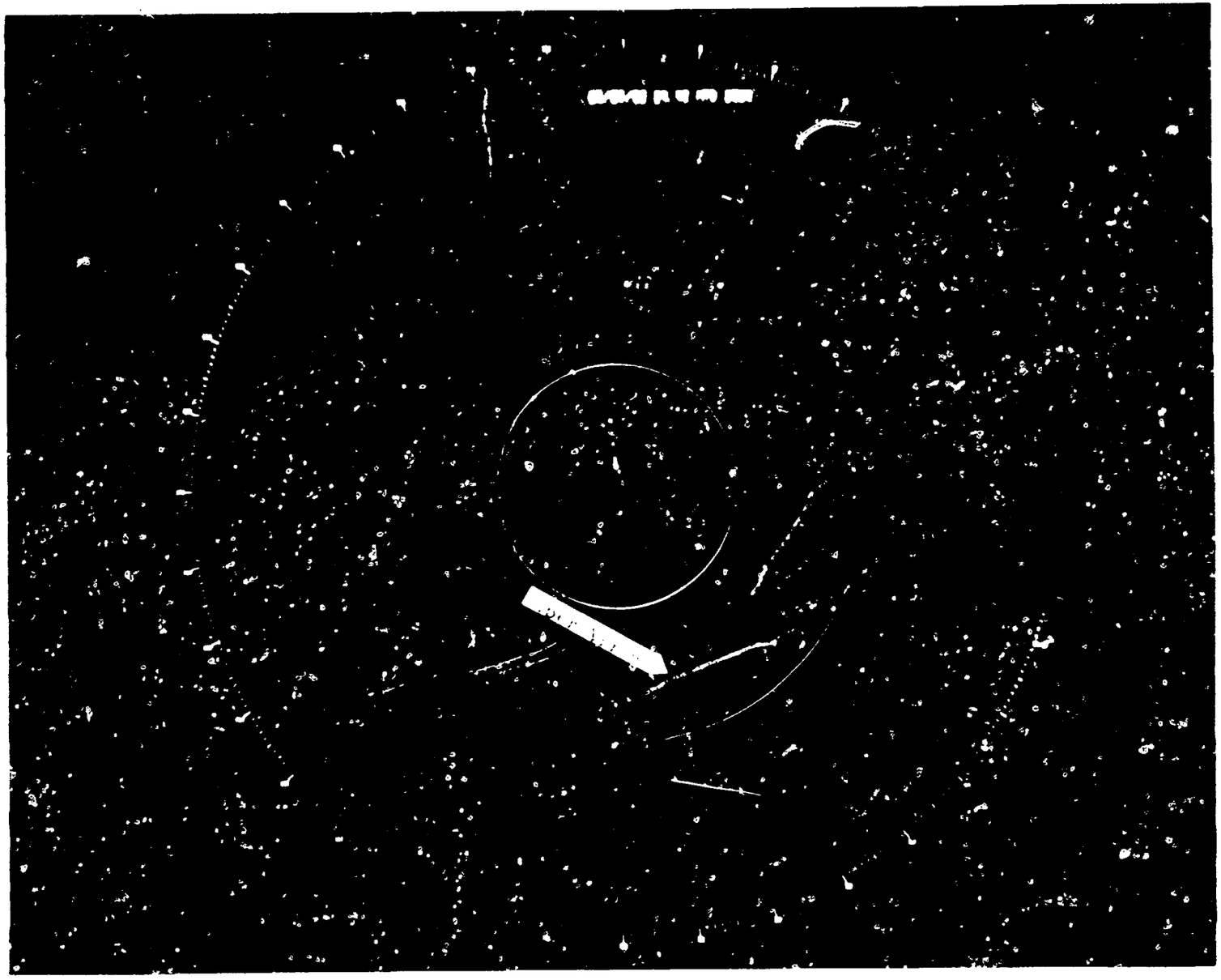

FIGURE 33. FPS-18/MTD TANGENTIAL DETECTION IN CLUTTER (5-nmi Range Rings)

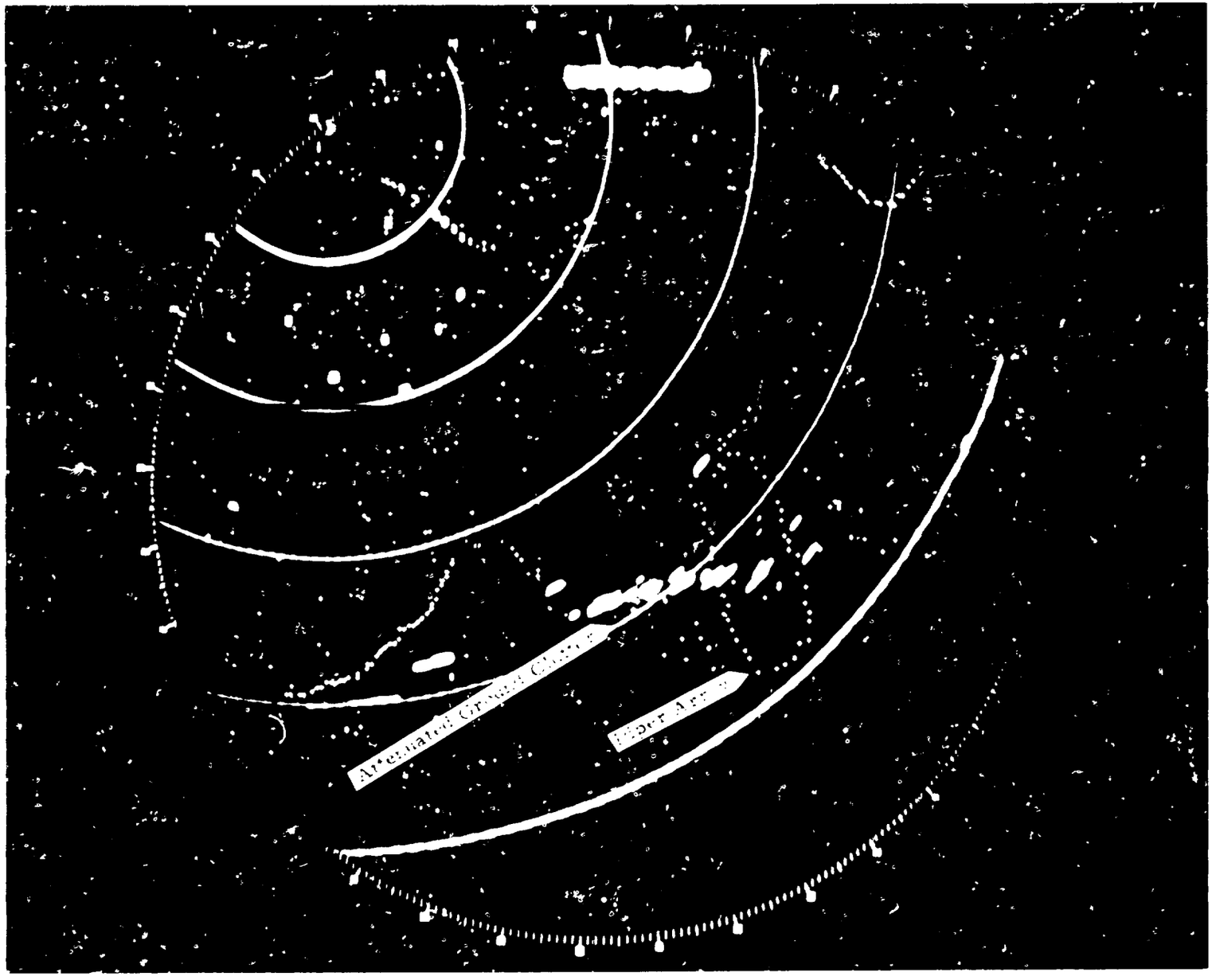

FIGURE 34. SCV TEST FLIGHT WITH SUPERIMPOSED ATTENUATED (25 dB) GROUND CLUTTER (2-nmi Range Rings)

FIGURE 35. FLIGHT TEST WEATHER (NORMAL VIDEO, 5-nmd Range Rings)

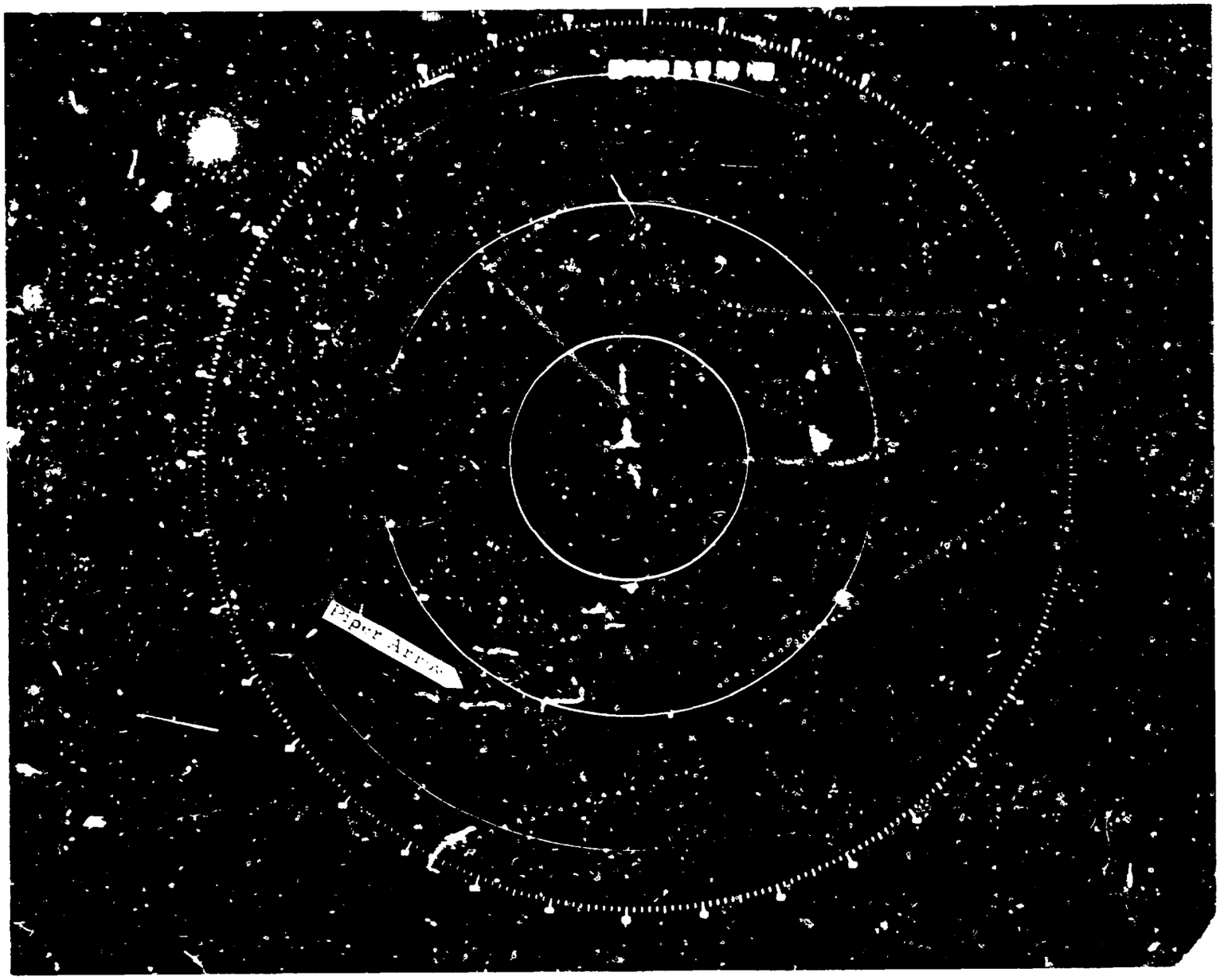

FIGURE 36. ASR-7/RVD-4 TARGET DETECTION IN WEATHER (5-nmi Range Rings)

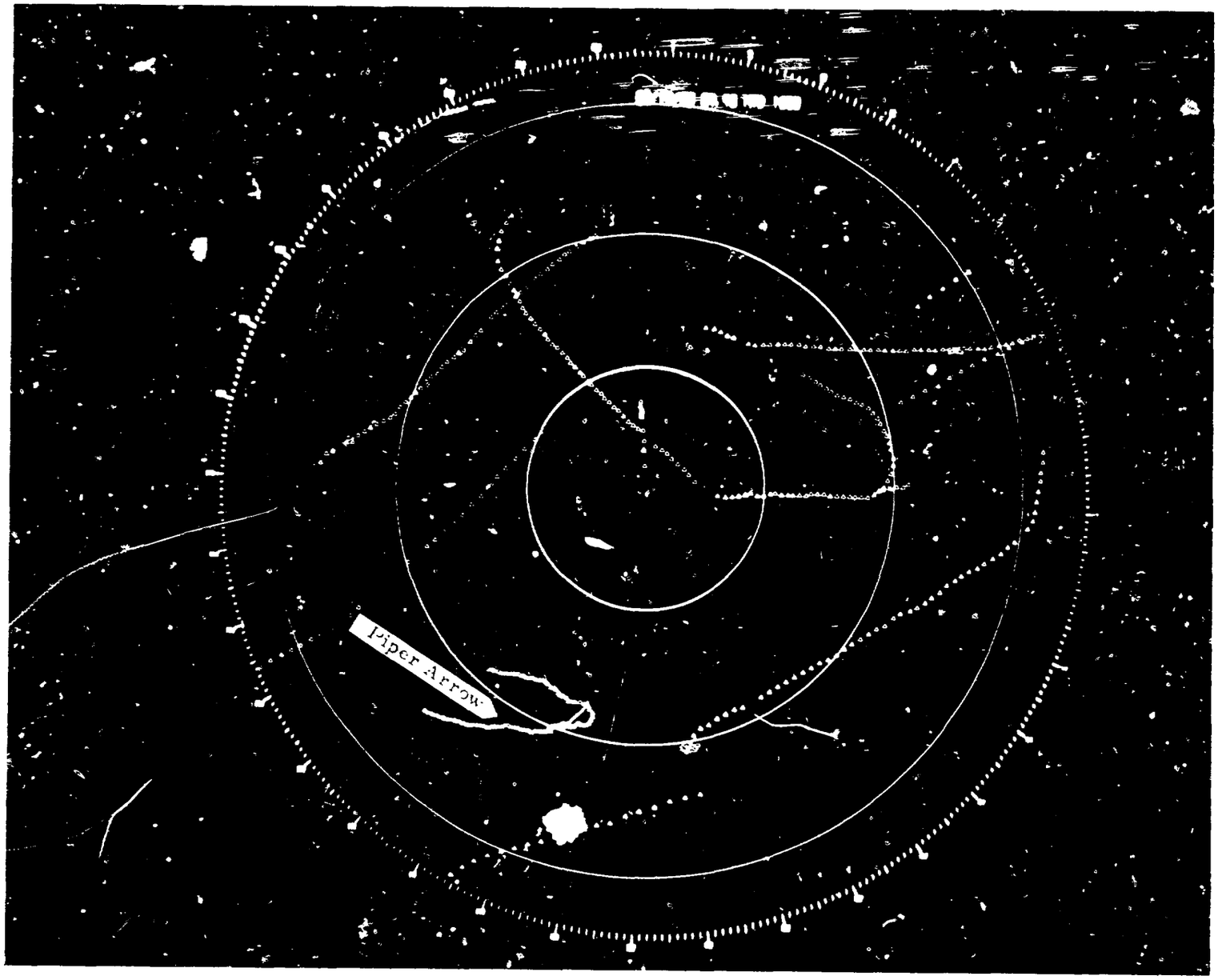

FIGURE 37. FPS-18/MTD TARGET DETECTION IN WEATHER (5-nmi Range Rings)

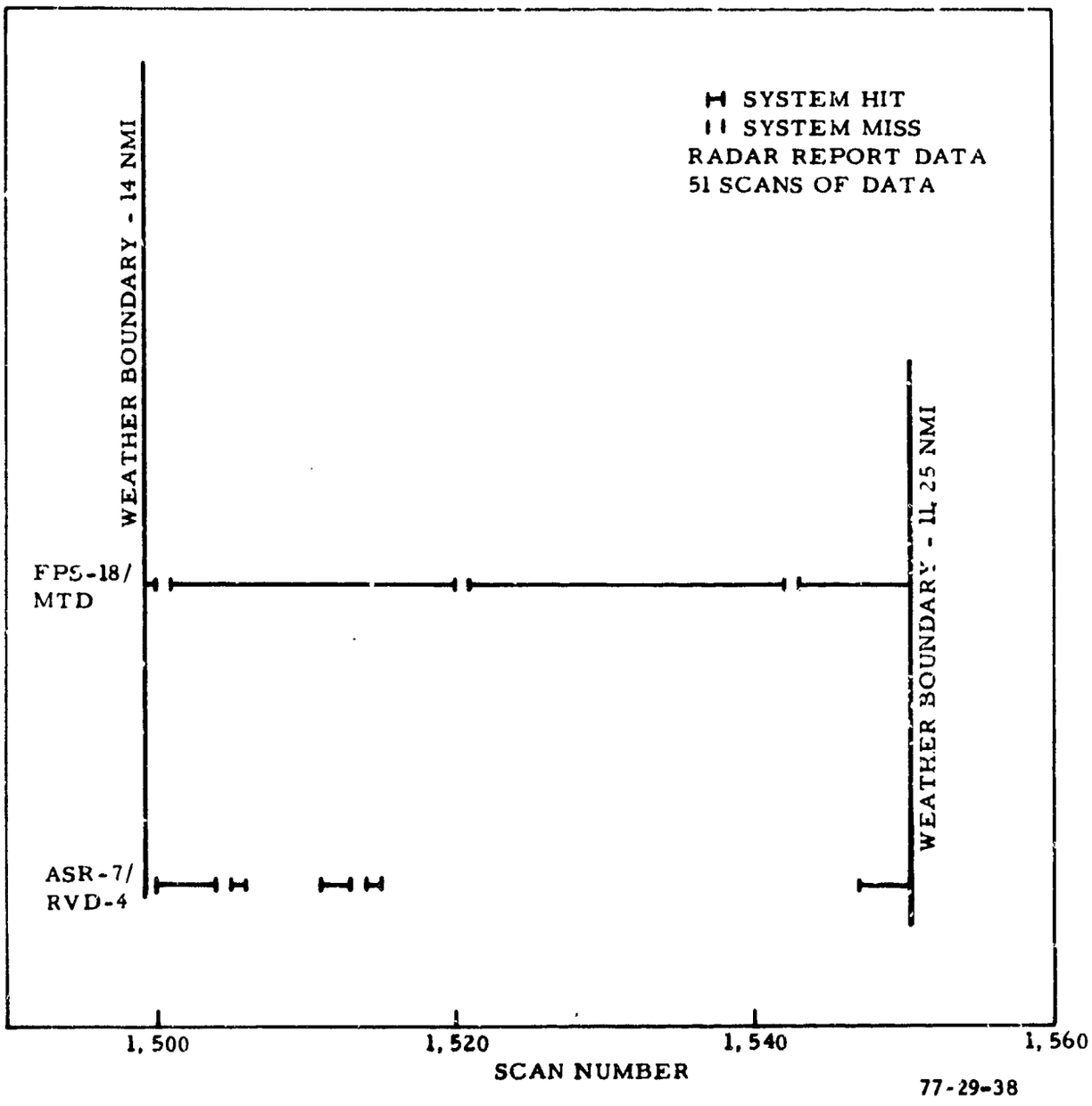

FIGURE 38. COMPARATIVE SYSTEM DETECTION IN WEATHER

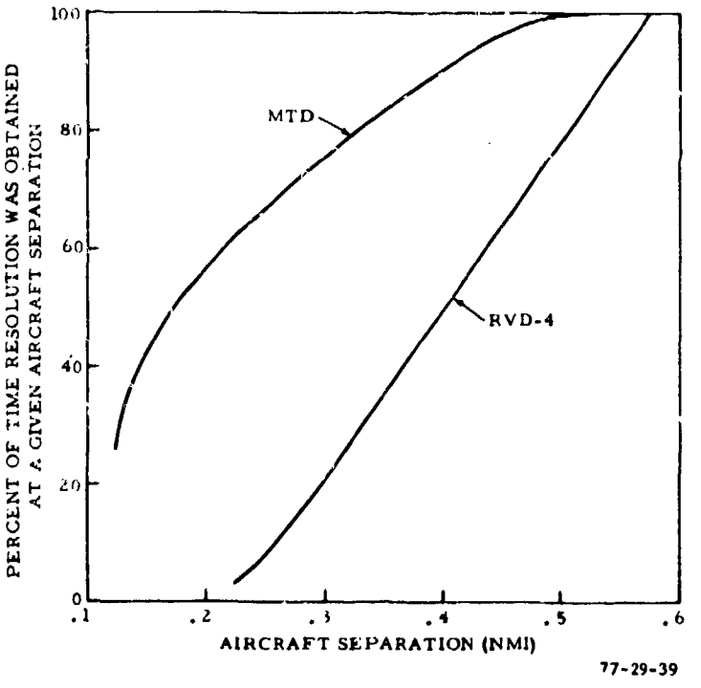

FIGURE 39. COMPARATIVE TARGET RESOLUTION CAPABILITY

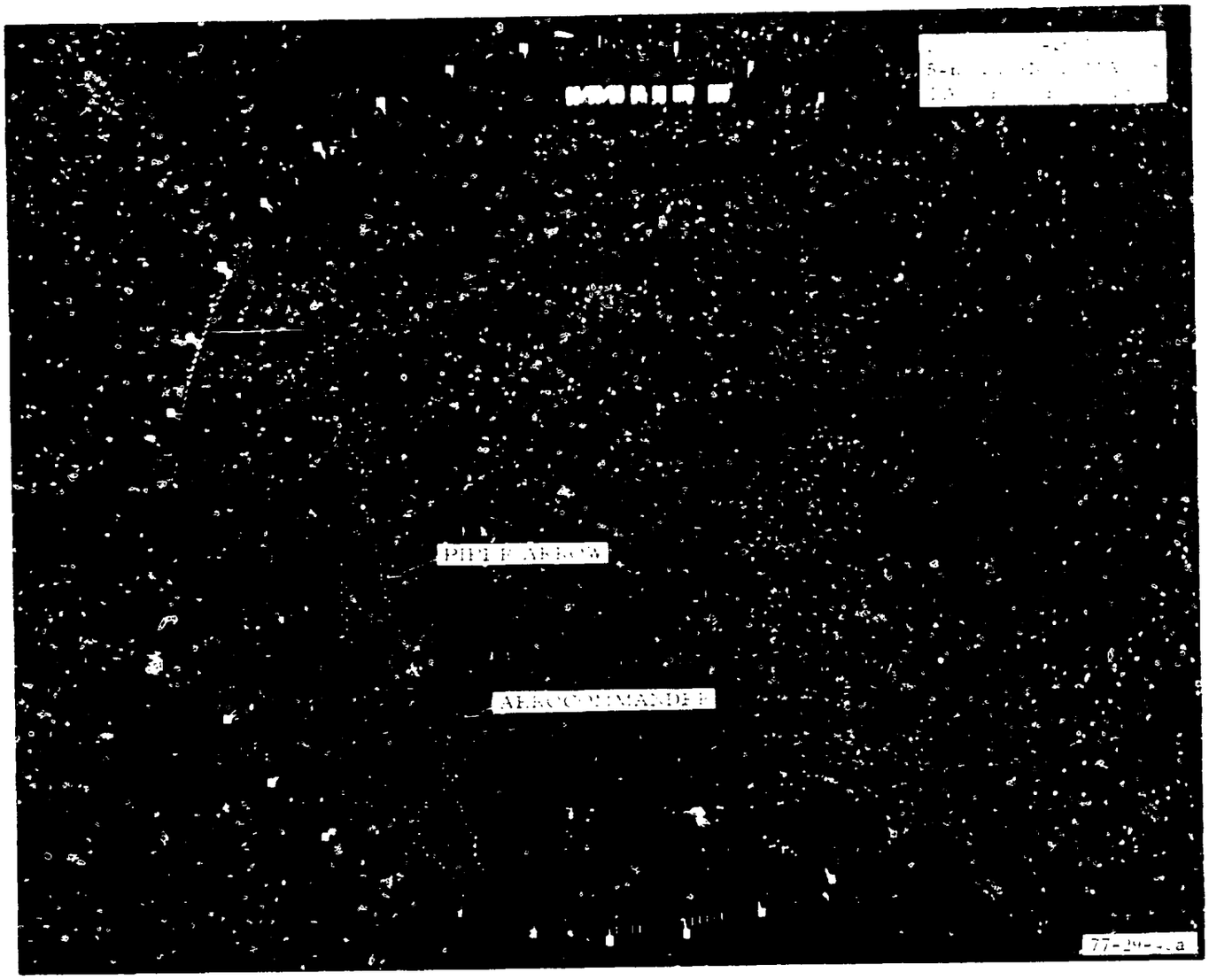

FIGURE 40. COMPARATIVE TARGET RESOLUTION CAPABILITY (Sheet 1 of 8)

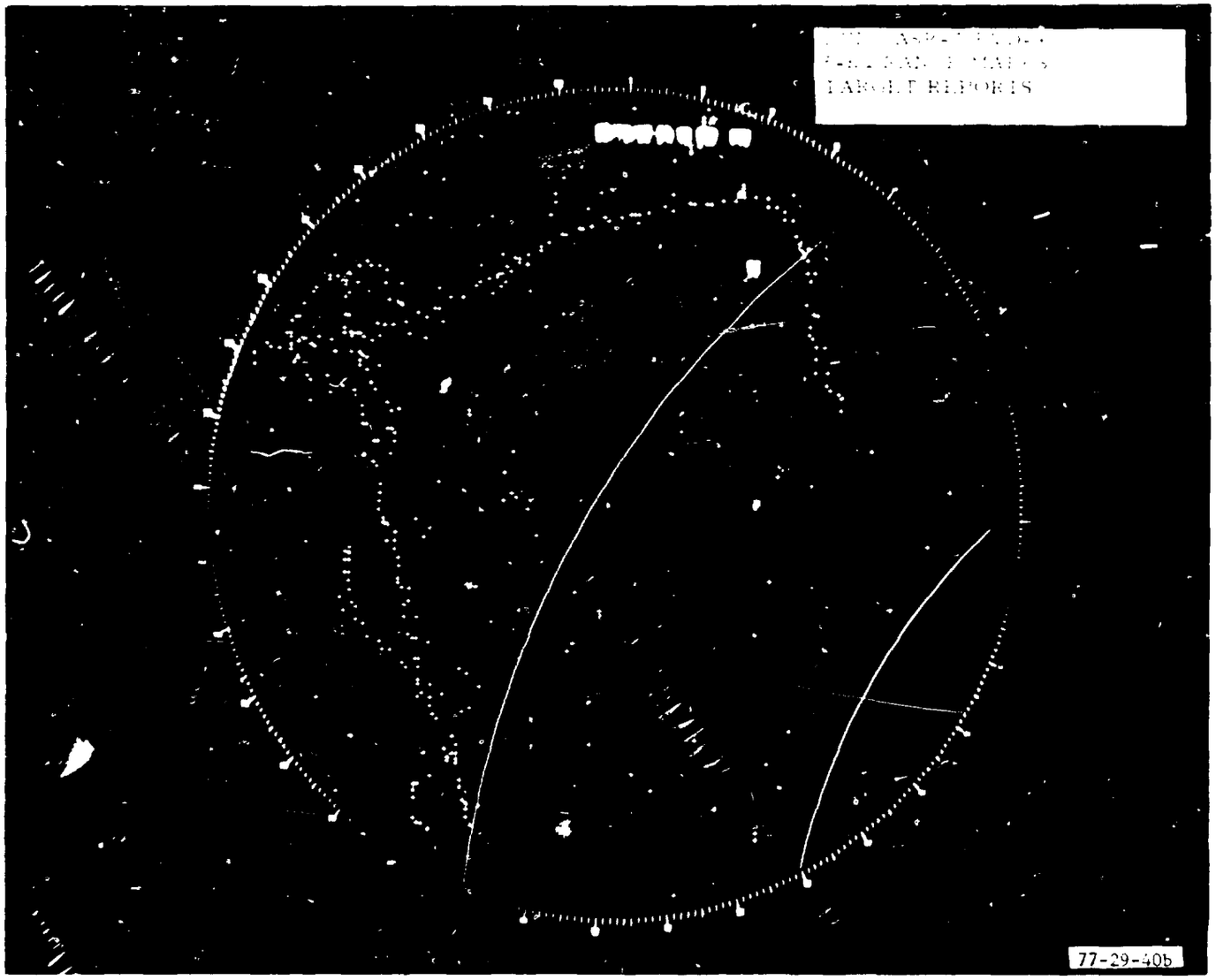

FIGURE 40. COMPARATIVE TARGET RESOLUTION CAPABILITY (Sheet 2 of 8)

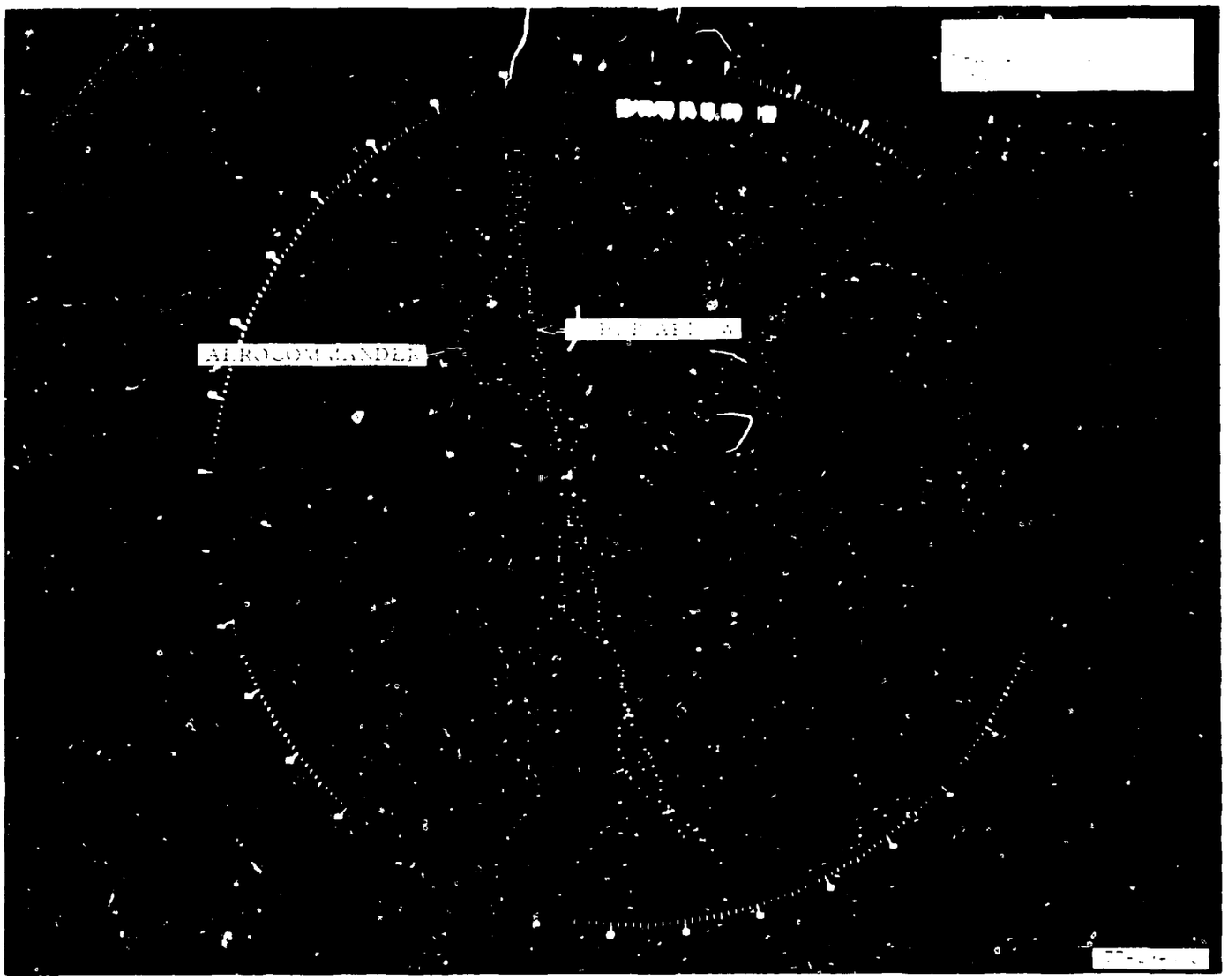

FIGURE 40. COMPARATIVE TARGET RESOLUTION CAPABILITY (Sheet 3 of 8)

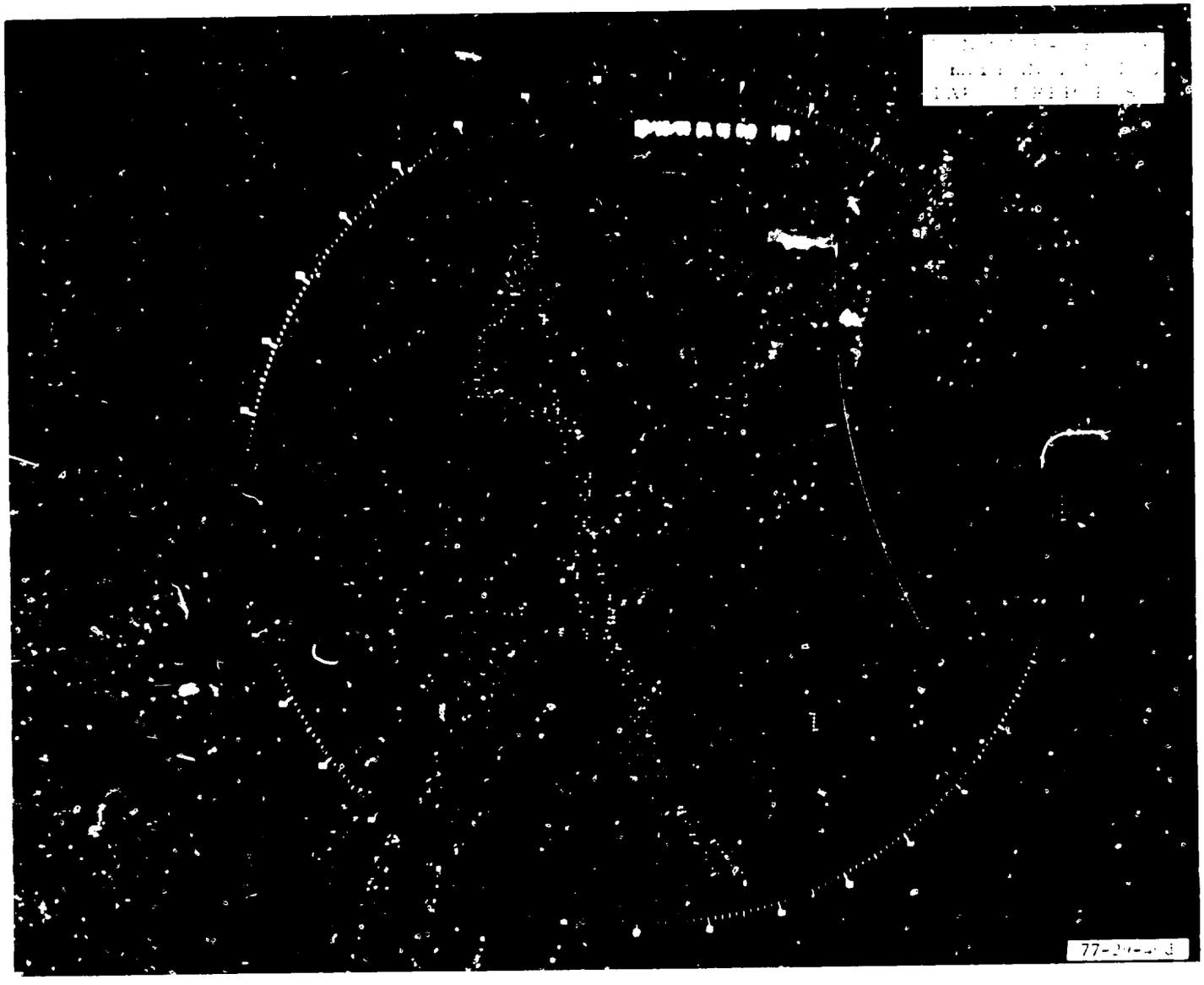

FIGURE 40. COMPARATIVE TARGET RESOLUTION CAPABILITY (Sheet 4 of 8)

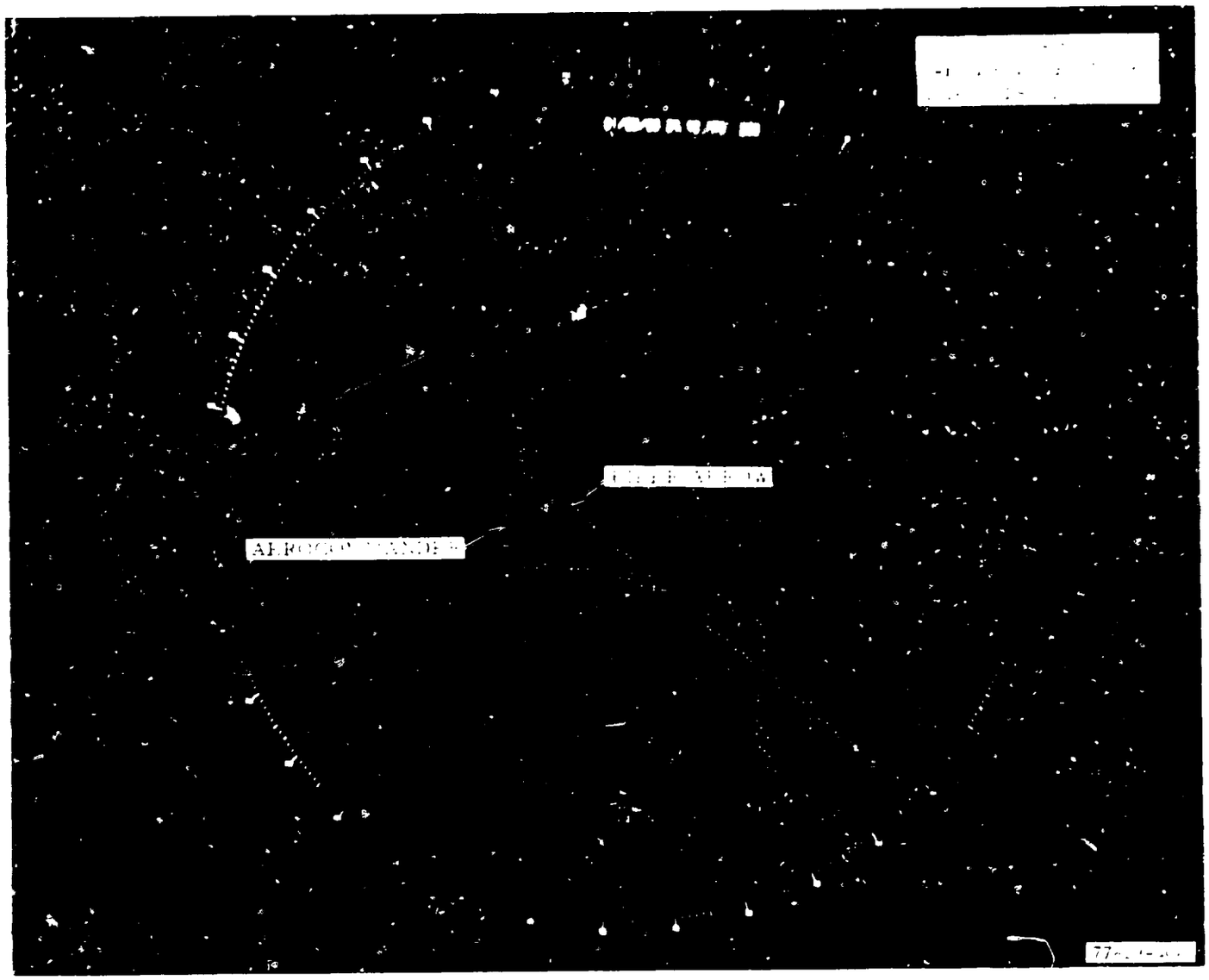

FIGURE 40. COMPARATIVE TARGET RESOLUTION CAPABILITY (Sheet 5 of

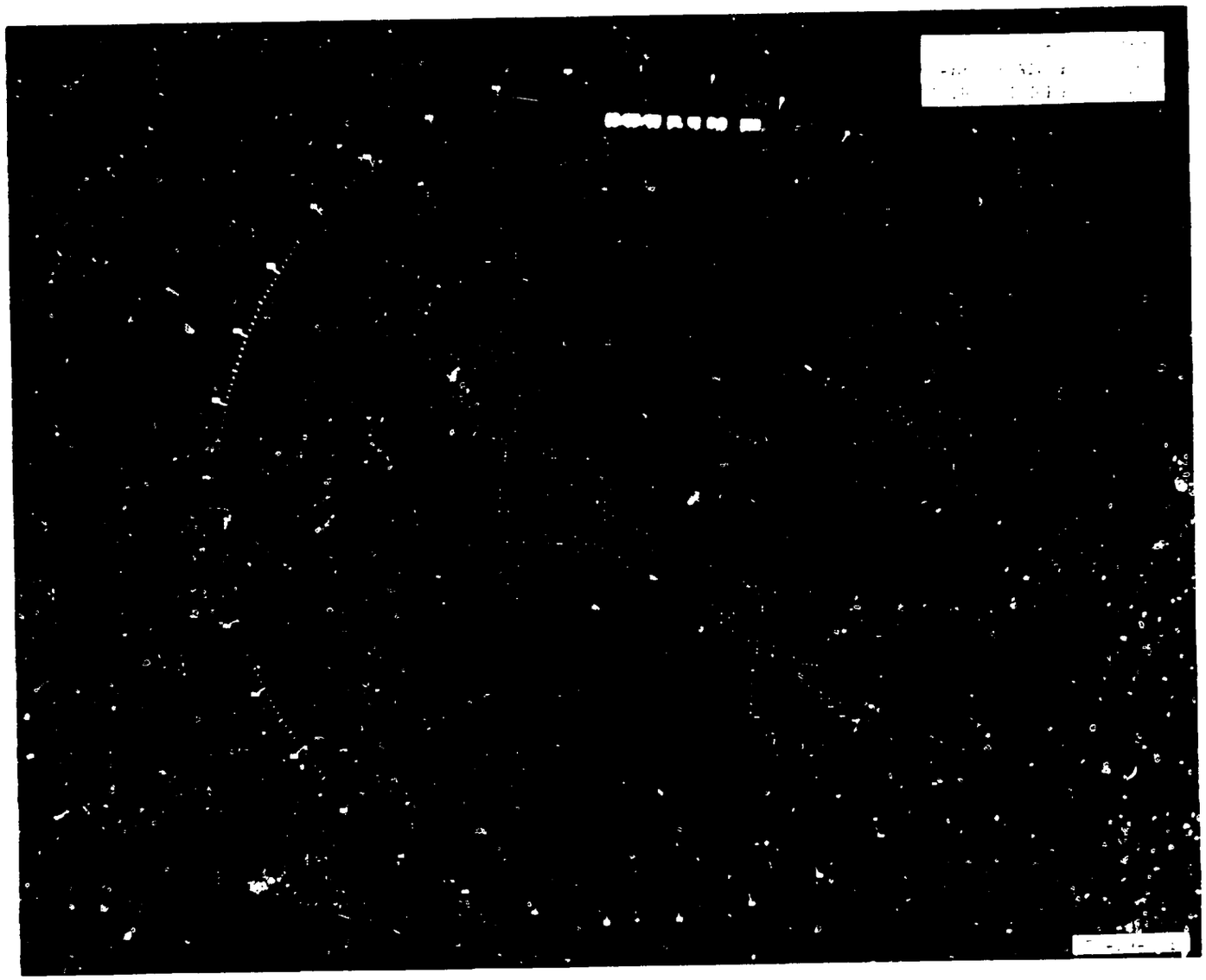

FIGURE 40. COMPARATIVE TARGET RESOLUTION CAPABILITY (Sheet 6 of 8)

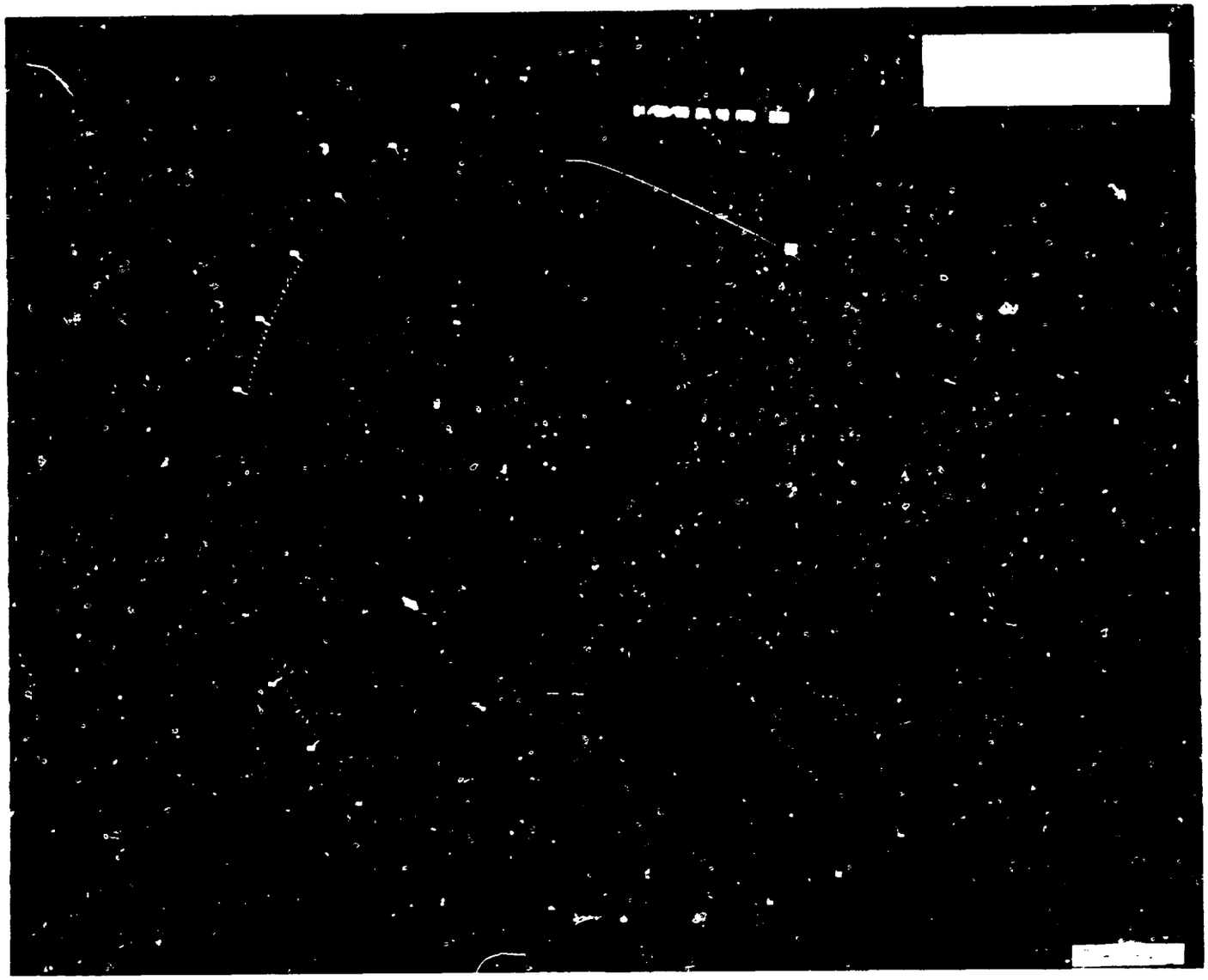

FIGURE 40. COMPARATIVE TARGET RESOLUTION CAPABILITY (Sheet 7 of 8)

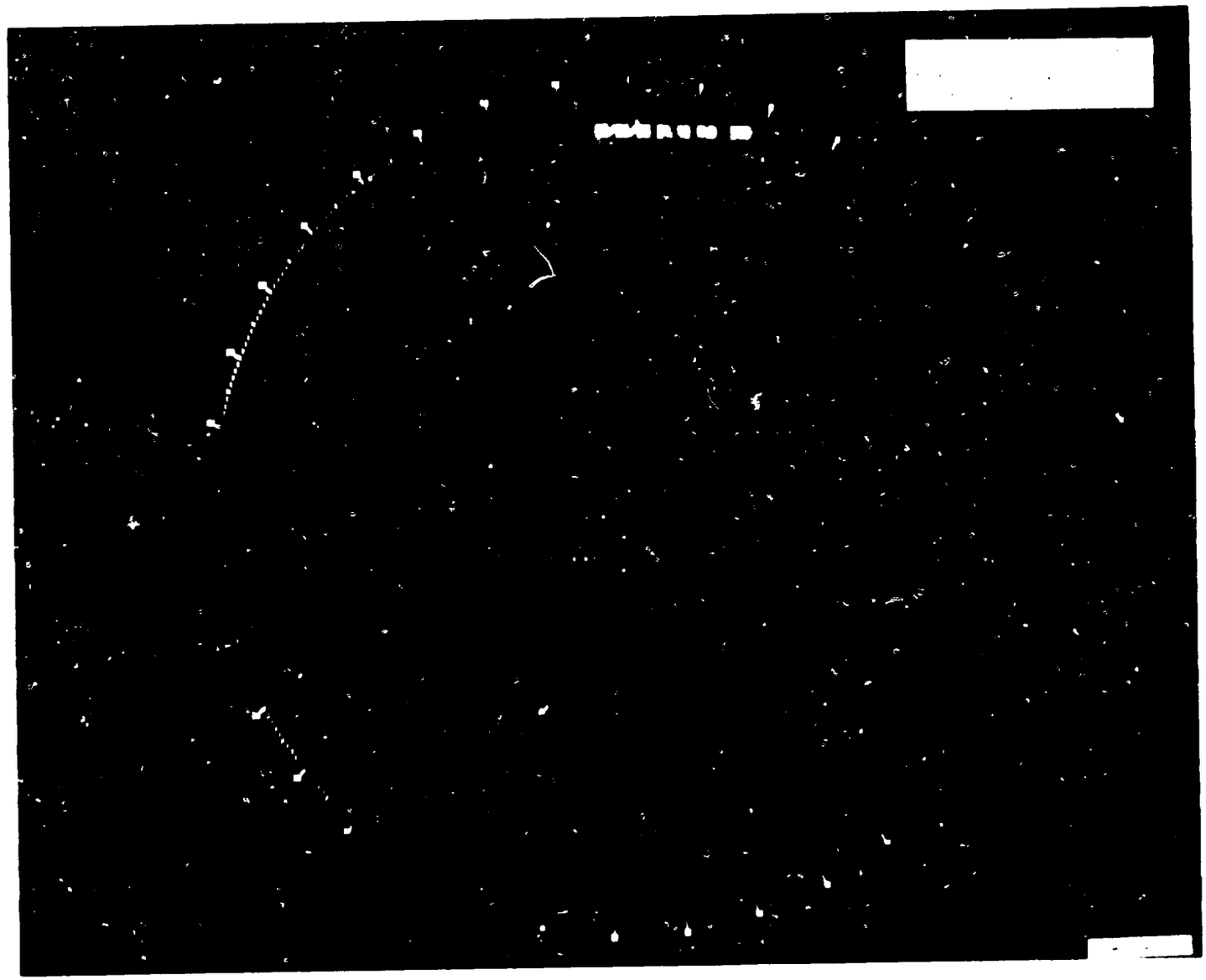

FIGURE 40. COMPARATIVE TARGET RESOLUTION CAPABILITY (Sheet 8 of 8)

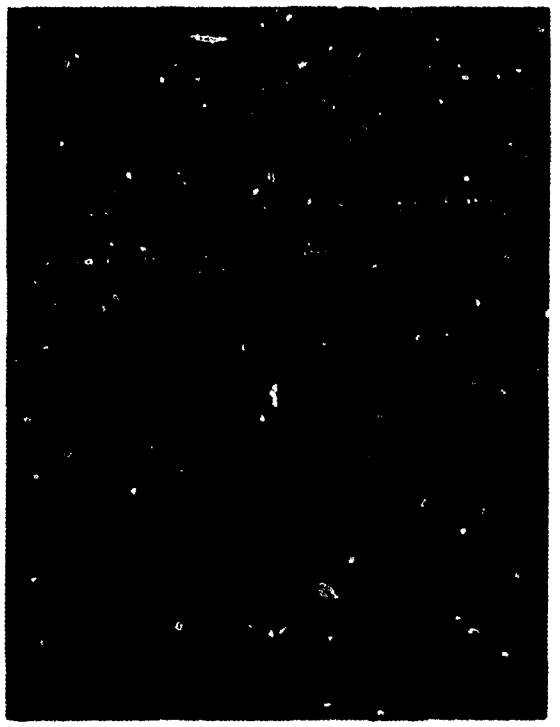

(a) ASR-5/MTD

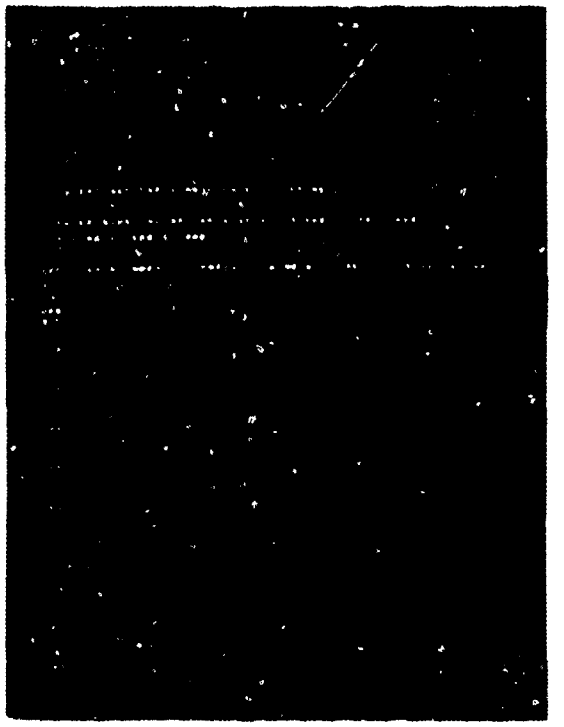

(b) ASR-7/MTD

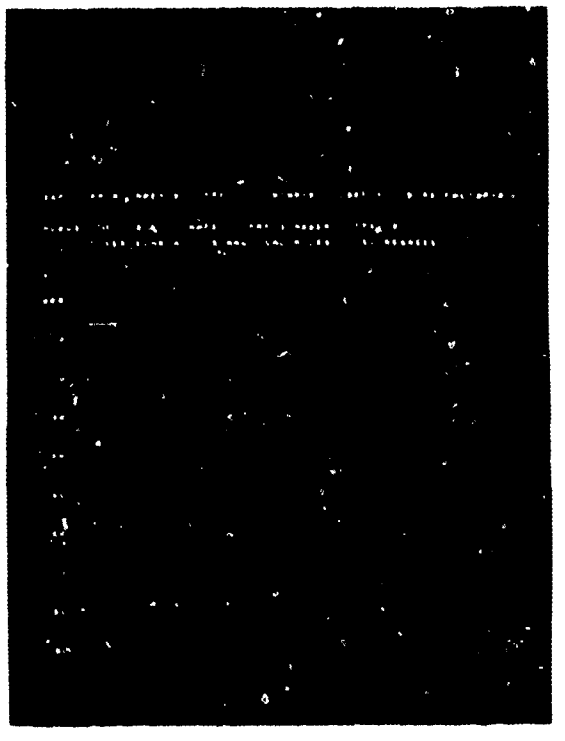

(c) FPS-18/MTD

FIGURE 41. SYSTEM STABILITY DETERMINED WITH SINGLE GATE PROCESSOR

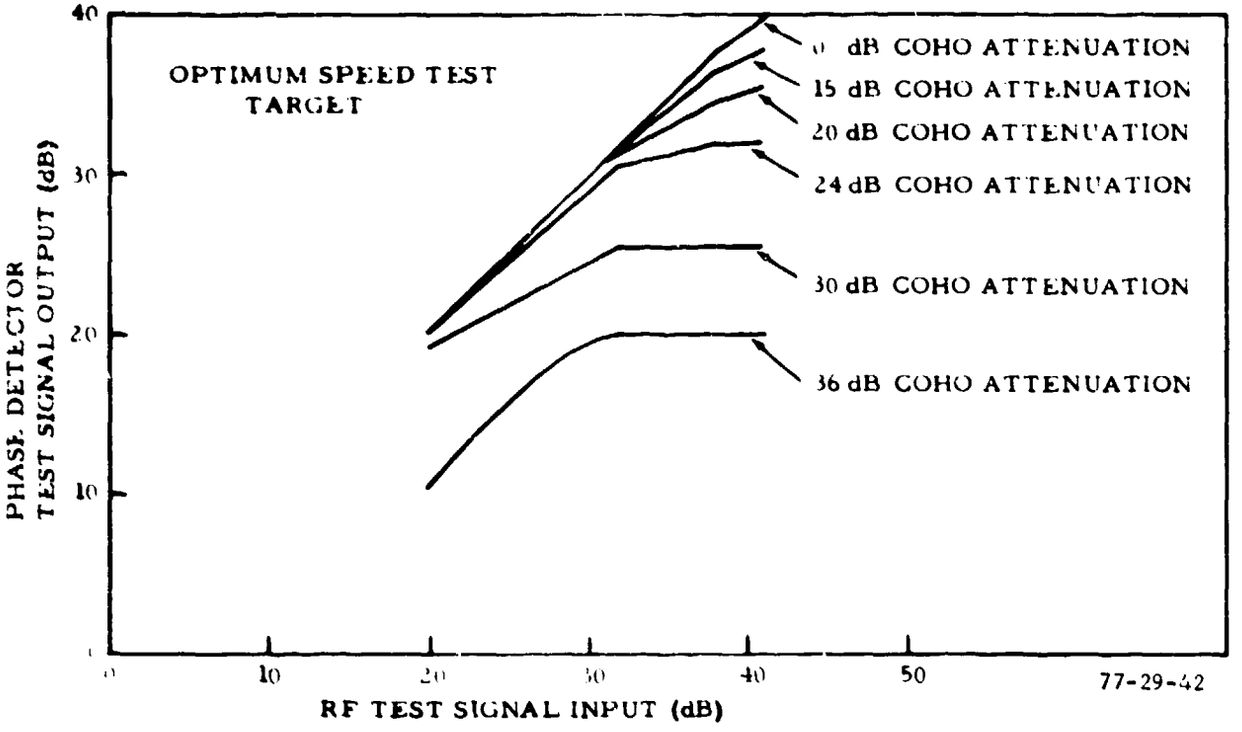

FIGURE 42. PHASE DETECTOR CONVERSION LOSSES

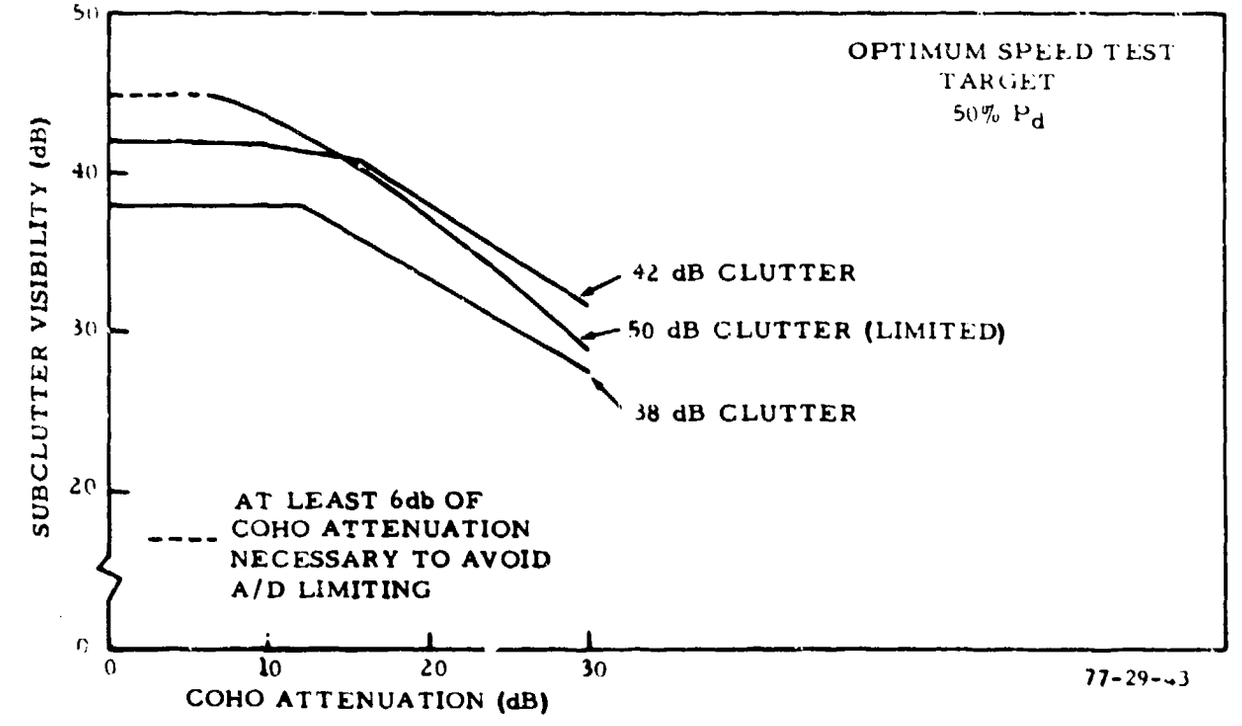

FIGURE 43. SUBCLUTTER VISIBILITY AS A FUNCTION OF COHO LEVEL

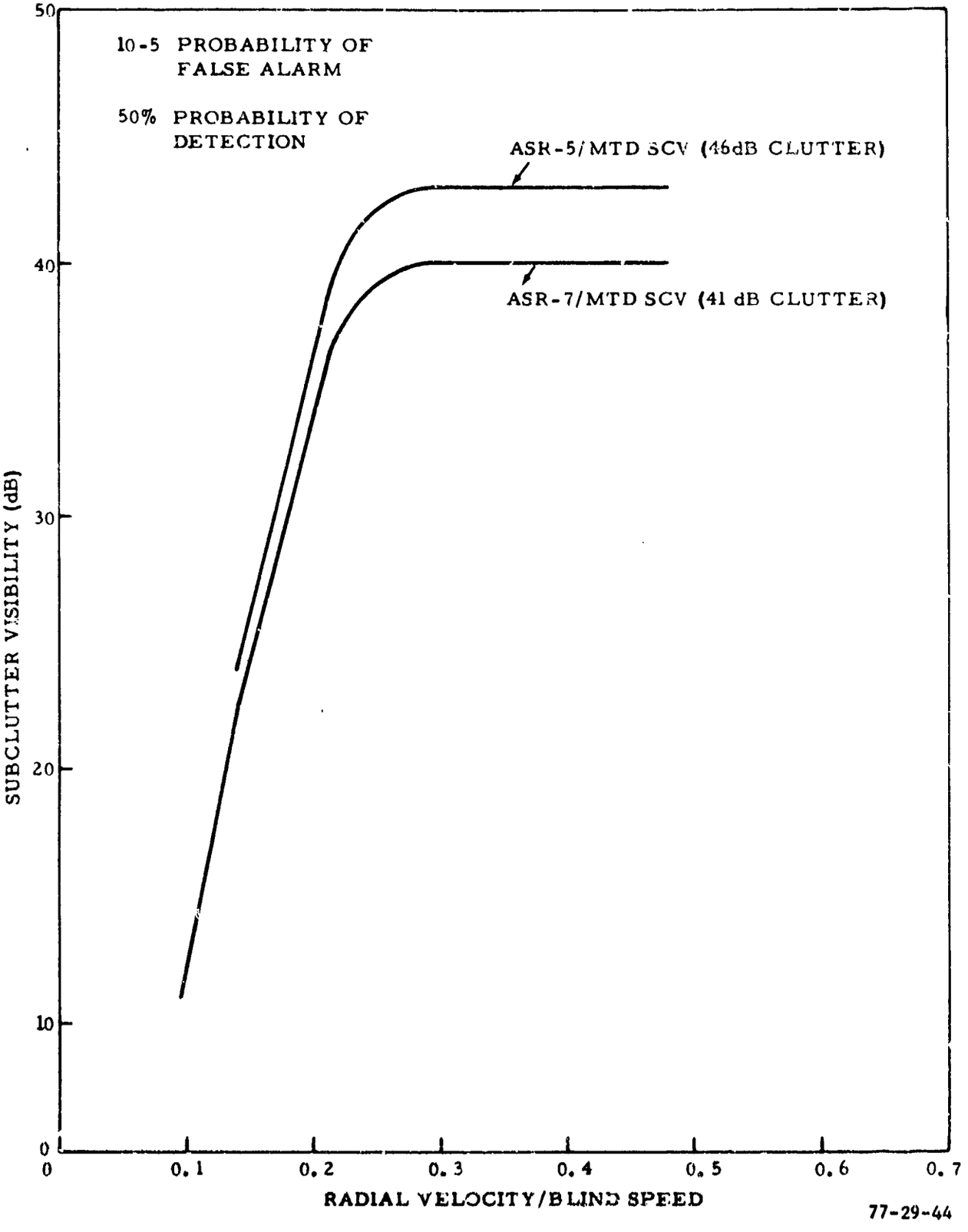

FIGURE 44. ASR-5 AND ASR-7 MTD SUBCLUTTER VISIBILITY

APPENDIX A

DESCRIPTION OF EQUIPMENT

APPENDIX A

LIST OF ILLUSTRATIONS

LIST OF TABLES

APPENDIX A

DESCRIPTION OF EQUIPMENT

The MIT Lincoln Laboratory MTD radar-signal processor (figure A-1) was a developmental system which was integrated into the existing TFAST (Terminal Facility for Automated Surveillance testing) at NAFEC. The sensor portion of the MTD was comprised of a modified Bendix FPS-18 S-band medium-power, short-range air search radar system previously employed in the SAGE system by the Air Force.

Important modifications to the radar analog system included the installation of a solid state receiver/exciter with additional filtering and regulation to the Klystron high-voltage power supply for improved stability. The thyratron modulator charging circuits were modified to allow for operation at variable pulse repetition rates. The receiver subsystem was redesigned to provide wide dynamic range, stability, and two-channel synchronous (quadrature video) detection.

The master timer for the radar transmitter was located in the MTD signal processor. It provided a 1-μs gated 30.987-MHz COHO signal, an HVPS gate, and a system trigger. The gated COHO signal was mixed with the 2741-MHz solid state crystal oscillator (STALO) to establish the basic radar frequency of 2710 MHz. The pulsed RF excitation signal was amplified through a Varian VA-87B water-cooled klystron which was modulated at intervals determined by the MTD timing and control unit.

Figure A-2 shows the signal flow of the receiver system. Received RF energy from the antenna/diplexer was channeled to a Hyletronics LS-25 microwave sensitivity-time control (STC) attenuator. STC timing was controlled by the digital control system through a D/A converter providing R^{-4} attenuation capability from 0 to 94 1/2 dB.

A standard ASR-7 parametric amplifier, tunable from 2.7 to 2.9 GHz, was installed after the RF STC unit to amplify incoming RF signals and provide an improved receiver noise figure.

The IF frequency was produced by mixing the 2710-MHz radar signal with the 2741-MHz STALO signal. A MPX2-4/2c RHG Electronics mixer-preamplifier was used to accomplish the mixing.

The MTD analog subsystem was assembled almost entirely from commercially available items. The low-pass filter which followed the double balanced mixers were fabricated by Lincoln Laboratory.

IF and COHO amplification was accomplished by using high-gain Avantek amplifiers, while IF filtering was achieved by using a CIR-Q-TEL 3.75-MHz(3-dB points) band-pass filter. IF signals were then distributed equally to the double-balanced mixers through a Merrimac PD-20-50 power divider. The COHO was fed to a Merrimac QHM-3-30 quadrature hybrid which established the 90°

phase difference necessary for in-phase and quadrature video detection. "I" and "Q" videos were channeled to the low-pass filters and then to the A/D converters.

The low-pass video filters were provided to filter out the excess noise passed by the wide IF band-pass filter. The in-phase (I) and quadrature (Q) bipolar video signals were sampled at 2.6 MHz rate by 10 bit, Computer Labs 5103, A/D converters. The sampled video was then interfaced into the MTD input processing logic.

A complete description of the MTD processor is contained in reference 1.

Figure A-3 shows the basic flow of MTD signals in the ARTS III system. Except for the new RIP and data extraction portions, standard TFAST ARTS III hardware and software were used. The data extraction capability shown in more detail in figure 4 (in the body of the report) produced magnetic extraction tapes and summaries of data as listed in tables A-1 and A-2.

A block diagram of the RIP is shown in figure A-4.

The MTD information to the RIP input buffer consisted of two 32-bit words. These were termed the PAS (PRF, azimuth, status) and VRS (velocity, range, strength) words. A PAS word occurred at the beginning of each CPI and provided basic information for processing VRS words within the CPI. Within the PAS word, the PRF field designated which one of four possible PRF's was used during the CPI. The azimuth field provided the CPI center azimuth data. The status field indicated whether the maximum of 40 target responses allowed in a CPI was exceeded and whether any communication problem existed between the MTD and RIP. The VRS word velocity and strength field contained the MTD Doppler filter number and amplitude of the target response. The range field contained the target position in range. A threshold field was included in the VRS word to define the levels of the weather and clutter thresholds.

The input control/buffer functions shown in figure A-4 provided the link between the MTD and the computer processing functions. These functions included the provision of synchronization between the MTD and the ARTS III and the detection of and response to parity error conditions. The input buffer contained 300 words of storage.

The CPI data consolidation function provided for the combining of multiple Doppler and range responses into a single response. Prior to the actual consolidation, normalization of the Doppler strengths was performed. This was made necessary by the effect of the three-pulse canceller preceding the DFT processor resulting in the lower velocity filters having a lesser output amplitude. This effect was discussed more fully in the body of this report under velocity response testing. Table A-1 contains the normalization factor for each filter. Normalization consisted of the division of the output of a filter by its normalization factor.

Following Doppler strength normalization, all adjacent Doppler responses at the same range were consolidated into a single response. For this purpose, Doppler adjacency was defined as occurring when signals within a CPI were in the same range gate and from adjacent Doppler filters. If an adjacency was found, an interpolated Doppler number and corrected strength value were determined as follows. First, determinations were made as to which of the multiple Doppler responses had the highest strength number and then as to which of the two possible adjacent responses had the larger strength. Then the following determinations were made:

1. A strength ratio was computed by dividing the selected adjacent normalized strength.

2. The Doppler was interpolated to six-bit accuracy (0-64) from table A-2 using Doppler filter numbers and strength ratio.

3. The strength of the largest response was corrected for off-filter (non-centered) loss by dividing it by correction factor from table A-2.

If a single isolated response was obtained (no adjacencies), the response was assumed to represent the maximum response of the Doppler filter identified by the VRS word. An interpolated Doppler number was derived from table A-2 using the Doppler number and a strength correction factor of unity.

The above consolidation procedure resulted in a single response with an interpolated Doppler number, normalized and corrected strength, range, threshold indicator (clutter or weather), and a count of the number in the range cell.

Range consolidation combined Doppler-consolidated responses satisfying the following range/Doppler adjacency criteria into a single response. Range adjacency was obtained when two responses occupied adjacent range gates (1/16-nmi separation). Doppler adjacency was obtained when two responses had an interpolated Doppler number separation of less than four (the 0 and 64 interval numbers were also adjacent). When two responses satisfied the above criteria, they were assumed to represent the same target, and the one with the largest target strength was selected as the output. Responses without adjacencies were passed directly to the output. The number of VRS words associated with a consolidated response was indicated by quality bits. Azimuth and PRF information were added to the output to complete the target response data.

Following CPI data consolidation, target record processing was performed. This function created or updated records of target data using the target response data. Each CPI's consolidated response data were entered separately. When the processing began with data from a new CPI, all target records from previous CPI's were located in target store A. The target record processing routine first performed a correlation between these records and the new consolidated response data on a comparative range basis. The basic operation performed for the match/no match determination is described below:

1. Match condition - Existing record and new data (within 1/16-nmi) were merged and updated into a new record and stored in record store B.

2. Miss Update - No new data to match existing record data. The record was updated to show the miss and put in record store B.

3. New target - No existing record to match new data. A new record was generated and put in store B.

4. Target report - Initiation of target finalization occurred when there were two consecutive misses (no target response for two information occurred in CPI's) or when information occurred in seven successive CPI's.

The target finalization routine processed completed target records into target reports or noise responses. The routine first checked the record bit count to determine the type of processing required. A bit count of 1 represented either a noise response or a single-CPI target response. Such a record with a quality number of zero was considered to be from a noise response and was entered in the noise count store. Those with a quality of greater than zero were considered to be from a valid target, and their range, strength, azimuth, and Doppler data were used to make up a target report. As a selectable option, all single-CPI records could be processed into noise responses.

A hit count greater than 1 (multiple-CPI responses) was processed as follows. The target record content was examined to determine which responses belonged together as representing data from the same target. Within a CPI, records with an interpolated Doppler number separation of less than 4 were considered to be from the same target. Responses from adjacent CPI's were then associated together to form a final set representing the target.

The target record was then completed by computing and entering its velocity and center azimuth. The velocity was computed using the Doppler information in the target records. The center of azimuth was computed by applying the formula:

$$\overline{AZ} = \sum_{k=1}^{N} \frac{[AZ(K)][S(K)]}{\sum_{k=1}^{N} s(K)}$$

where:

$\overline{AZ}$ = the target report azimuth
AZ(K) = the azimuth position of the K^{th} CPI response (from the target record)
S(K) = the corrected strength values of the responses (from the target record)
N = the number of responses in the target record

The resulting output was a 12-bit azimuth word to the target report store. The finalized target reports contained range, azimuth, strength, number of CPI's involved, and Doppler filter numbers.

Second-level thresholding was adopted to remove residual clutter signals, thereby utilizing the maximum sensitivity of the radar for track initiation. This thresholding was fully automatic and adaptive to the radar environment (weather, angels, inversion, etc.).

The algorithm employed divided the surveillance area (48 nmi) into 4 nmi by 22.5° sectors for a total of 192 sectors. Each sector contained eight independent thresholds (one for each MTD Doppler filter) yielding a total of 1,536 thresholds. The 48-nmi coverage area was further divided into two zones. The first zone extended from range zero to 16 nmi. This zone size was decided upon, since it contained most of the return from clutter experienced in the NAFEC radar environment. The second zone extended from 16 nmi to 48 nmi.

The adaptive threshold in each sector/Doppler filter was derived from the number of single CPI's it contained. These threshold levels were derived as described in the body of the report.

The thresholds were applied according to major range zone number. In the first zone (0 nmi to 16 nmi), all MTD replies were tested (by strength number) at the RIP input to determine if they exceeded the pertinent sector/Doppler filter threshold levels. In the second zone, only single-CPI replies were tested against the thresholds.

To initiate a track in the first zone, a target report was required to contain replies from at least two CPI's to have a tracker velocity of at least 50 knots and a scan history of three scans. However, single-CPI target reports were used for updating existing tracks.

All of the previous conditions for tracking were also required in zone two, except that track initiation was possible using single-CPI target reports.

Nonsynchronous interference detection and rejection was implemented in the RIP. The MTD employed an interference rejection algorithm as previously described. However, when interference and ground or weather clutter signals were concomitant, the algorithm did not function properly.

Interference signals were found to occur in one CPI and multiple Doppler filters. Being random in nature, they did not activate the second-level thresholds. To prohibit the interference from initiating false tracks, the number of single-CPI reports in each 5° by 48 nmi sector of the radar coverage area were counted. When this number exceeded a threshold value of 15, track initiation in that sector by single-CPI targets was prohibited. This effectivity eliminated track initiation by nonsynchronous interference. The radar/beacon correlation, tracking, and display functions shown in figure A-1 were accomplished using existing ARTS III software.

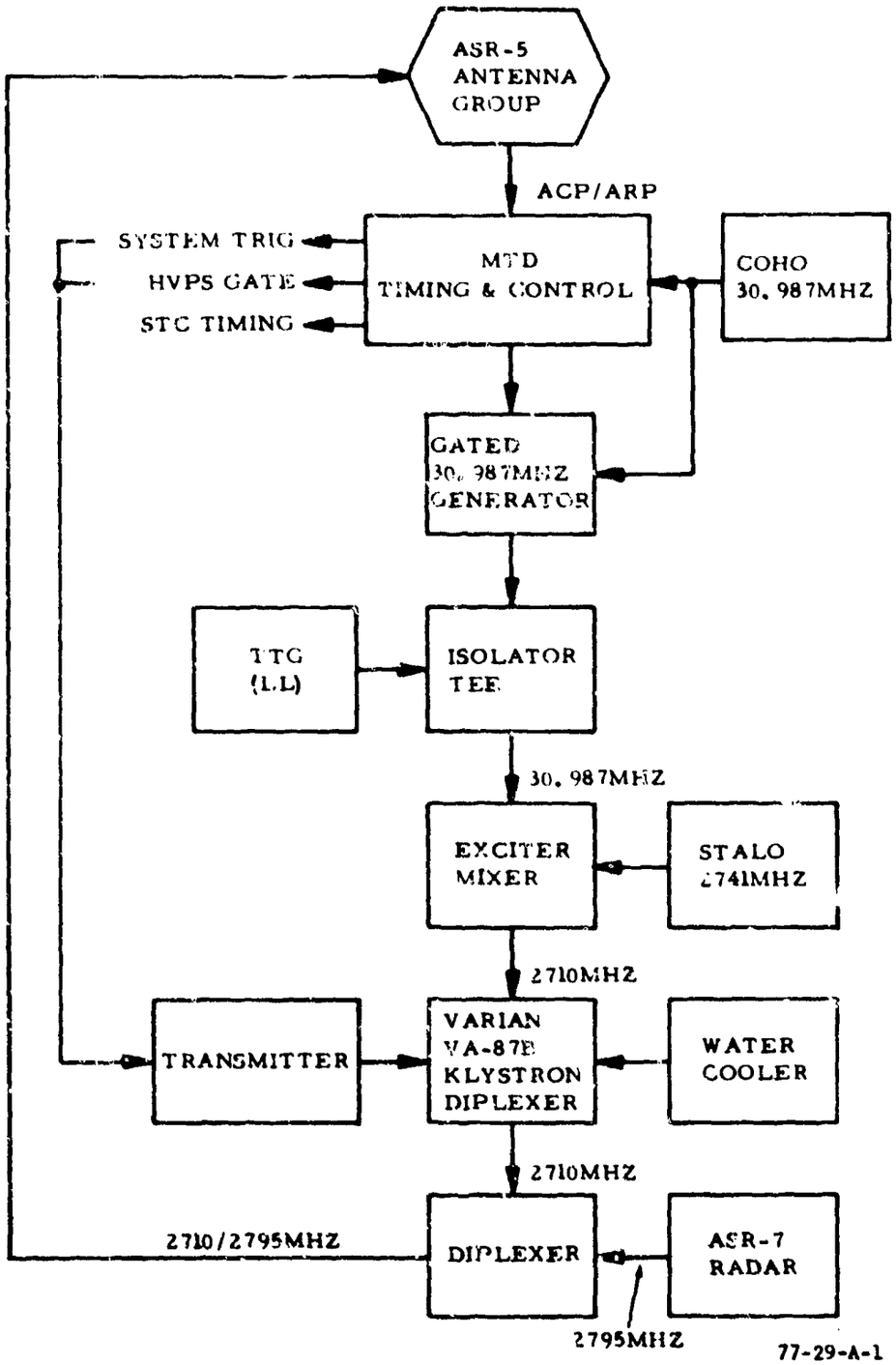

FIGURE A-1. TRANSMITTER SYSTEM SIMPLIFIED BLOCK DIAGRAM

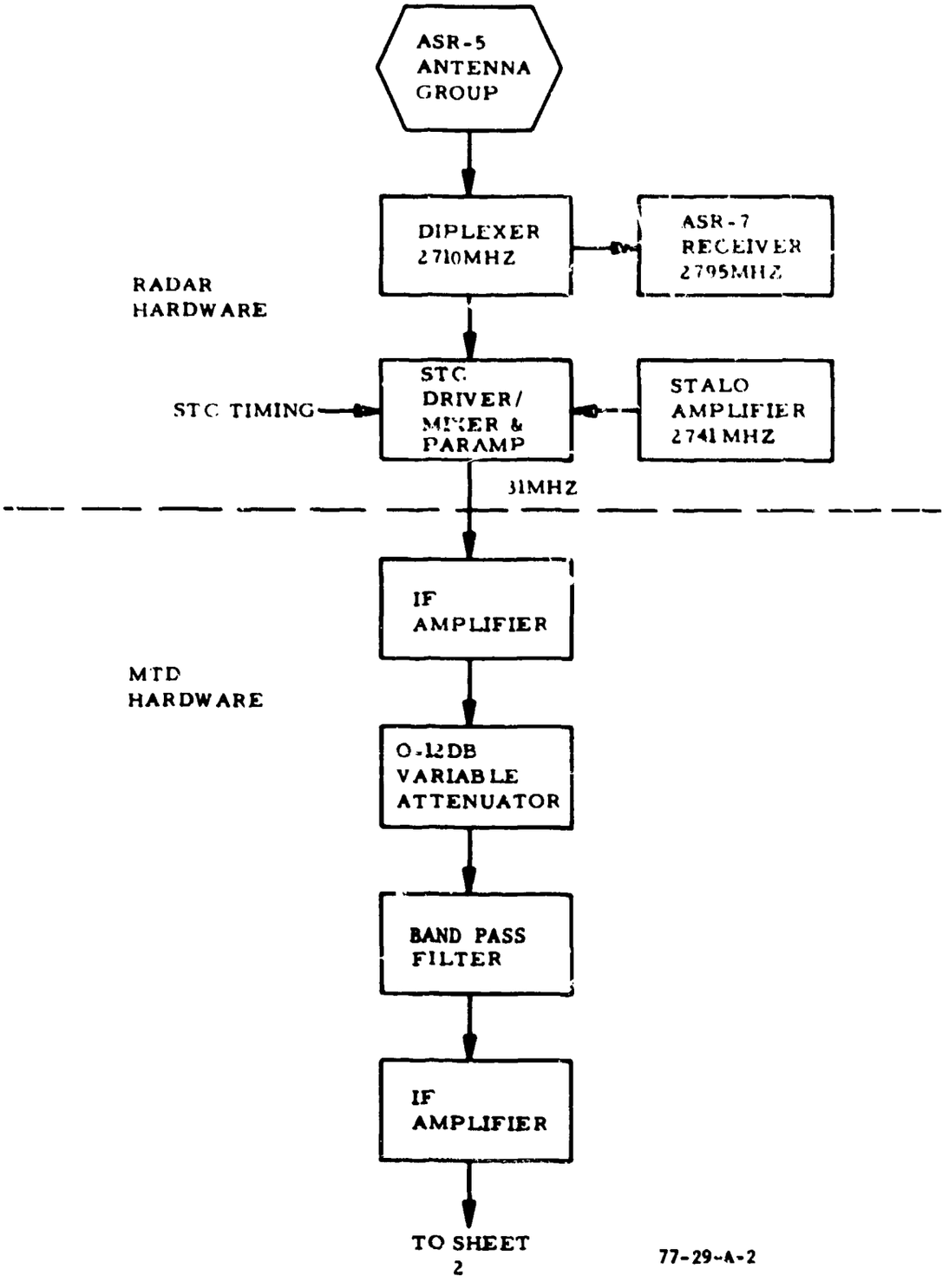

FIGURE A-2. FPS-18/MTD RECEIVER SIMPLIFIED BLOCK DIAGRAM (SHEET 1 OF 2)

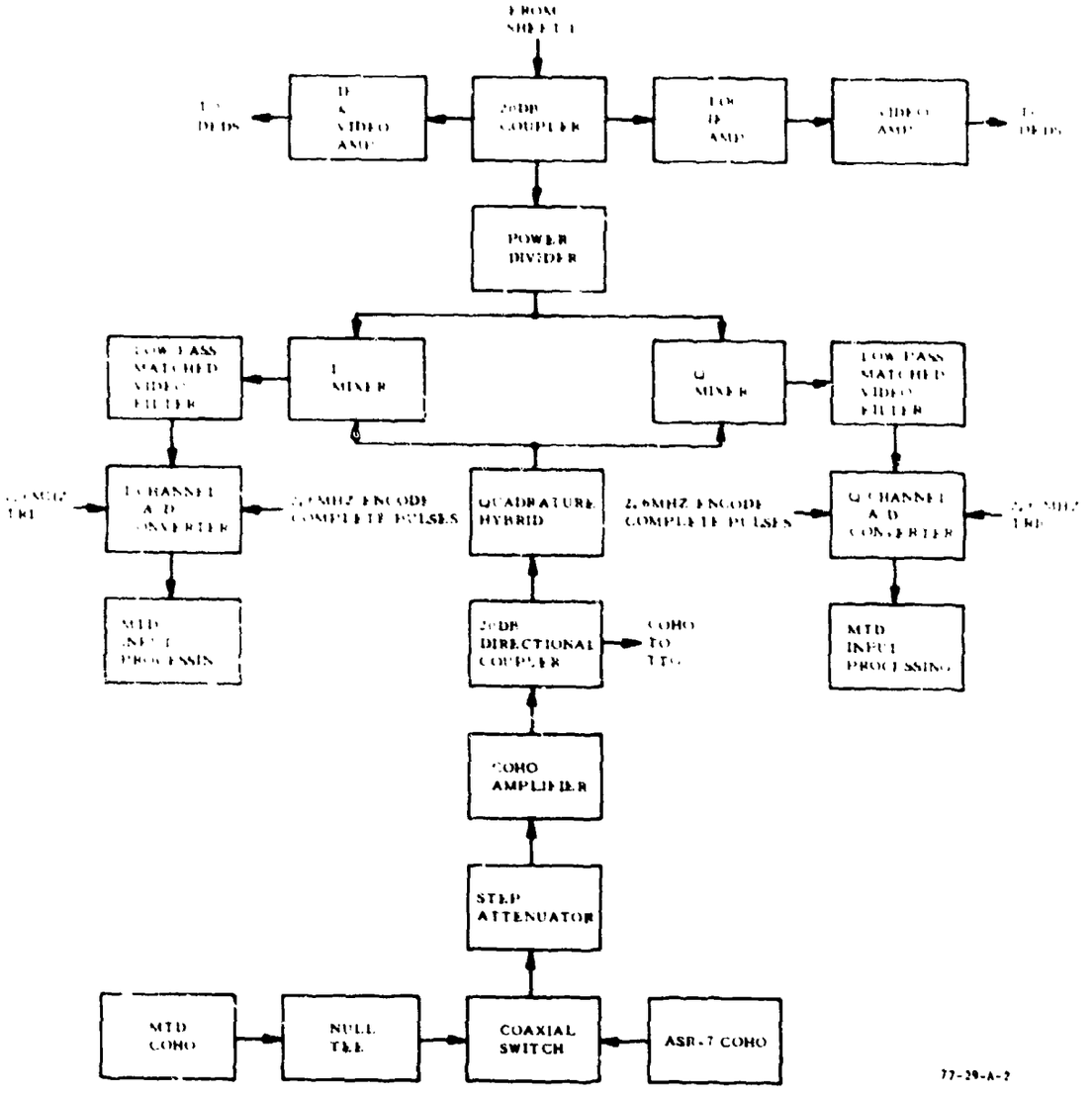

FIGURE A-2. FPS-18/MTD RECEIVER SIMPLIFIED BLOCK DIAGRAM (SHEET 2 OF 2)

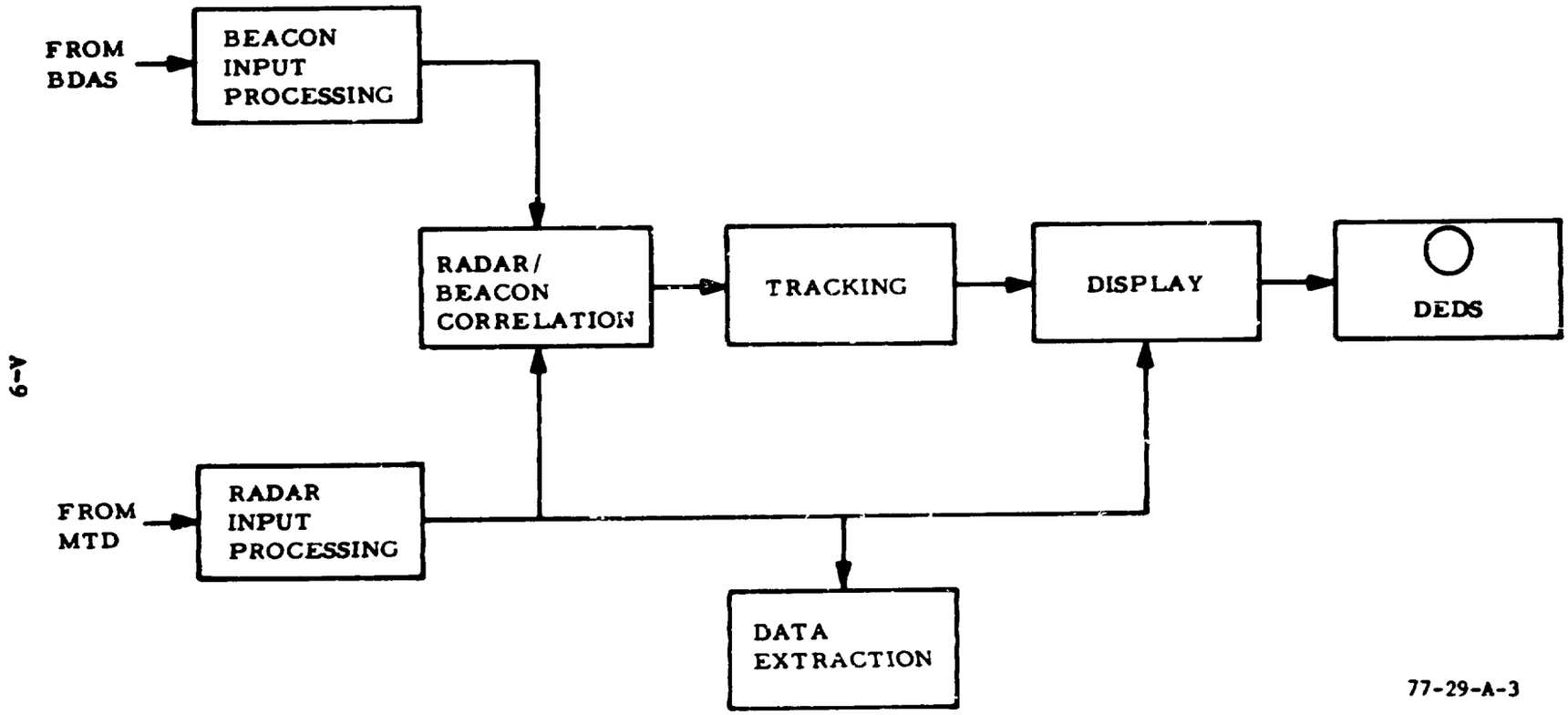

FIGURE A-3. ARTS III SYSTEM CONFIGURED FOR MTD TEST OPERATION

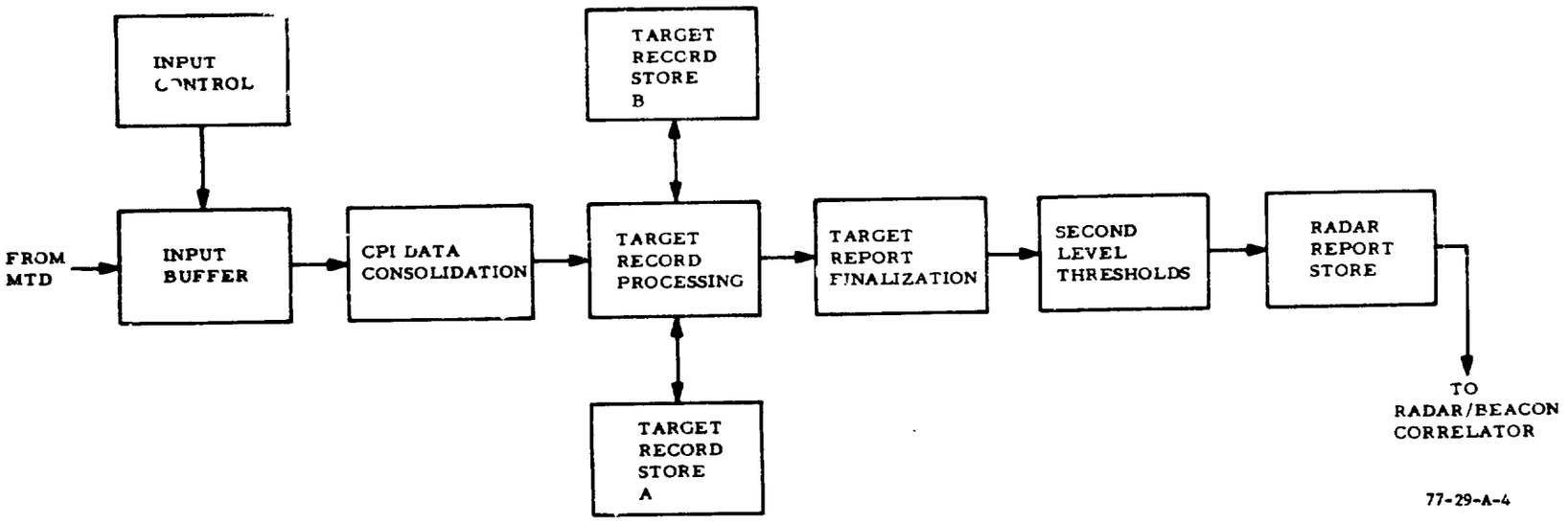

FIGURE A-4. RADAR INPUT PROCESSOR SIMPLIFIED BLOCK DIAGRAM

TABLE A-1. DOPPLER STRENGTH NORMALIZATION FACTORS

Filter Number	Normalization Factor
0	0.3363
1	0.01897
2	0.1057
3	0.2561
4	0.3363
5	0.2561
6	0.1057
7	0.01897

TABLE A-2. DOPPLER INTERPOLATION VALUES

Internal Number	Larger Filter	Smaller Filter	Larger Response Strength	Response Strength Ratio	Smaller Filter	Larger Filter	Interval Number
0			1.000	0			64
1			0.9880	0.000001832			63
2			0.9527	0.0005000			62
3			0.8960	0.003978			61
4	0	1	0.8211	0.01852			60
5			0.7319	0.06315			59
6			0.6331	0.1750			58
7			0.5297	0.4177			57
8			0.4268	0.8910			56
9			0.5740	0.5730			55
10	1	0	0.7704	0.3116	0	7	54
11			0.9262	0.1765			53
12			1.0000	0.1795			52
13	1	2	0.9683	0.3095	6	7	51
14			0.8358	0.5427			50
15			0.6350	0.9876			49
16			0.7957	0.5214			48
17			0.9693	0.2400			47
18			1.0000	0.1365			46
19			0.9906	0.2394			45
20	2	3	0.9005	0.4127	5	6	44
21			0.7471	0.7116			43
22			0.6992	0.8014			42
23	3	2	0.8497	0.4404	6	5	41
24			0.9570	0.2268			40
25			1.0000	0.1384			39
26			0.9693	0.2518			38
27	3	4	0.8697	0.4415	4	5	37
28			0.7195	0.7613			36
29			0.7159	0.7618			35
30	4	3	0.8631	0.4344	5	4	34
31			0.9641	0.2388			33
32			1.000	0.1229			32

APPENDIX B

TEST EQUIPMENT

APPENDIX B

TEST EQUIPMENT

The coherent S-band test Target Generator (TTG) used to generate simulated radar target information is described in this appendix. A list of standard equipments used in testing the MTD is also given.

The coherent RF TTG was designed by Westinghouse Electric Corporation for the FAA to provide realistic simulated RF radar targets for S-band radar sensors. The TTG was interfaced into the MTD/RVD test facility and was used extensively throughout the MTD test and evaluation. Figure B-1 illustrates the TTG/RADAR/MTD interface.

RF test targets were generated by mixing 30-MHz IF (ASR-7) test targets with a sample of the STALO frequency from the radar. The phase modulator was modified to accept 31-MHz IF test targets from the FPS-18. Two external switches enabled the TTG to accept either 30-MHz or 31-MHz IF signals. Coherent or noncoherent targets could be generated by selecting either the COHO signal from the radar or an internal 30-MHz oscillator as the IF signal source. All MTD/RVD tests used the controlled phase mode of operation (variable mode). The simulated RF test targets were controllable in azimuth, range, range rate, velocity, pulse width, and amplitude.

Azimuth control was accomplished by a counter which counted azimuth change pulses (ACP's) and was reset by the north azimuth reference pulse (ARP) from the azimuth pulse generator (APG). Thumbwheel switch control permitted the azimuth start to be set to any selected ACP, providing 4096 possible azimuth positions per 360°. Another thumbwheel switch controlled the selection of azimuth steps per target, up to a total of 99. The time interval between azimuth steps was controlled by another set of thumbwheel switches which were adjustable from 10 us to 10 ms. A manually programmable diode matrix was used to establish the antenna scan pattern. The test target could be window gated as programmed by the antenna pattern, or it could be of constant amplitude every PRP.

Range control was accomplished by a range counter which was reset by a zero mile trigger. A thumbwheel switch selected the range of the RF test target and was variable from 0 to 60 miles in 1 μs steps. Two modes of range control were available: the "fixed mode" provided a stationary target at a selected range and the "moving mode" simulated a radially moving target. Either incoming or outgoing test targets were selectable. Simulated velocity control selected the target velocity and controlled the range rate. The velocity control was variable from 0 to 1,000 knots. The FPS-18 and ASR-7 radars operated with 1.0 and 0.833 μs transmitted pulse widths, respectively. Therefore, the TTG was adjusted to provide the necessary test target pulse widths.

A Hewlett Packard direct-reading precision variable attenuator, model S382C, controlled the RF output amplitude to ±1 percent of reading or 0.1 dB, whichever was greater. The attenuation range was from 0 to 60 dB.

For the probability of detection test, a higher data rate was necessary to provide adequate sampling of RF levels from the TTG. This was accomplished by generating four concentric rings of test targets, each separated in range from the preceding target by approximately 3.75 nmi. An azimuth trigger which occurred 32 times per scan (RVD-4 azimuth 2^7 bit) was used to generate 32 test targets per scan at the same range providing 128 targets per scan. The velocity of the targets was controlled by the velocity-controlled crystal oscillator (VCXO) of the TTG. In addition, the azimuth trigger was incremented by one ACP each antenna scan to provide azimuth changes to test CPI boundaries.

Table B-1 contains a list of the test equipment used in maintenance and calibration of the MTD radar/digital signal processor.

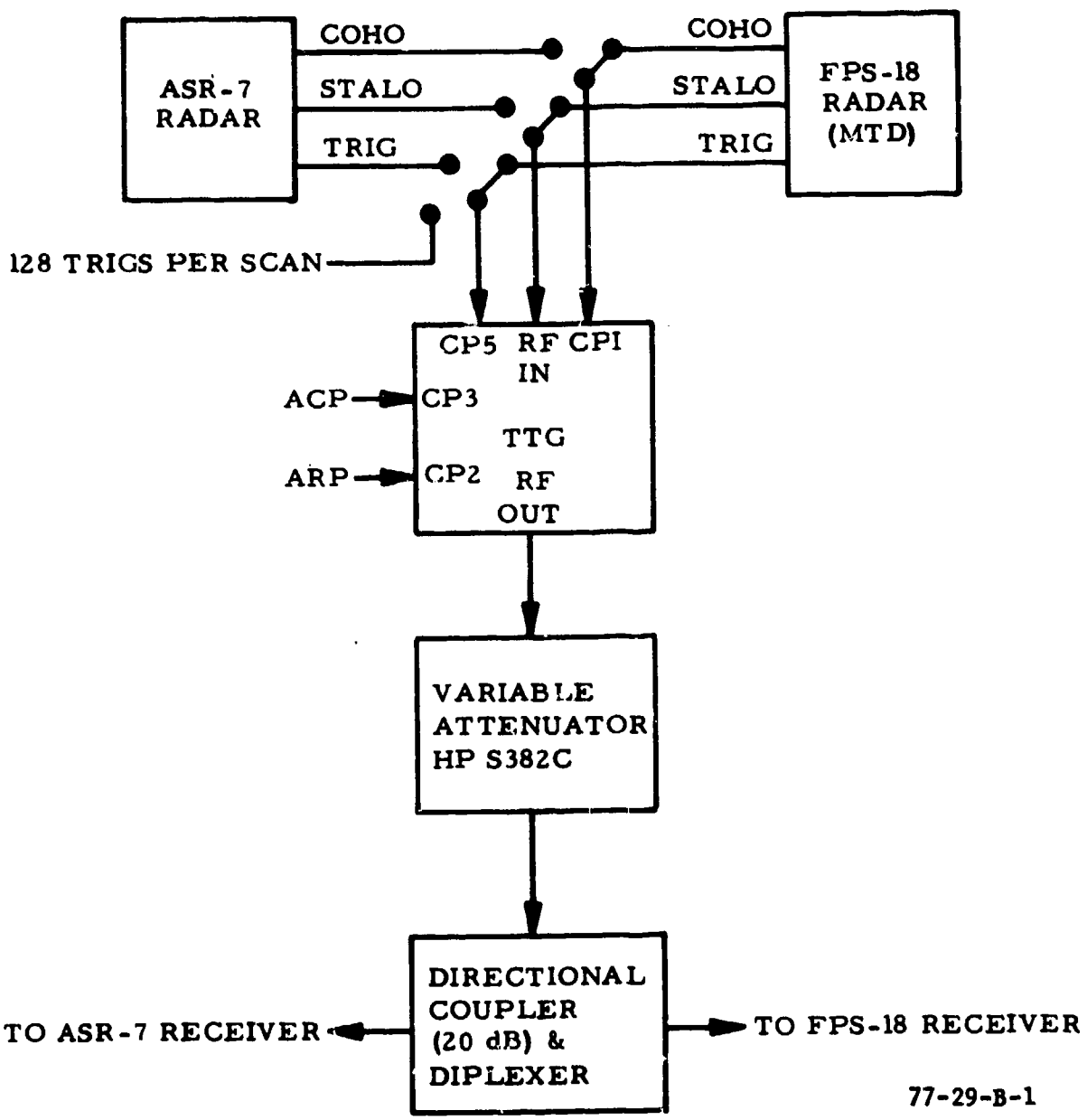

FIGURE B-1. TEST TARGET GENERATOR/RADAR INTERFACE

TABLE B-1

Type	Model	Source
Oscilloscope	7603	Tektronix
Time Base Unit	7B53A	Tektronix
Dual Trace Amplifier	7A26	Tektronix
Voltage Probe	P6053B	Tektronix
Voltage Probe	P6011	Tektronix
Oscilloscope	475	Tektronix
Power Meter	431B	Hewlett Packard
Thermistor Mount	478A	Hewlett Packard
True RMS Voltmeter	3403C	Hewlett Packard
Electronic Counter	5248M	Hewlett Packard
Frequency Converter	5254C	Hewlett Packard
Time Interval Unit	5267A	Hewlett Packard
Sweep Oscillator	8690B	Hewlett Packard
Solid State RF Plug In	8698B	Hewlett Packard
Solid State RF Plug In	8699B	Hewlett Packard
Variable Attenuator	S382C	Hewlett Packard
VHF Attenuator	355C	Hewlett Packard
VHF Attenuator	355D	Hewlett Packard
Attenuator Set	11581A	Hewlett Packard
Coaxial Frequency Meter	536A	Hewlett Packard
Signal Generator	8616A	Hewlett Packard
General Purpose Amplifier	465A	Hewlett Packard
Crystal Detector	420A	Hewlett Packard
Variable Phase Generator	203A	Hewlett Packard
RF Voltmeter	91CA	Boonton
RF Probe	91-12	Boonton
Digital Multimeter	8000A	Fluke
Pulse Generator	7260	Exact
Pulse Generator	100A	Systron Donner
Pulse Generator	110B	Systron Donner
Echo Box	TS-270-AUP	Johnson Elec. Co.
System Noise Monitor	-	Ailtech
Noise Source	-	Ailtech

APPENDIX C

MTD PROBABILITY OF FALSE ALARM IN THERMAL NOISE

APPENDIX C

LIST OF ILLUSTRATIONS

APPENDIX C

MTD PROBABILITY OF FALSE ALARM IN THERMAL NOISE

The MTD probability of false alarm in thermal noise (P_{fa}) was determined by measuring the time it took to receive 100 thermal false alarms and then calculating $P_{fa} = \frac{100}{t_{fa}} \times n$

where t_{fa} was the time elapsed in seconds per 100 false alarms and n was the number of independent opportunities for false alarm per second. In the MTD system, n for each Doppler filter was equal to the product of the number of range gates processed (760) in a coherent processing interval (CPI) and the number of CPI's processed per second (102.13). This product equaled 77,617 opportunities per second per filter. For all seven weather filters, there were therefore 543,319 false alarm opportunities per second. For all eight filters taken together, there were 620,936 false alarm opportunities per second which, at 4.70 seconds per antenna scan, yielded 2,918,400 false alarm opportunities per antenna scan.

It was desired to set the MTD system thresholding so that between 10 and 100 thermal false alarms would be outputted to the ARTS III system each antenna scan. Considering the above false alarm opportunity numbers, it follows that operating with approximately a ten to the minus fifth power probability of false alarm would yield the desired false alarm rate. To determine the correct thresholding levels, receiver noise only (radar transmitter OFF and receiver input connected to the system dummy load) was inputted to the MTD processor, and the false alarm time measured using the NOVA minicomputer. In initial testing, the MTD thresholding was varied to determine its effect on false alarm time. A threshold of 12 dB provided approximately the desired 10^{-5} P_{fa}. The receiver noise level was then varied in amplitude by means of a step attenuator, and the false alarm time of each of the eight Doppler filters was measured.

Figure C-1 shows the resulting data from the seven weather filters (numbers 1 through 7) and figure C-2 the corresponding data from the zero velocity filter. As seen in figure C-1, the number of false alarms increased at lower noise levels in the weather filters. The exact cause of the increase was not determined. Two possible causes were (1) the exact accuracy of the A/D converters was closer to 9 bits than to the rated 10 bits and (2) quantization noise in the MTD processor due to truncations. By operating with a 6-mV noise level (measured using a true voltmeter), the desired false alarm rate was obtained. Six millivolts corresponded to approximately three A/D converter counts. Originally, the system was desired to operate with a 2-mV noise level equal to one A/D least count. Operation with a 6-mV noise level resulted in the loss of approximately 9 dB in system dynamic range capability.

During the testing, it was found that a disproportionately large percentage of the false alarms were produced by the numbers one and seven filters. This was deemed to be due to the effect of the three-pulse canceller filter preceding the DFT filter. The canceller modified the velocity response obtained at the output of the individual FFT filters. Due to the significantly lesser canceller output at frequencies corresponding to the low velocity filters (particularly numbers one and seven), there resulted an increase in the false alarm rate. This was compensated for by operating the number one and seven filters with a higher threshold. While filters two through six had the desired false alarm rate when operated with a threshold 3.94 times (11.91 dB) the average noise level, filters one and seven required a threshold of 4.38 times (12.83 dB) the average noise level. As can be seen in figure B-1, when operated at the above thresholds and at 6-mV rms noise, each of the seven weather filters produced approximately the desired false alarm rate.

Due to the different nature (recursive filter and disc memory) of the zero velocity filter (ZVF), its probability of false alarm curve had a different shape. At the 6-mV operating point dictated by the other Doppler filters, the ZVF had approximately the desired false alarm rate when operated with a threshold of 5.5 times (14.8 dB) the value stored on the disc memory. The ZVF clutter map recursive filter could be adjusted to provide the desired rate of clutter map buildup. The algorithm for the recursive filter (which determined what information was to be stored on the clutter map each scan) was $M-1/2_n$ (M-N) where M and N represented information from the Map and New information from the magnituder, respectively, for each range/azimuth cell. The value of n was selectable, controlling the rate of clutter map update. Testing resulted in the selection of an n value of 3 (yielding an algorithm of M-1/8 (M-N)) so that 1/8 of the information on the clutter map was replaced with new information each antenna scan. This provided a good compromise between too fast a clutter map change (resulting in a high false alarm rate) and too slow a change (resulting in the inability of the clutter map to accurately follow environmental changes such as weather).

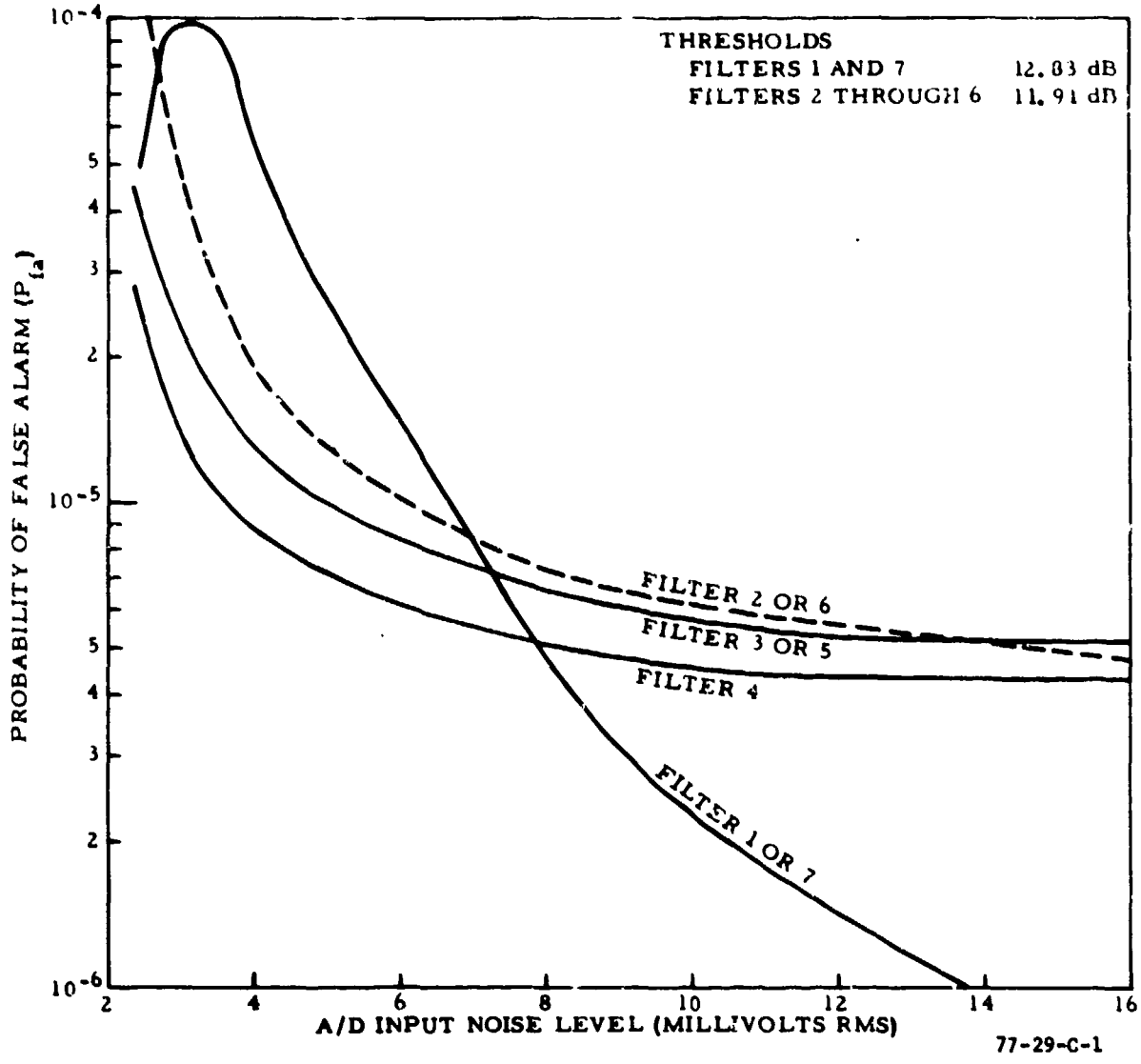

FIGURE C-1. PROBABILITY OF FALSE ALARM FROM RECEIVER NOISE FILTERS 1 THROUGH 7

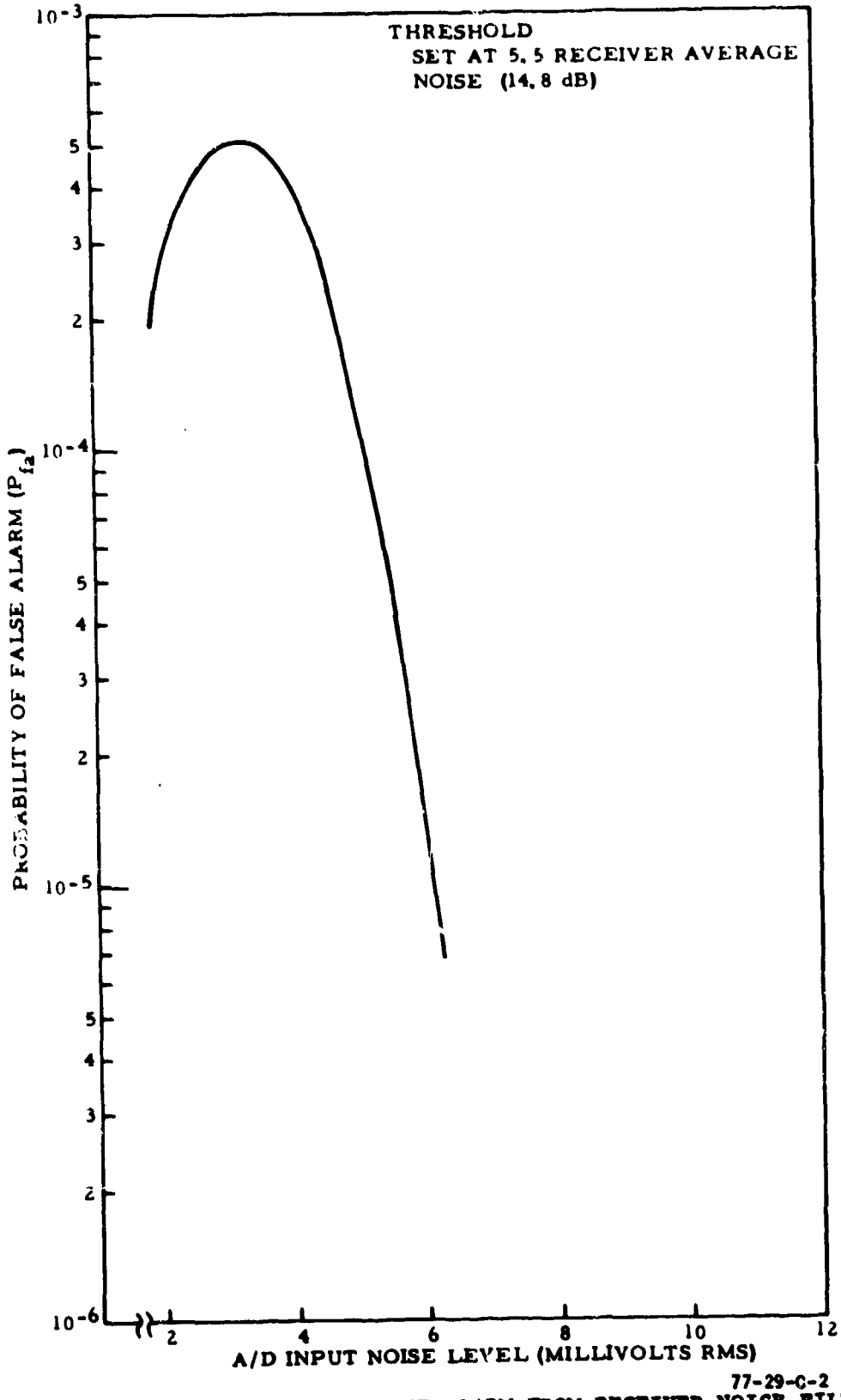

FIGURE C-2. PROBABILITY OF FALSE ALARM FROM RECEIVER NOISE FILTER 0

APPENDIX D

MTD INTERFACE WITH ASR-5 AND ASR-7 RADARS

APPENDIX D

LIST OF ILLUSTRATIONS

APPENDIX D

MTD INTERFACE WITH ASR-5 AND ASR-7 RADARS

The equipment modifications and interconnecting cabling changes necessary to interface the MTD with the TFAST ASR-7 and ASR-5 radars are shown in figures D-1 and D-2, respectively. Both radars were operated with fixed-frequency crystal controlled STALOS. The magnetrons were automatically tuned to maintain the correct frequency with respect to the STALOS. The ASR-7 radar was retuned to operate with the 31-MHz IF frequency used with the FPS-18. A new 30-MHz IF band-pass filter was subsequently procured for ASR-5 operation to avoid retuning it to 31 MHz.

To accommodate the timing interface between the ASR-7 and MTD, the ASR-7 control selector assembly, 6A2A19, was modified to enable the external tuning signal INT. This was accomplished by opening the printed circuit between Z5D pin 13 and Z8A pin 1 and inserting a jumper from Z5D pin 13 to ground for internal operation or open for external operation. An open at Z5D pin 13 enabled Z5C pin 8 which in turn enabled gates Z12D, Z1D, and Z20D on the repetition rate decoder module 6A2A39. The external timing signals from the MTD which appeared on 6A2A39 pins 7, 37, and 40 were then distributed throughout the ASR-7. The ASR-7 COHO and preamplifier output signals were inputted to the MTD. Inter-equipment trigger cabling is shown in figure D-1.

The following steps were taken to interface the ASR-5 and MTD equipments in addition to the trigger cable interconnection shown in figure D-2:

1. Connect MTD Mod trigger to J8805 using BNC "T".
2. Install Coax from J8805 (BNC "T") to J6614.
3. Connect MTD STC trigger to J6613 using BNC "T".
4. PRF stagger unit - remove V13.
5. Normal video realignment unit - remove V17 and V18.
6. Connect RG-58 Coax from ASR-5 COHO output to MTD COHO input.
7. Connect RG-58 Coax from ASR-5 preamplifier to MTD IF input.

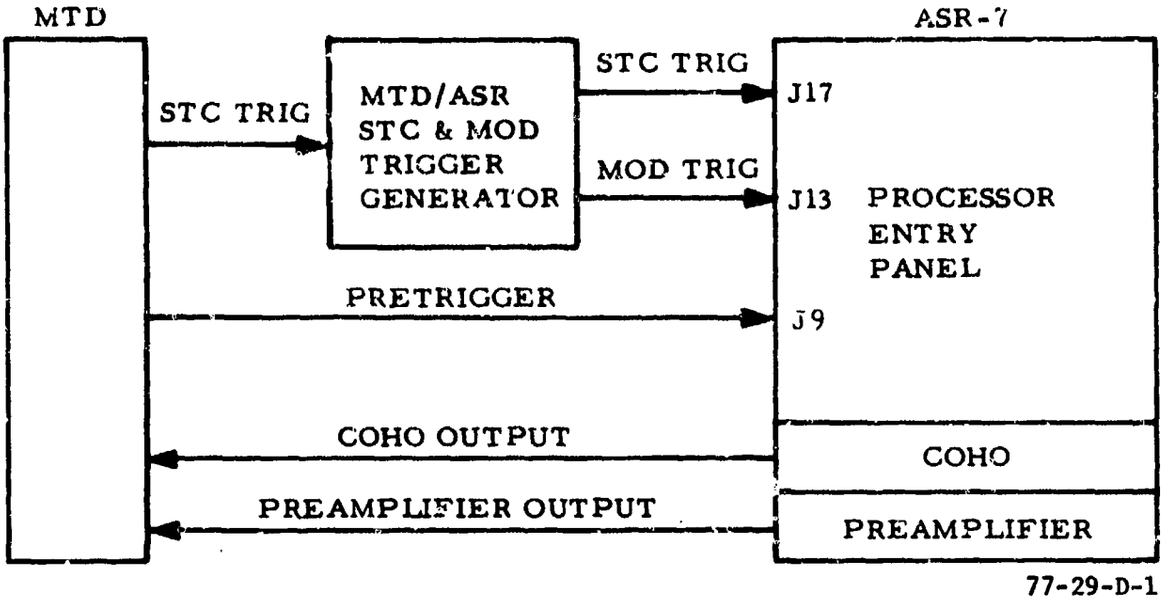

FIGURE D-1. ASR-7/MTD INTERCONNECTION DIAGRAM

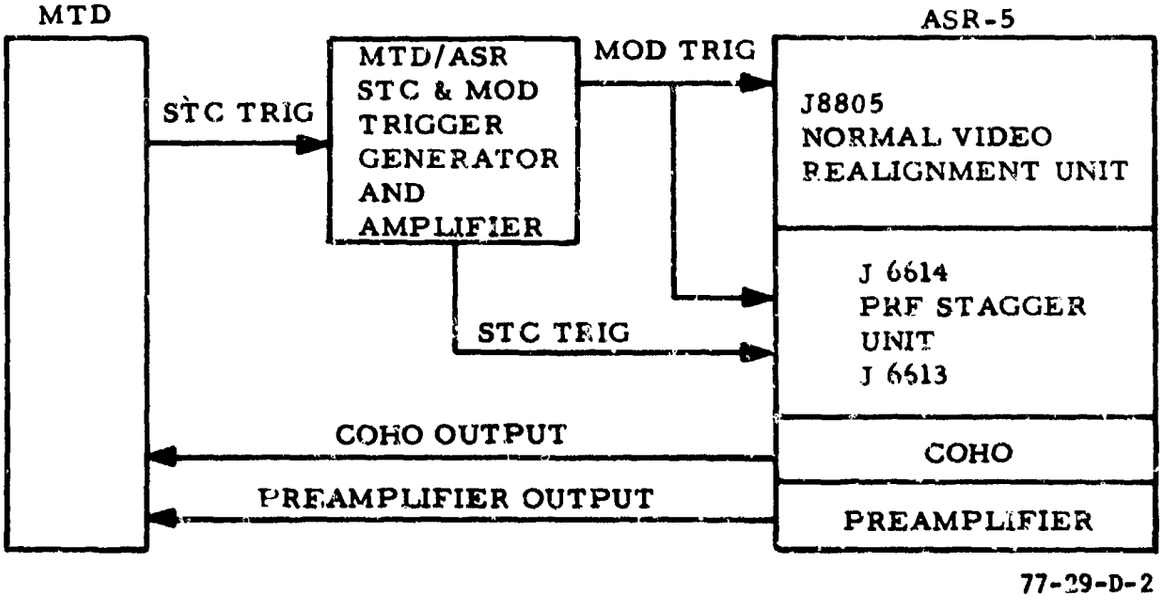

FIGURE D-2. ASR-5/MTD INTERCONNECTION DIAGRAM